Decays of Heavy-Light Mesons. Weak Matrix Elements From The Lattice

Christopher Michael Maynard

Doctor of Philosophy

The University of Edinburgh

1998

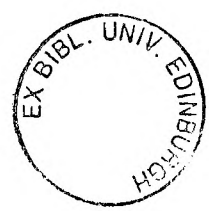

Abstract

This thesis describes a numerical study of weak matrix elements of the vector and axial vector currents relevant to the semi-leptonic and leptonic decays of B and D mesons from Lattice QCD. The simulation was performed in Quenched QCD on a $24^3 \times 48$ lattice at $\beta = 6.2$. The fermionic degrees of freedom were calculated using a non-perturbatively $\mathcal{O}(a)$ improved action.

For a pseudoscalar final state in a semi-leptonic decay, only the vector current contributes and can be parameterised by two form factors which are functions of the momentum transfer squared. The main results for the form factors of the decays $B \to \pi$ at zero momentum transfer are;

$$f_+(0) = f_0(0) = 0.33^{+4}_{-3\ \text{stat}}\ ^{+10}_{-\ 2\ \text{sys}}$$

The momentum dependence was found to be reasonably modelled by pole dominance models. The decay rate for $B \to \pi$ is calculated and compared to experiment allowing the CKM matrix element V_{ub} to be extracted,

$$V_{\text{ub}} = 0.0026^{+1}_{-2\ \text{stat}}\ ^{+1}_{-3\ \text{sys}}\ ^{+4}_{-5\ \text{exp}}$$

The form factors for $D \to K, \pi$ were calculated and the momentum dependence was found to be reasonably modelled by pole dominance.

For leptonic decays of pseudoscalar mesons, the axial current is parameterised by the decay constant, for B and D decays the results are

$$f_B = 174^{+5}_{-3\ \text{stat}}\ ^{+17}_{-11\ \text{sys}}\ \text{MeV}$$
$$f_D = 194^{+2}_{-2\ \text{stat}}\ ^{+20}_{-\ 7\ \text{sys}}\ \text{MeV}$$

The soft pion relation for the B meson which relates the ratio f_B/f_π to $f_0(q^2_{\text{max}})$, is evaluated and found to be substantially violated.

Declaration

This thesis has been wholly composed by me and presents work carried out as part of the UKQCD collaboration. This calculation used gauge configurations and light quark propagators generated by the UKQCD collaboration. I used UKQCD computer code to generate the heavy propagators used in the calculation as well as the two-point correlation functions. The code to generate the three-point functions was adapted by me from the two-point code with some contributions from Victor Lesk. The three-point and heavy-light two-point functions were generated by me. All the results were analysised by me under the guidance of Dave Richards and Ken Bowler. The analysis code was adapted by me based on existing UKQCD statistical analysis routines.

Preliminary results of these calculation are to appear in

- Semileptonic decays of Heavy Mesons. C. Maynard, UKQCD Collaboration, `hep-lat/9809064`, proceedings of Lattice 98.

C.M. Maynard.

Acknowledgements

I would like to thank David Lin and Bálint Joó with whom I shared many a Banana Time and an office. I would also like to thank my supervisors, Ken Bowler and David Richards, whose helpful discussions and suggestions have been invaluable. I would also like to thank Jonathan Flynn for advice in all matters heavy. I would like to thank the other postgraduate students in the group for useful discussions and many distractions.

I am also indebted to many people not involved in particle physics who have made my student life in Edinburgh a happy and a fulfilled one.

Mostly I would like to thank Pauline for coming to Edinburgh in the first place and then putting up with someone self-centred enough to do a Ph.D.

Errata

In the Abstract, the value for $V_{\rm ub}$ should be

$$V_{\rm ub} \;=\; 0.0036^{+6}_{-4\ \rm stat}\ ^{+1}_{-5\ \rm sys}\ ^{+6}_{-6\ \rm exp}.$$

On page 93, equation (5.20) should be

$$\frac{\Gamma}{|V_{\rm ub}|^2} \;=\; 9.1^{+2.7}_{-1.8\ \rm stat}\ ^{+3.2}_{-0.4\ \rm sys}\ 10^{12}\ \rm s^{-}$$

On page 94, equation (5.23) should be

$$V_{\rm ub} \;=\; 0.0036^{+6}_{-4\ \rm stat}\ ^{+1}_{-5\ \rm sys}\ ^{+6}_{-6\ \rm exp}.$$

Contents

Chapter 1

Introduction

The Standard Model (SM) of particle physics [1, 2, 3, 4] has been in existence for 25 years. Based on the gauge group of $SU(3) \otimes SU(2) \otimes U(1)$, it has had remarkable success at predicting phenomena over a huge range of scales. However, the SM has in total 19 free parameters, 22 including 2 masses and a mixing angle for the neutrinos [5]. This is too many for the theory to be thought of as fundamental. Despite the many successes of the SM some of these free parameters are not at all well known. In particular some of the quark mixing angles of the *Cabibbo-Kobayashi-Maskawa* (CKM) matrix [6, 7] are amongst the least well known.

Our knowledge of some of the CKM matrix elements has large uncertainties coming from both experiment and theory, particularly those related to the b quark. The experimental situation is about to be radically altered by the so called B-factory experiments, at KEK in Japan and *BaBar* at SLAC in the USA. This wealth of experimental data will make possible the accurate determination of the under-determined CKM matrix elements. However, the theoretical predictions from the SM must also be accurately known. In addition, some of the processes to be measured at the B-factories are sensitive to possible new physics beyond the SM. If the SM predictions are known sufficiently accurately then experimental deviations can be interpreted as signals of new physics. This thesis is concerned with the calculation of physical observables from the SM relevant to the semi-

leptonic and leptonic decays of B and D mesons.

1.1 The Standard Model

The SM has two groups of particles, the half-integer spin fermions and the integer spin bosons. In the SM all the fermions are spin $\frac{1}{2}$ and come from one of two families; quarks which feel the strong interaction, and leptons which do not. This pattern is repeated in 3 generations. The bosons are either gauge bosons which mediate the interactions, or the scalar Higgs boson. In this section the Glashow-Weinberg-Salam model of $SU(2)_L \otimes U(1)_Y$ describing the electroweak interaction is considered. Quantum Chromodynamics, the $SU(3)$ gauge theory of the strong interaction will be discussed in chapter 2.

The Lagrangian density of the electroweak interaction can be divided into three additive parts

$$\mathcal{L} = \mathcal{L}_F + \mathcal{L}_G + \mathcal{L}_H \tag{1.1}$$

where F stands for Fermion, G for gauge and H for Higgs.

The gauge boson piece of the Lagrangian is written as

$$\mathcal{L}_G = -\frac{1}{4} F^a_{\mu\nu} F^{a\mu\nu} - \frac{1}{4} G_{\mu\nu} G^{\mu\nu}. \tag{1.2}$$

$F^a_{\mu\nu}$ $(a = 1, 2, 3)$is the non-abelian $SU(2)$ field strength tensor,

$$F^a_{\mu\nu} = \partial_\mu W^a_\nu - \partial_\nu W^a_\mu - g_2 \epsilon^{abc} W^b_\mu W^c_\nu. \tag{1.3}$$

The W^a are isospin gauge fields, and g_2 the coupling constant. The structure constant for $SU(2)$ is the Levi-Cevita alternating tensor. Similarly, $G_{\mu\nu}$ is the field strength tensor for the abelian $U(1)$ gauge group,

$$G_{\mu\nu} = \partial_\mu B_\nu - \partial_\nu B_\mu, \tag{1.4}$$

and B_μ is the weak hyper-charge gauge field.

Consider one generation of chiral fermions where only the left handed fermions transform non-trivially under $SU(2)_L$ of weak isospin. The fermion fields are

$$v\psi_L = \begin{pmatrix} u \\ d \end{pmatrix}_L , \qquad u_R,\ d_R$$

$$l_L = \begin{pmatrix} \nu \\ e \end{pmatrix}_L \quad , \qquad e_R \tag{1.5}$$

where it is assumed there is no right-handed neutrino.

Table 1.1: Quantum Numbers in the Standard Model

field/Q_n	T	T_3	Y	Q_{em}
ν_L	$\frac{1}{2}$	$\frac{1}{2}$	-1	0
e_L	$\frac{1}{2}$	$-\frac{1}{2}$	-1	-1
e_R	0	0	-2	-1
u_L	$\frac{1}{2}$	$\frac{1}{2}$	$\frac{1}{3}$	$\frac{2}{3}$
d_L	$\frac{1}{2}$	$-\frac{1}{2}$	$\frac{1}{3}$	$-\frac{1}{3}$
u_R	0	0	$\frac{4}{3}$	$\frac{2}{3}$
d_R	0	0	$-\frac{2}{3}$	$-\frac{1}{3}$

Particle states under $SU(2)_L \otimes U(1)_Y$ are specified by three quantum numbers, T and T_3 of the weak isospin group and Y of the weak hyper-charge group. The fermion fields are assigned the quantum numbers in table 1.1. The electromagnetic charge Q_{em} is related to the hyper-charge and isospin quantum numbers by

$$Q_{em} = T_3 + \frac{1}{2}Y. \tag{1.6}$$

The Lagrangian density for the Fermion fields is given by

$$\mathcal{L}_F = \sum_{F_L} \bar{\psi}_L i \not{D} \psi_L + \sum_{F_R} \bar{\psi}_R i \not{D} \psi_R \tag{1.7}$$

where D^μ is the *covariant* derivative and the sum over F is over all the fermion fields. Right-handed fields do not couple to the weak isospin gauge fields, so they only couple to the weak hyper-charge through their covariant derivative,

$$D_\mu \psi_R = \left(\partial_\mu + i\frac{g_1}{2} Y B_\mu\right) \psi_R. \tag{1.8}$$

The covariant derivative for the left-handed fermions is

$$D_\mu \psi_L = \left\{ \mathbf{I}\left(\partial_\mu + i\frac{g_1}{2} Y B_\mu\right) + i\frac{g_2}{2} \tilde{\tau} \cdot \widetilde{W}_\mu \right\} \psi_L \tag{1.9}$$

Here the τ's are the Pauli matrices, and $\mathbf{I}$ the identity matrix and

$$\widetilde{W}_\mu = \left(W_\mu^1, W_\mu^2, W_\mu^3\right). \tag{1.10}$$

The third piece of the Lagrangian density is the Higgs sector. The Higgs interaction splits into two, the Higgs-fermion coupling and the Higgs-gauge coupling. Considering the latter, let Φ be a complex scalar doublet, where both components have hyper-charge 1,

$$\Phi = \begin{pmatrix} \phi^+ \\ \phi^0 \end{pmatrix} \tag{1.11}$$

then the Lagrangian density can be written as

$$\mathcal{L}_{HG} = D_\mu \Phi^\dagger D^\mu \Phi - \mathcal{V}(\Phi). \tag{1.12}$$

The potential $\mathcal{V}(\Phi)$ is given by

$$\mathcal{V}(\Phi) = -\mu^2 \Phi^\dagger \Phi + \lambda \left(\Phi^\dagger \Phi\right)^2, \tag{1.13}$$

and the covariant derivative is given by equation 1.9.

The fermion fields couple to the Higgs field by a Yukawa interaction. The Lagrangian density is

$$\mathcal{L}_{HF} = -Q_u \bar{\psi}_L \bar{\Phi} \psi_R^u - Q_d \bar{\psi}_L \Phi \psi_R^d - Q_l \bar{l}_L \Phi l_R + h.c. \tag{1.14}$$

where the Q's are the coupling constants and $\bar{\Phi}$ is defined as

$$\bar{\Phi} = i\tau_2 \Phi^\star. \tag{1.15}$$

1.1.1 Spontaneous Symmetry Breaking

Both the fermions and the gauge bosons acquire mass through the spontaneous breaking of the $SU(2)_L \otimes U(1)_Y$ symmetry. The ground state Higgs configuration can be found by minimising the potential.

$$\Phi(-\mu^2 + 2\lambda \Phi^\dagger \Phi) = 0. \tag{1.16}$$

This has two solutions for the vacuum expectation value of the Higgs field. The trivial solution $\langle\Phi\rangle = 0$ and the non-trivial

$$|\langle\Phi\rangle|^2 = \frac{v^2}{2} \tag{1.17}$$

where

$$v \equiv \sqrt{\frac{\mu^2}{\lambda}}. \tag{1.18}$$

One vacuum expectation value for the Higgs field which satisfies 1.17 is

$$\langle\Phi\rangle = \begin{pmatrix} 0 \\ v/\sqrt{2} \end{pmatrix}. \tag{1.19}$$

The Higgs field Φ can be substituted by

$$\Phi(x) \rightarrow \langle\Phi\rangle + \Phi'(x). \tag{1.20}$$

Firstly define the charged fields, $W^\mu_\pm$, as

$$W^\mu_\pm = \frac{1}{\sqrt{2}}\left(W^\mu_1 \pm iW^\mu_2\right). \tag{1.21}$$

The Higgs Lagrangian density then contains the terms

$$\begin{aligned} \mathcal{L}_H &= -\frac{v}{\sqrt{2}}\left(Q_u\bar{\psi}^u_L\psi^u_R + Q_d\bar{\psi}^d_L\psi^u_R + Q_l l^e_L l^e_R\right) \\ &\quad +\frac{v^2}{4}\left(g_2^2 W^\mu_+ W^-_\mu + \left[g_2 W^\mu_3 - g_1 B^\mu\right]^2\right). \end{aligned} \tag{1.22}$$

The fermion fields now have masses which are proportional to their Yukawa couplings,

$$m_f = \frac{v}{\sqrt{2}}Q_f \tag{1.23}$$

and the $W^\pm$ fields have acquired a mass of

$$M_W = g_2\frac{v}{2}. \tag{1.24}$$

What has happened to the neutral fields is not so clear. Two new neutral fields can be defined which are linear combinations of the original two;

$$Z^\mu = W^\mu_3\cos\theta_W - B^\mu\sin\theta_W \tag{1.25}$$

$$A^\mu = W^\mu_3\sin\theta_W + B^\mu\cos\theta_W, \tag{1.26}$$

where θ_W is the *weak-mixing angle* defined as

$$\tan\theta_W = \frac{g_1}{g_2}. \tag{1.27}$$

In particular, if we use equations 1.25 and 1.26 to substitute into equation 1.22, the gauge part can be written as

$$\mathcal{L}_{HG} = \frac{v^2}{4}\left(g_2^2 W_+^\mu W_\mu^- + \frac{g_2^2}{\cos^2\theta_W} Z^\mu Z_\mu\right). \tag{1.28}$$

It can now be seen that the Z field has acquired a mass, M_Z

$$M_Z = g_2 \frac{v}{2\cos\theta_W}, \tag{1.29}$$

and

$$M_W = M_Z \cos\theta_W. \tag{1.30}$$

These mass terms break the gauge symmetry. Crucially there is no quadratic term in the neutral A field, so it has zero mass and that gauge group remains unbroken. This field is associated with the photon of electromagnetism, i.e.

$$SU(2)_L \otimes U(1)_Y \rightarrow U(1)_{\text{em}} \tag{1.31}$$

The interaction of fermion fields with the gauge fields comes through the covariant derivative (equation 1.9). Writing the covariant derivative in terms of the new fields, $W_\pm^\mu$, Z^μ, and A^μ generates the weak and electromagnetic currents.

1.1.2 The CKM Matrix

The CKM matrix arises in the SM because the gauge basis states of the electroweak interaction are not the mass eigenstates. Generalising the above discussion to three generations of quarks and leptons, consider the quark content of the electroweak sector in the gauge interaction basis.

$$\mathcal{L}_{HF} = -\bar{\psi}_L Q_u \bar{\Phi} \psi_R^u - \bar{\psi}_L Q_d \Phi \psi_R^d + h.c. \tag{1.32}$$

The Q's are now are coupling *matrices*. The quark fields are now

$$\begin{aligned}\psi_L &= \left(\begin{pmatrix} u \\ d \end{pmatrix}_L, \begin{pmatrix} c \\ s \end{pmatrix}_L, \begin{pmatrix} t \\ b \end{pmatrix}_L, \right) \\ \psi_R^u &= (u_R, c_R, t_R) \\ \psi_R^d &= (d_R, s_R, b_R)\,, \end{aligned} \tag{1.33}$$

where u, d, c, s, t, b are flavours of quark. Following Spontaneous Symmetry Breaking the Lagrangian 1.32 becomes

$$\mathcal{L}_{qm} = -\bar{\psi}_L^u \mathbf{M}^u \psi_R^u - \bar{\psi}_L^d \mathbf{M}^d \psi_R^d + h.c. \tag{1.34}$$

where

$$\mathbf{M} = \frac{v}{\sqrt{2}} Q. \tag{1.35}$$

and

$$\begin{aligned}\psi_L^u &= (u_L, c_L, t_L) \\ \psi_L^d &= (d_L, s_L, b_L) \end{aligned} \tag{1.36}$$

In general these 3×3 mass matrices are not diagonal. They can be transformed to the mass basis where they are diagonal.

The fields can then be transformed, or rotated to the mass basis as follows

$$\begin{aligned}\psi_L^f \to \psi_L'^f &= R_L^f \psi_L^f \\ \psi_R^f \to \psi_R'^f &= R_R^f \psi_R^f. \end{aligned} \tag{1.37}$$

The mass matrices then transform as

$$\mathbf{M}^f \to \mathbf{M}'^f = R_L^f \mathbf{M}^f R_R^{\dagger f}. \tag{1.38}$$

This implies,

$$\begin{aligned}\mathcal{L}_{qm} \to \mathcal{L}'_{qm} &= -\bar{\psi}_L'^u \mathbf{M}'^u \psi_R'^u - \bar{\psi}_L'^d \mathbf{M}'^d \psi_R'^d + h.c. \\ &= -\bar{\psi}_L^u R_L^{\dagger u} R_L^u \mathbf{M}^u R_R^{\dagger u} R_R^u \psi_R^u - \bar{\psi}_L^d R_L^{\dagger d} R_L^d \mathbf{M}^d R_R^{\dagger d} R_R^d \psi_R^u + h.c. \\ &= -\bar{\psi}_L^u \mathbf{M}^u \psi_R^u - \bar{\psi}_L^d \mathbf{M}^d \psi_R^d + h.c. \end{aligned} \tag{1.39}$$

where $\mathbf{M}'^f$ are the diagonal mass matrices,

$$\mathbf{M}'^u = \begin{pmatrix} m_u & 0 & 0 \\ 0 & m_c & 0 \\ 0 & 0 & m_t \end{pmatrix} \quad \text{and} \quad \mathbf{M}'^d = \begin{pmatrix} m_d & 0 & 0 \\ 0 & m_s & 0 \\ 0 & 0 & m_b \end{pmatrix} \tag{1.40}$$

The differentiation between the mass eigenstate basis and the gauge interaction basis has no effect until the coupling to the gauge fields is considered. Consider the gauge quark coupling in the electroweak sector, in particular the *charged current.*

$$\mathcal{L}_{ch} = -\frac{g_2}{\sqrt{8}} \left\{ W^+_\mu J^\mu_{ch} + W^-_\mu J^{\mu\dagger}_{ch} \right\}. \tag{1.41}$$

where $J^\mu_{ch} = J^\mu_q + J^\mu_l$,

$$J^\mu_q = \bar{\psi}^u_L \Gamma^\mu \psi^d_L \quad \text{and} \quad \Gamma^\mu = \gamma^\mu(1-\gamma^5), \tag{1.42}$$

and similarly for the leptonic current. The current for quarks can be written in either basis

$$\begin{aligned} J^\mu &= \bar{\psi}^u_L \Gamma^\mu \psi^d_L \\ &= \bar{\psi}'^u_L \Gamma^\mu R^u_L R^{\dagger d}_L \psi'^d_L \\ &= \bar{\psi}'^u_L \Gamma^\mu \psi''^d_L. \end{aligned} \tag{1.43}$$

That is the weak interaction sees a linear combination of the 'down type' mass eigenstates. ψ''^d is,

$$\psi''^d_{\alpha,L} = V_{\alpha\beta} \psi^d_{\beta,L}. \tag{1.44}$$

This V is the CKM matrix,

$$V_{CKM} = \begin{pmatrix} V_{ud} & V_{us} & V_{ub} \\ V_{cd} & V_{cs} & V_{cb} \\ V_{td} & V_{ts} & V_{tb} \end{pmatrix} \tag{1.45}$$

The unitarity of this matrix plus fermion phase invariance constrains the elements such that there are only 4 independent parameters. This matrix is often written in the *Wolfenstein* parameterisation [8]. To $\mathcal{O}(\lambda^4)$

$$V = \begin{pmatrix} 1 - \frac{\lambda^2}{2} & \lambda & A\lambda^3(\rho - i\eta) \\ -\lambda & 1 - \frac{\lambda^2}{2} & A\lambda^2 \\ A\lambda^3(1 - \rho - i\eta) & -A\lambda^2 & 1 \end{pmatrix} \tag{1.46}$$

This takes account of the hierarchy in the matrix, $A \sim 1$, $\lambda \sim 0.22$ (the Cabibbo angle), and the two least well known, ρ and η. From equations 1.41, 1.43 and 1.45, the transition $b \to uW^-$ or $\bar{b} \to \bar{u}W^+$ is dependent on ρ and η.

As the parameters of the CKM matrix are free parameters of the SM, they cannot be calculated in the SM. However, if we compute some observable which is dependent on the above transition, and measure experimentally that observable, the CKM matrix element can be determined.

1.2 Weak Matrix Elements

Calculating the above transitions in the weak interaction is relatively easy as they correspond to tree level diagrams (plus radiative corrections). However, quarks feel the strong interaction and are bound into hadrons, and this has to be accounted for in the calculation of such a transition. Figure 1.1 shows a schematic of the decay $B^0 \to \pi^+ l\bar{\nu}_l$. To calculate, for instance, the decay rate of such a transition,

Figure 1.1: $B^0 \to \pi^+ l\bar{\nu}_l$

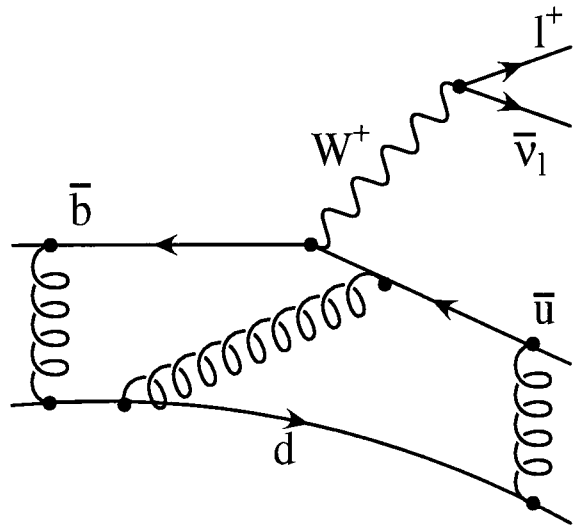

$$\Gamma(B^0 \to \pi^+ l \bar{\nu}_l) = \frac{1}{2E_{B^0}} \int \frac{d^3\vec{q}_1 d^3\vec{q}_2 d^3\vec{k}_1}{(2\pi)^3 2E_{l^-}(2\pi)^3 2E_{\nu_l}(2\pi)^3 2E_{\pi^+}} \times (2\pi)^4 \delta^4(p - k - q_1 - q_2) \sum_{\epsilon} |\mathcal{A}|^2 , \quad (1.47)$$

where the sum over ϵ is over the internal degrees of freedom, we must consider the transition amplitude, $\mathcal{A}$.

$$\mathcal{A} = \left\langle l^-(\vec{q_1}), \bar{\nu}(\vec{q_2}), \pi^+(\vec{k}) \mid \mathbf{H} \mid B^0(\vec{p}) \right\rangle \quad (1.48)$$

where $\mathbf{H}$ is the effective Hamiltonian discussed below.

For small momentum transfers ($q^2/M_W^2 \ll 1$) then the $SU(2) \otimes U(1)$ Lagrangian (equation 1.41) can be written as an effective Fermi Lagrangian,

$$\mathcal{L}_{\text{eff}} = -\frac{G_F}{\sqrt{2}} J_{ch}^{\mu\dagger} J_{ch}^{\mu}, \quad (1.49)$$

where the Fermi constant G_F is

$$\frac{G_F}{\sqrt{2}} = \frac{g_2^2}{8M_W^2}. \quad (1.50)$$

The effective Hamiltonian in equation 1.48 is then

$$\mathbf{H} = -\mathcal{L}_{\text{eff}}. \quad (1.51)$$

The transition amplitude can then be written,

$$\mathcal{A} = \frac{G_F}{\sqrt{2}} V_{ub} L_{\mu}^{\dagger} H^{\mu}. \quad (1.52)$$

The amplitude $\mathcal{A}$ is factorized into purely leptonic and purely hadronic parts, where

$$L^{\mu} = \bar{l}(\vec{q}_1)\gamma^{\mu}(1 - \gamma^5)\nu_l(\vec{q}_2) \quad (1.53)$$

and

$$H^{\mu} = \left\langle \pi^+(\vec{k}) \left| J^{\mu} \right| B^0(\vec{p}) \right\rangle \quad (1.54)$$

where J^{μ} is the $V - A$ current.

H^{μ} is known as a weak matrix element. The name is something of a misnomer, as it describes the non-perturbative strong interaction effects of quarks bound together in hadrons. There are several methods for calculating this, and other matrix elements. However, this thesis is concerned with calculating this, and other weak matrix elements numerically using Lattice Gauge Field theory.

1.3 Form Factors and Decay Constants

Equation 1.54 is not the only weak matrix element that can be used to extract V_{ub}. In general *any* process that has a b quark decaying to a u quark can be used. For instance, the matrix element for $B^0 \to \rho^+ l^- \bar{\nu}_l$ can be calculated. In this thesis, only pseudoscalar to pseudoscalar semileptonic transitions are calculated.

The weak matrix element can be parameterised by considering its Lorentz transformation properties. Consider the matrix element,

$$\left\langle P_F(\vec{k})\right|J^\mu\left|P_I(\vec{p})\right\rangle = \left\langle P_F(\vec{k})\right|V^\mu - A^\mu\left|P_I(\vec{p})\right\rangle, \tag{1.55}$$

where $\left|P_I(\vec{p})\right\rangle$ is the initial pseudoscalar state with momentum $\vec{p}$, and $\left\langle P_F(\vec{k})\right|$ is the final pseudoscalar state with momentum $\vec{k}$. Then

$$\begin{aligned}\left\langle P_F(\vec{k})\right|V^\mu\left|P_I(\vec{p})\right\rangle &= f_+(q^2)(p+k-q\Delta_{m^2})^\mu + f_0(q^2)q^\mu\Delta_{m^2} \\ \left\langle P_F(\vec{k})\right|A^\mu\left|P_I(\vec{p})\right\rangle &= 0,\end{aligned} \tag{1.56}$$

where $q = p - k$ and

$$\Delta_{m^2} = \frac{m_I^2 - m_F^2}{q^2}. \tag{1.57}$$

The form factors f_+ and f_0 are both real, dimensionless functions of the four-momentum transfer squared.

The weak matrix element is a strong interaction quantity, and as such it contains no information about flavour. The only difference between quarks of different flavour in the strong interaction is their mass. Taking advantage of this property, several different matrix elements of different decays can be calculated by changing one parameter, the mass of the quark. The results presented in this thesis are for the decays

$$\begin{aligned}D &\to K l \nu \\ D &\to \pi l \nu \\ B &\to \pi l \nu\end{aligned}$$

Other important weak matrix elements are for the leptonic decays of the pseudoscalar and vector mesons, in particular the leptonic decays of B, B^*, D and D^*.

Figure 1.2: $B^- \to l\bar{\nu}_l$

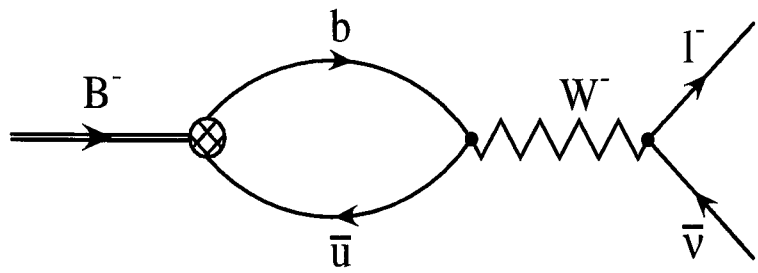

Figure 1.2 shows the leptonic decay of a B meson. The decay rate is given by,

$$\Gamma(B^- \to l\bar{\nu}_l) = \frac{1}{2E_{B^-}} \int \frac{d^3\vec{q}_1 d^3\vec{q}_2}{(2\pi)^3 2E_{l^-}(2\pi)^3 2E_{\nu_l}} \times (2\pi)^4 \delta^4(p - q_1 - q_2) \sum_{\epsilon} |\mathcal{A}|^2 . \quad (1.58)$$

The amplitude $\mathcal{A}$ is

$$\mathcal{A} = \left\langle l(\vec{q}_1), \bar{\nu}(\vec{q}_2) \middle| \mathbf{H} \middle| B^-(\vec{p}) \right\rangle, \quad (1.59)$$

where again $\mathbf{H}$ is the effective Hamiltonian 1.51. The transition amplitude can again be written as equation 1.52 though the hadronic part of the current is given by

$$H^\mu = \left\langle 0 \middle| J^\mu \middle| B^-(\vec{p}) \right\rangle. \quad (1.60)$$

This weak matrix element can be parameterised by considering the Lorentz transformations, as,

$$\langle 0|A^\mu|P(\vec{p})\rangle = p^\mu f_P. \quad (1.61)$$

Similarly for the vector meson,

$$\langle 0|V^\mu|V(\vec{p},\epsilon)\rangle = \epsilon^\mu \frac{M_V^2}{f_V}, \quad (1.62)$$

where ϵ^μ is the polarisation vector of the vector state. Unlike the form factors $f_+(q^2)$ and $f_0(q^2)$, the decay constants f_V and f_P are not functions of the momentum transfer. f_P is a dimensionful quantity with dimensions of mass, whereas f_V is dimensionless. In principle V_{ub} could be extracted from these decays as well.

Chapter 2

Numerical Calculations in Lattice QCD

2.1 QCD

Quantum Chromodynamics is the gauge field theory of the strong interaction. It is defined in terms of fundamental constituents, quarks and gluons. However the observed spectrum of states is made up of composite particles, mesons and baryons. To compute this spectrum one requires a non-perturbative approach. In this chapter I shall present a brief review of Lattice QCD and the construction of correlation functions from which hadronic quantities, such as the spectrum may be extracted. More detailed accounts can be found in [9, 10, 11]

The Lagrangian of the pure QCD sector of the standard model is given by

$$\mathcal{L} = -\frac{1}{4} F^a_{\mu\nu} F^{\mu\nu a} - \sum_{\psi=u,d,c,s,t,b} \bar{\psi}^p(x) \left(i \not{D}^{pq} - m\delta^{pq} \right) \psi^q(x) \tag{2.1}$$

where $a = 1, 2 \cdots, 8$ are colour indices of the gluons and $p, q = 1, 2, 3$ the colour indices of the quarks. The gauge fields live in the adjoint representation of $SU(3)$ and the fermion fields in the fundamental. The covariant derivative is defined as

$$\not{D} = D^\mu \gamma_\mu \quad \text{and} \quad D^\mu = \partial^\mu - igA^\mu(x) \tag{2.2}$$

The gauge fields are collected in the matrix

$$A_\mu(x) = T^a A^a_\mu(x). \tag{2.3}$$

The T^a's are the 8 generators of the $SU(3)$ group and satisfy the Lie algebra

$$[T^a, T^b] = if^{abc}T^c \quad \text{and} \quad \mathrm{Tr}\left(T^a T^b\right) = \frac{1}{2}\delta^{ab} \tag{2.4}$$

The gauge field strength tensor is defined as

$$\begin{aligned} F_{\mu\nu} &= -\frac{i}{g}[D_\mu, D_\nu] \\ F^a_{\mu\nu} &= \partial_\mu A^a_\nu(x) - \partial_\nu A^a_\mu(x) - g f^{abc} A^b_\mu(x) A^c_\nu(x) \end{aligned} \tag{2.5}$$

In the path integral formalism, the expectation value of an observable $\mathcal{O}$ can be written as

$$\langle \mathcal{O} \rangle = \frac{1}{\mathcal{Z}} \int \mathcal{D}A \mathcal{D}\bar{\psi} \mathcal{D}\psi \mathcal{O} e^{iS}, \tag{2.6}$$

where $\mathcal{Z}$ is the partition function given by

$$\mathcal{Z} = \int \mathcal{D}A \mathcal{D}\bar{\psi} \mathcal{D}\psi e^{iS}, \tag{2.7}$$

and S is the action given by

$$S = \int \mathcal{L} d^4x. \tag{2.8}$$

The path integral is a functional integral. It is also complex and the integrand is strongly oscillating. The integrand cannot be interpreted as a probability, which is required for numerical simulations. The theory thus far has been formulated in *Minkowski* space-time, the complexity of the integrand can be removed by formulating the theory in *Euclidean* space-time.

2.1.1 Euclidean Field Theory

The following is a brief discussion of the Euclidean formulation. A more detailed discussion can be found in [9]. Euclidean field theory is formulated by simply rotating the time coordinate to imaginary time.

$$x^0 = -ix^4, \quad \text{and} \quad x^4 \in \mathbf{R}. \tag{2.9}$$

This results in a change in the metric tensor from $g^{\mu\nu}$ to $\delta^{\mu\nu}$, and the action becomes

$$S_E = -iS_M. \tag{2.10}$$

The Dirac matrices are related to their Minkowski counter parts by

$$\gamma_i^E \equiv -i\gamma_i^M \quad \text{and} \quad \gamma_4^E \equiv -i\gamma_4^M \equiv \gamma_0^M \tag{2.11}$$

and satisfy the anti-commutation relations

$$\{\gamma_\mu, \gamma_\nu\} = \delta_{\mu\nu}. \tag{2.12}$$

The path integral in equation 2.6 is now manifestly real and the oscillatory integrand has become damped. In general the observables in equation 2.6 are constructed from time ordered *Green's functions*

$$\mathcal{G}(x_1, \cdots, x_n) = \langle 0 \,|T\left\{\phi(x_1), \cdots, \phi(x_n)\right\}| \, 0\rangle \,. \tag{2.13}$$

These Euclidean correlation functions can be analytically continued to Minkowski space-time by Wick rotation, provided that they obey *reflection positivity.*

Consider some Euclidean field ϕ, evolving according to,

$$\phi(x) = e^{Hx^4}\phi(\vec{x}, 0)e^{-Hx^4}. \tag{2.14}$$

Defining the Euclidean time reflection by

$$\theta(\vec{x}, x^4) = (\vec{x}, -x^4) \tag{2.15}$$

then the operator Θ can be defined as

$$\Theta\phi(x) = \overline{\phi(\theta x)} \tag{2.16}$$

where the bar indicates complex conjugation. The action of Θ is extended to arbitrary functions F by requiring anti-linearity,

$$\Theta(\lambda F) = \overline{\lambda}\Theta F \tag{2.17}$$

and associativity

$$\Theta(FG) = \Theta F \Theta \, G. \tag{2.18}$$

This Θ can be thought of as roughly corresponding to Hermitian conjugation in Minkowski space. Now consider some function F_p which is a function of fields at positive times, then reflection positivity states

$$\langle(\Theta F_p)F_p\rangle \geq 0. \tag{2.19}$$

2.2 Quantum Field Theory on a Lattice

Lattice QCD is a Euclidean field theory formulated on a hyper-cubic space-time lattice, of spacing a. This introduces a momentum cutoff of order the inverse lattice spacing. Consider the finite volume case, with periodic boundary conditions, with the linear extent given by

$$\frac{L}{a} = N \in \mathbf{Z}. \tag{2.20}$$

The Fourier transform of a square integrable function $f(x)$ is defined by

$$f(x) = \int_{-\infty}^{\infty} \frac{dk}{2\pi} \bar{f}(k) e^{ikx}. \tag{2.21}$$

Now consider the fourier transform when $x \to \hat{x} = na,\ 0 \leq n < N$,

$$f(na) = \sum_{k \in \mathcal{B}} \frac{dk}{2\pi} \bar{f}_a(k) e^{ikna} \tag{2.22}$$

where the momentum is restricted to the first *Brillouin zone*

$$\mathcal{B} = \left\{ -\frac{\pi}{a} < k_\mu \leq \frac{\pi}{a} \right\},$$
$$k_\mu = \frac{2n_\mu \pi}{a}, \quad n_\mu \in [0, N-1] \tag{2.23}$$

The cutoff and indeed the lattice regulates the theory without recourse to perturbation theory, and as such is a non-perturbative regulator of the theory.

2.2.1 Gauge Fields

In order to construct the gauge fields on the lattice, the concept of *parallel transport* must be considered. Parallel transport describes how a vector transforms along some curve in space time. Consider a curve $\mathcal{C}$ from x to y and some vector $\phi(x)$ which is an element of the vector space V_x. Consider the case when the gauge group is $SU(3)$. Let $U \in SU(3)$ matrix, such that

$$U(\mathcal{C}) : V_x \to V_y \tag{2.24}$$

The $U(\mathcal{C})$ now maps the vector $\phi(x)$ onto the space V_y, along the curve $\mathcal{C}$. In general each curve or path in space time will have its own parallel transporter.

There are other conditions necessary for parallel transport U:

$$\begin{aligned} U(0) &= \mathbf{1} \\ U(\mathcal{C}_2 \circ \mathcal{C}_1) &= U(\mathcal{C}_2)U(\mathcal{C}_1) \\ U(-\mathcal{C}) &= U^{-1}(\mathcal{C}) \end{aligned} \tag{2.25}$$

where $\mathcal{C}_1 \circ \mathcal{C}_2$ implies a path $\mathcal{C}_1$ followed by a path $\mathcal{C}_2$.

Consider the parallel transporter and the vector under a local gauge transformation $\Lambda(x) \in SU(3)$

$$\begin{aligned} \phi(x) \to \phi'(x) &= \Lambda^{-1}(x)\phi(x) \\ U(\mathcal{C}_{xy}) \to U'(\mathcal{C}_{xy}) &= \Lambda^{-1}(x)U(\mathcal{C}_{xy})\Lambda(y). \end{aligned} \tag{2.26}$$

Gauge invariant objects can be built from closed loops of Us, or 2 vectors linked by a chain of Us.

For the case of an infinitesimal straight path x to $x + dx$, the corresponding parallel transporter can only deviate infinitesimally from the unit matrix,

$$U(\mathcal{C}_{x+dx,x}) = \mathbf{1} + igA_\mu(x)dx^\mu \tag{2.27}$$

where $A_\mu(x)$ is an element of the algebra $SU(3)$. The choice of symbol, $A_\mu(x)$, is no coincidence; this is in fact the gauge field of equation 2.3. Indeed the parallel transport of a vector around a closed path can be used to obtain the Yang-Mills action. Again the reader is referred to [9]. By varying the path and then solving the resulting differential equation one arrives at the following result

$$U(\mathcal{C}) \equiv \mathbf{P}e^{ig\int_C A_\mu(x)dx^\mu} \tag{2.28}$$

where $\mathbf{P}$ denotes path ordering.

The smallest path of non-zero length on the lattice is the straight line of length a between two points of the lattice. Thus the elementary parallel transporters on the lattice are associated with a *link*.

$$U_\mu(x) = \mathbf{P}e^{iga\int_0^1 A_\mu(x+(1-y)a\hat{\mu})dy} \tag{2.29}$$

Figure 2.1: The Plaquette

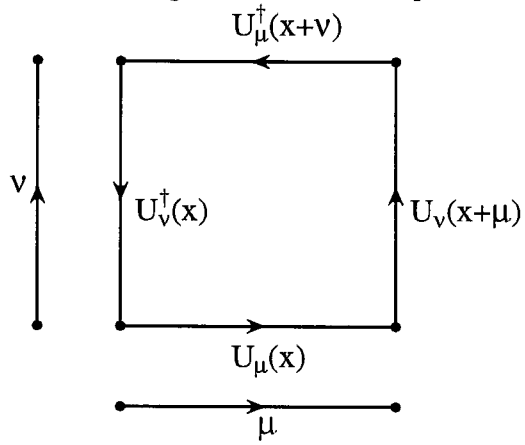

where $\hat{\mu}$ is a unit vector in the direction μ. The elementary closed path on the lattice is the plaquette, Figure 2.1. The plaquette variable is defined as

$$\mathrm{Tr}U_{\mu\nu}(x) = \mathrm{Tr}\left\{U_\mu(x)U_\nu(x+\mu)U_\mu^\dagger(x+\nu)U_\nu^\dagger(x)\right\} \tag{2.30}$$

where

$$U_\nu^\dagger(x) = U_{-\nu}(x+\nu) \tag{2.31}$$

from equation 2.25. The action proposed by Wilson [12] is defined in terms of plaquette variables

$$S_{WG} = \beta \sum_x \sum_{\mu<\nu} \left\{1 - \frac{1}{N_c}\mathbf{R}\ \mathrm{Tr}U_{\mu\nu}(x)\right\} \tag{2.32}$$

where

$$\beta = \frac{2N_c}{g^2} \tag{2.33}$$

and N_c is the number of colours in $SU(N_c)$. It can be shown [13] that this action reduces to the continuum Yang-Mills action in the classical continuum limit, $a \to 0$

$$\lim_{a\to 0} S_{WG} = \int d^4x \left\{\frac{1}{4}F_{\mu\nu}^2 + \mathcal{O}(a^2)\right\}. \tag{2.34}$$

2.2.2 Fermion Fields

The simplest discretisation of the fermionic part of the action is as follows. Place the anti-commuting Grassmann four-component spinors ψ on the lattice sites

$$\psi(x) \to \psi(\hat{x}) \quad \text{where} \quad \hat{x} = an, \quad n \in \mathbf{Z} \tag{2.35}$$

where a is the lattice spacing. Replacing the derivative in the Dirac equation with a finite difference, and dropping the hats, the free field action can be written as

$$S_F = \sum_x \left\{ \frac{1}{2a} \sum_\mu \bar{\psi}(x)\gamma_\mu \left[\psi(x+\mu) - \psi(x-\mu)\right] + m\bar{\psi}(x)\psi(x) \right\}. \tag{2.36}$$

In a more compact notation

$$S_F = \sum_{x,y} \bar{\psi}(x) M_{xy} \psi(y) \tag{2.37}$$

where M is called the fermion matrix

$$M_{xy} = \frac{1}{2a} \sum_\mu \gamma_\mu \left[\delta_{x+\mu,y} - \delta_{x-\mu,y}\right] + m\delta_{xy}. \tag{2.38}$$

Its inverse is the free field propagator, which can be computed by taking the Fourier transform and diagonalising

$$M^{-1}_{xy} = \int_{-\pi/a}^{\pi/a} \frac{d^4p}{(2\pi)^4} e^{ip(x-y)} \frac{\hat{m} - i\hat{p}}{a^{-1}\hat{m}^2 + a^{-1}\hat{p}^2} \tag{2.39}$$

where the hats denote quantities in lattice units

$$\hat{m} = m_{\text{phys}} a \quad \text{and} \quad \hat{p} = \gamma_\mu \sin(ap_\mu). \tag{2.40}$$

Letting $a \to 0$ such that

$$\lim_{a\to 0} \frac{\hat{m}}{a} = m_{\text{phys}} \tag{2.41}$$

results in a pole in the propagator when $\hat{p} = i\hat{m}$ associated with a fermion state. However, this occurs not only when

$$\hat{p} = i \sin(\hat{m}') = i\hat{m}, \tag{2.42}$$

as expected in the naive continuum limit, but also when

$$\hat{p} = i \sin(n\pi\hat{m}') = i\hat{m}, \tag{2.43}$$

at the corners of the Brillioun zone. This is the well known fermion doubling problem. It results in 2^d species of fermions where d is the number of dimensions.

In order to remove these doublers the Nielsen and Ninomiya [14] 'no-go' theorem must be considered. It states that:

> *If a lattice action is local and bilinear in the fermion fields and is translationally invariant, possesses continuous chiral symmetry and is hermitian, then in the continuum limit the fermion propagator contains equal numbers of right-handed and left-handed fermions which are otherwise identical.*

This essentially tells us that for every fermion on the lattice there is a partner with the opposite chirality. One method, known as *staggered fermions* [15] accepts these extra fermions by placing each component of the spinor on different lattice sites and interpreting the remaining doublers as different flavours. This will not be discussed here. The Nielsen-Ninomiya theorem does not say anything about the behaviour of the masses, nor their couplings in the continuum limit. The other main approach is to add an irrelevant term to the action which *explicitly breaks* the chiral symmetry of the action. This gives the extra fermion species a mass proportional to the cut-off and so they decouple from the low energy behaviour. This is known as the *Wilson action* [16].

The *irrelevant* term that Wilson added to the action is a 2nd derivative term which vanishes in the continuum limit.

$$S_{WF} = S_F - \frac{r}{2}\sum_x \left\{ \sum_\mu \bar{\psi}(x)\gamma_\mu[\psi(x+\mu) + \psi(x-\mu) - 2\psi(x)] \right\} \psi(x) \qquad (2.44)$$

After a redefinition of the parameters it is more usual to express the Wilson action as

$$S_{WF} = \sum_x \left\{ \bar{\psi}(x)\psi(x) + \kappa \sum_\mu \bar{\psi}(x)\left[(\gamma_\mu - r)\psi(x+\mu) - (\gamma_\mu + r)\psi(x-\mu)\right] \right\} \qquad (2.45)$$

where κ is the Hopping parameter,

$$\kappa = \frac{1}{2m + 8r}. \qquad (2.46)$$

2.2.3 The Lattice Action

The action for lattice QCD for Wilson fermions can be expressed as

$$S_{LQCD} = S_g + S_{WF} \tag{2.47}$$

where S_g from equation 2.32 for the $SU(3)$ gauge group is given by

$$S_g = \beta \sum_p \left(1 - \frac{1}{3}\mathbf{R}\ \mathrm{Tr} U_{\mu\nu}(x)\right) \tag{2.48}$$

where $\sum_p$ means sum over plaquettes. Recalling from equation 2.26 that gauge invariant objects can be constructed from closed loops of links or chains of links connecting vectors (spinors), S_{WF} in the presence of gauge fields can be written as

$$\begin{aligned} S_{WF} &= \sum_x \Big\{ \bar{\psi}(x)\psi(x) + \kappa \sum_\mu \big[U_\mu(x)(\gamma_\mu - 1)\psi(x+\mu) \\ &\quad - U_\mu^\dagger(x-\mu)(\gamma_\mu + 1)\psi(x-\mu) \big] \Big\} \end{aligned} \tag{2.49}$$

choosing $r = 1$. It can be shown that the Wilson Fermion action is equivalent to

$$S_{WF} = \int d^4x \bar{\psi} \left(\not{\partial} + ig\not{A} + m \right) \psi + \mathcal{O}(a) \tag{2.50}$$

2.3 Improvement

This discussion follows a series of lectures [17, 18, 19] given at the NATO Advanced Study Institute as part of the Newton Institute; Non-Perturbative Aspects of QCD.

The leading discretisation errors in the action are $\mathcal{O}(a)$. In order to control the cutoff effects one has to compute at several lattice spacings and extrapolate to the continuum limit. However, as noted above, a lattice action which reduces to QCD in the continuum is not unique. In particular Symanzik [20, 21] proposed that at energies less than the cutoff, lattice QCD is equivalent to an effective continuum theory whose action is given by

$$S_{\text{eff}} = S_0 + aS_1 + a^2 S_2 + \cdots \tag{2.51}$$

where S_1 is the action constructed from a linear combination of dimension 5 operators.

$$\begin{aligned}
\mathcal{O}_1 &= \bar{\psi}\sigma_{\mu\nu}F_{\mu\nu}\psi \\
\mathcal{O}_2 &= \bar{\psi}D_\mu D_\nu\psi + \bar{\psi}\overleftarrow{D}_\mu\overleftarrow{D}_\nu\psi \\
\mathcal{O}_3 &= m\mathrm{Tr}\{F_{\mu\nu}F_{\mu\nu}\} \\
\mathcal{O}_4 &= m\left\{\bar{\psi}\not{D}\psi - \bar{\psi}\overleftarrow{\not{D}}\psi\right\} \\
\mathcal{O}_5 &= m^2\bar{\psi}\psi
\end{aligned} \tag{2.52}$$

In a similar fashion any any renormalised local lattice fields $Z_\phi\phi$ can be constructed from local continuum fields,

$$\phi_{\text{eff}} = \phi_0 + a\phi_1 + a^2\phi_2 + \cdots \tag{2.53}$$

The number of operators required can be reduced by considering on-shell quantities only. $\mathcal{O}_2$ and $\mathcal{O}_4$ then vanish by the field equations. Thus an $\mathcal{O}(a)$ *counter term* that cancels the S_1 term in the effective action 2.51 can be constructed by considering only three additional operators.

$$S_{\text{ct}} = a^5\sum_x\left\{c_1\hat{\mathcal{O}}_1 + c_3\hat{\mathcal{O}}_3 + c_5\hat{\mathcal{O}}_5\right\} \tag{2.54}$$

where $\hat{\mathcal{O}}_n$ are a lattice representation of $\mathcal{O}_n$. Terms proportional to $\hat{\mathcal{O}}_3$ and $\hat{\mathcal{O}}_5$ can be dropped as these correspond to a renormalisation of the bare coupling and mass. An $\mathcal{O}(a)$ on-shell improved action first proposed by Sheikholeslami and Wohlert [22]

$$S_{\text{SW}} = a^5\sum_x c_{SW}\bar{\psi}(x)\frac{i}{2}\sigma_{\mu\nu}F_{\mu\nu}(x)\psi(x), \tag{2.55}$$

is known as the *clover action* due to the four plaquettes used to approximate $F_{\mu\nu}(x)$. The coefficient c_{SW} then has to be determined.

2.3.1 Improved Operators

If one wishes to compute matrix elements as well as spectral quantities one must also improve the corresponding lattice operators. In general five bare operators,

bilinear in the quark fields, can be constructed:

$$\begin{aligned} V^a_\mu(x) &= \bar{\psi}(x)\gamma_\mu\frac{1}{2}\tau^a\psi(x) \\ A^a_\mu(x) &= \bar{\psi}(x)\gamma_\mu\gamma_5\frac{1}{2}\tau^a\psi(x) \\ T^a_{\mu\nu}(x) &= \bar{\psi}(x)\sigma_{\mu\nu}\frac{i}{2}\tau^a\psi(x) \\ S^a(x) &= \bar{\psi}(x)\frac{1}{2}\tau^a\psi(x) \\ P^a(x) &= \bar{\psi}(x)\gamma_5\frac{1}{2}\tau^a\psi(x) \end{aligned} \tag{2.56}$$

where τ^a are the Pauli matrices. By considering the symmetry properties of the operators, the $\mathcal{O}(a)$ improved fields may be chosen to be

$$\begin{aligned} V^I_\mu &= V_\mu + c_V a\tilde{\partial}_\nu T_{\mu\nu} \\ A^I_\mu &= A_\mu + c_A a\tilde{\partial}_\mu P \\ T^I_{\mu\nu} &= T_{\mu\nu} + c_T a\left[\tilde{\partial}_\mu V_\nu - \tilde{\partial}_\nu V_\mu\right] \\ P^I &= P \\ S^I &= S \end{aligned} \tag{2.57}$$

where $\tilde{\partial}$ is the symmeterised lattice derivative

$$\tilde{\partial}_\mu = \frac{1}{2a}\left[\delta_{x+\mu,y} - \delta_{x-\mu,y}\right] \tag{2.58}$$

These coefficients have to be calculated, usually in lattice perturbation theory with the bare lattice coupling, α_{latt}, as the expansion parameter. At tree level $c_{SW} = 1$ and $c_A = 0$. This corresponds to removing discretisation errors to $\mathcal{O}(\alpha_s a)$. These can be reduced further by calculating to higher orders in perturbation theory. However, the notion that the bare coupling in a cut off theory is approximately the running coupling evaluated at the cut off badly underestimates the lattice coupling. This is a symptom of the 'Tadpole problem' [23].

All gluonic variables are built from the link variable, equation 2.29, which can be approximated to

$$U_\mu(x) \approx e^{iagA_\mu}. \tag{2.59}$$

Consider the leading order coupling with the quark fields, $\bar{\psi}U_\mu\gamma_\mu\psi/a$, this has the desired $g\bar{\psi}\not{A}\psi$ as well as all the higher order powers suppressed by the same

power of the lattice spacing. For quantised fields, pairs of A_μ's contracted together generate factors of $1/a^2$ which cancel the suppressing powers of a. These higher order vertices are suppressed by powers of g^2 and are the so called 'tadpole' contributions which spoil naive perturbation theory. Fortunately they are process independent, and so they can be corrected for. The mean link operator consists only of tadpoles,

$$u_0 = \left\langle \frac{1}{3}\mathrm{Tr}(U_{\mu\nu}(x)) \right\rangle^{\frac{1}{4}} \tag{2.60}$$

or it can be evaluated as

$$u_0 = \left\langle 0 \middle| \frac{1}{3}\mathbf{R}\mathrm{Tr}\, U_\mu \middle| 0 \right\rangle_{L.G.} \tag{2.61}$$

where the subscript L.G. stands for Landau Gauge which maximises the value of the mean link. The tadpole contributions can then be cancelled by dividing the link variables by the mean link value,

$$U_\mu(x) \to \frac{U_\mu(x)}{u_0} \tag{2.62}$$

in the action.

The motivation for many lattice gauge theory calculations is that they are non-perturbative. A more consistent approach would be to calculate these improvement coefficients non-perturbatively. The Alpha collaboration have implemented a program to calculate these improvement coefficients and the renormalisation constants in a mass independent renormalisation scheme [24, 25, 26] non-perturbatively. The renormalised improved operators are given by

$$\mathcal{O}_R = Z_\mathcal{O}(1 + b_\mathcal{O} a m_q)\mathcal{O}_I \tag{2.63}$$

where $\mathcal{O}$ are the improved operators V, A, T, P, S. The renormalisation constants Z_A and Z_V are calculated by imposing the continuum chiral Ward identities at finite values of the cutoff.

In order to evaluate c_{SW} and the other improvement coefficients to completely eliminate $\mathcal{O}(a)$ contributions to on-shell quantities one needs to impose some condition. The Alpha collaboration use the lattice PCAC relation

$$\left\langle \partial_\mu A^R_\mu(x)\mathcal{X} \right\rangle = 2m_R \left\langle P^R(x)\mathcal{X} \right\rangle + \mathcal{O}(a^n) \tag{2.64}$$

and tune c_{SW} and c_A such that the error is reduced from $\mathcal{O}(a)$ to $\mathcal{O}(a^2)$ for any product $\mathcal{X}$ of fields localised in a region not containing x. The operators are computed in the *Schrödinger Functional* scheme. This is formulated on a 'hyper-cylinder' $[0,T] \times S^1 \times S^1 \times S^1$ with periodic boundary conditions in the spatial directions and Dirichlet boundary conditions at the caps $t = 0, T$. The Schrödinger functional is then the partition function with sources for the gauge and fermionic sources on the temporal boundaries.

The values for c_{SW} and c_A quoted by the Alpha collaboration are for g_0 in the range $0 \leq g_0^2 \leq 1$

$$c_{SW}(g_0) = \frac{1 - 0.656g_0^2 - 0.152g_0^4 - 0.054g_0^6}{1 - 0.992g_0^2} \tag{2.65}$$

$$c_A(g_0) = -0.00756 \times g_0^2 \frac{1 - 0.748g_0^2}{1 - 0.977g_0^2} \tag{2.66}$$

2.4 The Quenched Approximation and Numerical Integration

The expectation value of some operator (equation 2.6) re-expressed with the lattice action can be written as

$$\langle \mathcal{O} \rangle = \frac{1}{\mathcal{Z}} \int [dU d\bar{\psi} d\psi] \mathcal{O} e^{-S_{LQCD}} \tag{2.67}$$

where the partition function

$$\mathcal{Z} = \int [dU d\bar{\psi} d\psi] e^{-S_{LQCD}}. \tag{2.68}$$

Defining

$$[dU] = \prod dU \tag{2.69}$$

where dU is the *Haar measure* over the gauge group G and obeys the following

$$\int [dU] = 1 \quad \text{and} \quad \int [dU] F(U) = \int [dU] F(UV) \quad \forall V \in G. \tag{2.70}$$

The fermionic terms in the action are bilinear in the fermion fields, 2.49 and 2.55

$$S_F[U, \psi, \bar{\psi}] = \sum_{xy} \bar{\psi}(y) M[U] \psi(x) \tag{2.71}$$

where $M[U]$ is the fermion matrix

$$\begin{aligned} M[U]_{xy} &= \delta_{xy}\left[1 - \frac{i}{2}c_{SW}\sigma_{\mu\nu}F_{\mu\nu}(x)\right] \\ &\quad -\kappa\sum_{\mu} U_{\mu}(x)\delta_{x,y+\mu}(\gamma_{\mu}-1) - U^{\dagger}_{\mu}(x-\mu)\delta_{x,y-\mu}(\gamma_{\mu}+1). \end{aligned} \quad (2.72)$$

The integral over the fermionic Grassmann variables is in fact Gaussian, and so the fermionic degrees of freedom can be integrated out (appendix A).

$$\int [d\bar{\psi}d\psi]e^{-S_F} = \det M[U]. \quad (2.73)$$

The action can now be re-written as an effective action

$$S_{\text{eff}}[U] = S_g[U] - \log\det M[U] = S_g[U] - \text{Tr}\log M[U] \quad (2.74)$$

The remaining integration can be carried out numerically.

The number of integration variables in

$$[dU] = \prod_{x,\alpha} dU_{x\alpha} \quad (2.75)$$

is rather large. The volume of typical lattices $V \sim \mathcal{O}(10^6)$. This requires *Monte Carlo* methods. Rather than generate *gauge configurations* $[U_n]$ randomly, it is more efficient to use the configurations that contribute most to the integral. This achieved through *importance sampling* of the gauge configurations. An *ensemble of configurations* is an infinite number of gauge configurations, with the probability of a configuration U being $P[U]$ defined on the measure dU. For the *Canonical ensemble* the probability is proportional to the Boltzmann factor;

$$P_c[U] \propto e^{-S[U]}. \quad (2.76)$$

Numerical algorithms have to generate a sample of a large number of gauge configurations $[\{U_n\}|\ n = 1, 2, \cdots, N]$ such that the sample distribution approximates the canonical ensemble. The sample average $\bar{\mathcal{O}}$ is given by

$$\bar{\mathcal{O}} \equiv \frac{1}{N}\sum_{n=1}^{N} \mathcal{O}[U_n] \approx \langle\mathcal{O}\rangle. \quad (2.77)$$

The configuration sample is generated as a sequence. This sequence is constructed by the repeated application of an algorithm. This updating is a stochastic process, and in general a large number of updates is needed to generate independent gauge configurations. In particular this updating is done by a *Markov*

process. A Markov process is a stochastic process which generates a chain of states (configurations) such that the probability of getting a state U_n from U_{n-1} depends only on U_n and U_{n-1}. i.e.

$$\mathcal{P}(U_n \leftarrow U_{n-1}|U_{n-1} \leftarrow U_{n-2}, \cdots) = \mathcal{P}(U_n \leftarrow U_{n-1}) \tag{2.78}$$

Considering again the fermion matrix (equation 2.72) one can see the order of the matrix is proportional to the volume and the internal degrees of freedom of the fermions. This results in a very large matrix, $\mathcal{O}(10^7)$, which is in principle non-local. The amount of computation in constructing the sequence of gauge configurations can be greatly reduced by avoiding the need to calculate det M for every update. The *Quenched approximation* does this by setting this determinant to a constant. A perturbative expansion in the gauge coupling of the fermion determinant generates closed quark loops. The quenched approximation has the effect of ignoring closed quark loops. The gauge fields can then be integrated independently of the fermionic fields.

2.5 The Quark Propagator

The starting point for the construction of hadronic quantities is the two point Green's function, or quark propagator. Considering equation 2.67 and integrating out the fermionic fields

$$\left\langle \psi(x)\bar{\psi}(0) \right\rangle = \frac{1}{\mathcal{Z}} \int [dU] M^{-1}(x, 0; U) e^{-S_g} \tag{2.79}$$

In the quenched approximation. The quark propagator is a gauge dependent quantity and is the inverse of the fermion matrix.

$$M_{ij}^{\alpha\beta}(x, y; U) G_{jk}^{\beta\gamma}(y, 0; U) = \delta(x, 0)\delta^{\alpha\gamma}\delta_{ik} \tag{2.80}$$

where the Greek indices label the spin components, and the Latin indices label the colour components. The fermion matrix can be inverted by solving equation 2.80. This is hard work, as it involves solving a large sparse system of linear equations, and the fermion matrix is very large. Equation 2.80 is solved for each spin-colour component on the point source. The twelve spin-colour components

of G correspond to a quark propagating from the origin to any point y. This still requires an iterative solution using linear solvers and considerable computer power.

In order to simulate light quarks (i.e. u, d, or s) on the lattice the propagators are calculated for several different quark masses in the vicinity of m_s. The results for physical quantities then have to be extrapolated to the physical quark masses. The main reason for this is that the linear equation solvers used to invert the fermion matrix equation 2.80 typically have a condition number C_n,

$$C_n = \frac{|\lambda|_{\max}}{|\lambda|_{\min}}, \tag{2.81}$$

where λ are the eigen values of the fermion matrix which is proportional the inverse of the quark mass. So the number of iterations required to invert the fermion matrix grows linearly as the quark mass decreases. This is computationally very expensive. Whilst this is the limiting factor, finite size-effects are likely to be large for small pseudoscalar meson mass, *i.e* the 'pion' would not fit in the box.

The simulation of heavy quarks (c and b) on the lattice can also present difficulties. Typical lattice spacings in simulations are of order $a^{-1} \sim 2.5 - 3$ Gev. The b quark has a mass of $m_b \sim 4.3$ GeV, and so its Compton wavelength is smaller than the lattice spacing. The lattice is not sufficiently fine to resolve the wavefunction of the b quark. One method to solve this problem and used in this thesis is to simulate at several quark masses in the vicinity of charm and extrapolate the results to the physical quark mass.

2.5.1 Symmetries of the Quark Propagator

By applying the discrete Lorentz transformations, parity (**P**), charge conjugation (**C**),time reversal (**T**) and the hermiticity (**H**) transformation to the fermion matrices, it can be seen that

$$G(x,y;U) = \mathbf{H}G^{\dagger}(y,x;U)\mathbf{H}^{-1} \tag{2.82}$$

$$G(x,y;U) = \mathbf{P}G(y^{\mathbf{P}},x^{\mathbf{P}};U^{\mathbf{P}})\mathbf{P}^{-1} \tag{2.83}$$

$$G(x,y;U) = \mathbf{C}G^T(y^{\mathbf{C}},x^{\mathbf{C}};U^{\mathbf{C}})\mathbf{C}^{-1} \quad (2.84)$$

$$G(x,y;U) = \mathbf{T}G(y^{\mathbf{T}},x^{\mathbf{T}};U^{\mathbf{T}})\mathbf{T}^{-1} \quad (2.85)$$

where

$$\begin{aligned} \mathbf{H} &= \gamma^5 \\ \mathbf{P} &= \gamma^4 \\ \mathbf{C} &= \gamma^4\gamma^2 \\ \mathbf{T} &= \gamma^4\gamma^5 \end{aligned} \quad (2.86)$$

These relations will be useful when considering the hadronic correlation functions.

2.6 Hadronic Correlation Functions

The spectrum and matrix elements can be extracted from lattice calculations by studying correlation functions of time-ordered products of operators, themselves constructed from gauge invariant products of quark and gauge fields. In general, there is no unique correspondence between particle states and operators; in order to measure the mass of a state A, all that is required is that the operators have a non-zero overlap with the state in question,

$$\langle 0 \left| \mathcal{O}_A \right| A \rangle \neq 0. \quad (2.87)$$

This can be achieved by constructing operators that have the same quantum numbers as the state. The vacuum expectation values of the correlation functions can then be computed through equations 2.67 and 2.77.

2.6.1 Meson Correlation Functions

Meson operators are bilinear in the quark fields. The simplest operator is the local product.

$$\Omega_A(x) = \bar{\psi}^a(x)\Gamma\psi^b(x) \quad (2.88)$$

where Γ is a Dirac matrix such that $\Omega_A(x)$ has the same quantum numbers as state A. This can be thought of as a meson *annihilation* operator. The corresponding meson *creation* operator is

$$\Omega_A^\dagger(x) = -\bar{\psi}^b(x)\bar{\Gamma}\psi^a(x) \tag{2.89}$$

where

$$\bar{\Gamma} = \gamma_4\Gamma^\dagger\gamma_4 \tag{2.90}$$

Two-point correlation functions are constructed from a creation operator at source and an annihilation operator at sink. Using equation 2.67 the two-point correlation function is

$$\left\langle \Omega_A(x)\Omega_A^\dagger(0)\right\rangle = \frac{1}{\mathcal{Z}}\int [dU d\bar{\psi} d\psi]\Omega_A(x)\Omega_A^\dagger(0)e^{-S_{LQCD}}. \tag{2.91}$$

Integrating out the fermion fields yields

$$\begin{aligned}&\left\langle \Omega_A(x)\Omega_A^\dagger(0)\right\rangle \\ &= \frac{1}{\mathcal{Z}}\int [dU]\mathrm{Tr}\left\{\Gamma M_a^{-1}(x,0;U)\Gamma M_b^{-1}(0,x;U)\right\}e^{-S_g}.\end{aligned} \tag{2.92}$$

The quark propagators are evaluated on each gauge configuration using equation 2.80. The hermiticity property (equation 2.82) is used to re-write the propagator

$$G^b(0,x;U) = \gamma^5 G^{b\dagger}(x,0;U)\gamma^5 \tag{2.93}$$

The expectation value is then, by equation 2.77,

$$\left\langle 0\left|\mathcal{T}\left\{\Omega_A(x)\Omega_A^\dagger(0)\right\}\right|0\right\rangle = \left\langle \mathrm{Tr}\left\{\gamma^5\Gamma G^a(x,0;U)\Gamma\gamma^5 G^{b\dagger}(x,0;U)\right\}\right\rangle_U \tag{2.94}$$

where the notation $\langle\rangle_U$ means the average over gauge configurations.

To proceed further it is usual to take the Fourier transform. The two-point correlation function is then

$$C(\vec{p},t)_{2pt} = \left\langle \sum_{\vec{x}} e^{-i\vec{p}\cdot\vec{x}}\left\{\gamma^5\Gamma G^a(x,0;U)\Gamma\gamma^5 G^{b\dagger}(x,0;U)\right\}\right\rangle_U \tag{2.95}$$

Two-point correlation functions of different operators at source and sink can be constructed in a similar fashion.

Using the lattice completeness relation,

$$\frac{1}{L^3}\sum_{n,N}\frac{|N,\vec{k}_n\rangle\langle N,\vec{k}_n|}{2E_N(\vec{k}_n)} = \mathbf{1}, \tag{2.96}$$

and inserting a complete set of states in the two-point function:

$$C(\vec{p},t)_{2pt} = \sum_{n,N,\vec{x}}\frac{e^{-i\vec{p}\cdot\vec{x}}}{2L^3E_N(\vec{k}_n)}\left\langle 0\left|\Omega_A(x)\right|N,\vec{k}_n\right\rangle\left\langle N,\vec{k}_n\left|\Omega_A^\dagger(0)\right|0\right\rangle \tag{2.97}$$

Now considering the (Minkowski) translation operator χ,

$$\mathcal{O}(\vec{x},t)) = e^{i(\hat{E}t-\vec{p}\cdot\vec{x})}\mathcal{O}(0)e^{-i(\hat{E}t-\vec{p}\cdot\vec{x})} = e^{\chi}\mathcal{O}(0)e^{-\chi}, \tag{2.98}$$

the two-point correlation function becomes

$$\begin{aligned} C(\vec{p},t)_{2pt} &= \sum_{n,N,\vec{x}}\frac{e^{-i\vec{p}\cdot\vec{x}}}{2L^3E_N(\vec{k}_n)}\left\langle 0\left|e^{\chi}\Omega_A(0)e^{-\chi}\right|N,\vec{k}_n\right\rangle\left\langle N,\vec{k}_n\left|\Omega_A^\dagger(0)\right|0\right\rangle \\ &= \sum_{n,N,\vec{x}}\frac{e^{i(\vec{k_n}-\vec{p})\cdot\vec{x}}e^{-iE_Nt}}{2L^3E_N(\vec{k}_n)}\left|\left\langle 0\left|\Omega_A(0)\right|N,\vec{k}_n\right\rangle\right|^2. \end{aligned} \tag{2.99}$$

Defining the lattice delta function as

$$\delta(\vec{r},\vec{s}) = \frac{1}{L^3}\sum_{\vec{x}}e^{i(\vec{r}-\vec{s})\cdot\vec{x}}, \tag{2.100}$$

then

$$C(\vec{p},t)_{2pt} = \sum_N\frac{e^{-iE_Nt}}{2E_N(\vec{p})}\left|\langle 0\left|\Omega_A(0)\right|N,\vec{p}\,\rangle\right|^2. \tag{2.101}$$

The correlation function is calculated in Euclidean space, so the oscillating exponential becomes exponential decay as $\tau \to it$. In the limit $t \to \infty$ the groundstate will dominate.

$$\lim_{t\to\infty}C(\vec{p},t)_{2pt} = \frac{e^{-E(\vec{p})t}}{2E(\vec{p})}\left|Z_A(p^2)\right|^2 \tag{2.102}$$

where E is the ground state energy and $Z_A(p^2)$ is the matrix element of the interpolating operator of equation 2.87

$$Z_A(p^2) = \langle 0\left|\Omega_A(0)\right|A,\vec{p}\,\rangle. \tag{2.103}$$

Figure 2.2: The Three-Point Correlation Function

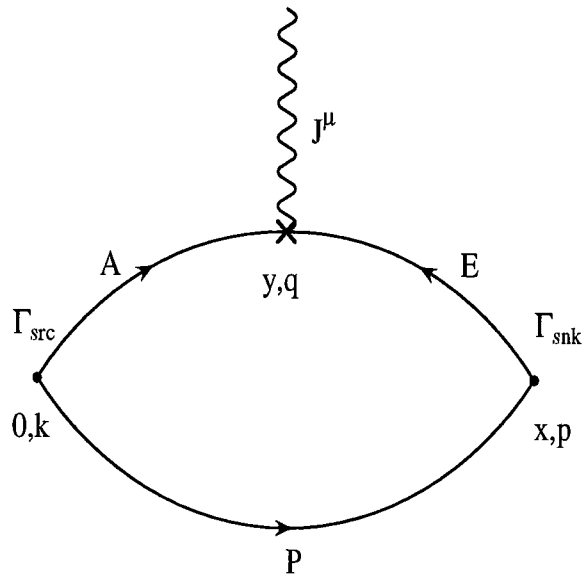

2.6.2 Three-Point Functions

A correlation function can be constructed which contains the matrix element of equation 1.54 in much the same way as for the two-point function. Define the three-point correlation function as

$$C^{\mu}_{3pt}(\vec{p},t_x,\vec{q},t_y)_{B\to A} = \sum_{\vec{x},\vec{y}} e^{-i(\vec{p}\cdot\vec{x}+\vec{q}\cdot\vec{y})} \left\langle 0 \left| \mathcal{T}\left\{\Omega_B(x)J^{\dagger\mu}(y)\Omega^{\dagger}_A(0)\right\}\right| 0\right\rangle \quad (2.104)$$

where

$$\left\langle 0 \left| \mathcal{T}\left\{\Omega_B(x)J^{\dagger\mu}(y)\Omega^{\dagger}_A(0)\right\}\right| 0\right\rangle = \frac{1}{\mathcal{Z}}\int [dUd\bar{\psi}d\psi]\Omega_B(x)J^{\dagger\mu}(y)\Omega^{\dagger}_A(0)e^{-S} \quad (2.105)$$

The creation, annihilation and current operators are defined by

$$\begin{aligned} \Omega^{\dagger}_A(0) &= -\bar{\psi}_a(0)\Gamma_{src}\psi_p(0) \\ \Omega_B(x) &= \bar{\psi}_p(x)\Gamma_{snk}\psi_e(x) \\ J^{\dagger\mu}(y) &= \bar{\psi}_e(y)\Gamma^C\psi_a(y) \end{aligned} \quad (2.106)$$

where the Latin subscripts refer to different flavours of quark. The form of Γ^C depends on the current. For a vector current $\Gamma^C = \gamma^\mu$. From equation 1.54 the

matrix element required is for a vector current between two pseudoscalar states. Thus

$$\Gamma_{src} = \Gamma_{snk} = \gamma^5 \tag{2.107}$$

and

$$\begin{aligned} V^\mu(x) &= \bar{\psi}_a(x)\gamma^\mu\psi_e(x) \\ \Rightarrow V^{\dagger\mu}(x) &= \psi_e^\dagger(x)\gamma^0\gamma^\mu\gamma^0\gamma^0\psi_a(x) \\ &= \bar{\psi}_e(x)\gamma^\mu\psi_a(x). \end{aligned} \tag{2.108}$$

Note that the current operator is flavour changing.

Carrying out the integration over the fermionic degrees of freedom the three-point correlation function can be written as

$$\begin{aligned} &C^\mu_{3pt}(\vec{p}, t_x, \vec{q}, t_y)_{B\to A} = \sum_{\vec{x},\vec{y}} e^{-i(\vec{p}\cdot\vec{x}+\vec{q}\cdot\vec{y})} \\ &\frac{1}{\mathcal{Z}}\int [dU] \mathrm{Tr}\left\{\Gamma_{src} M_P^{-1}(0,x;U)\Gamma_{snk} M_E^{-1}(x,y;U)\Gamma_C M_A^{-1}(y,0;U)\right\} e^{-S_g} \end{aligned} \tag{2.109}$$

As with the two-point correlation functions, point-to-all propagators can be calculated, again using the hermiticity property of the propagators (equation 2.82) to express the correlation function in terms of point-to-all propagators. However the propagator labelled E is an all-to-all propagator. Calculating an all-to-all propagator can be avoided by defining an *extended propagator.*

$$\begin{aligned} S(\vec{y}, 0; \vec{p}, t_x; U) &= \sum_{\vec{x}} e^{i\vec{p}\cdot\vec{x}} G^E(x,y;U)\gamma^5 G^P(0,x;U) \\ \Rightarrow S^\dagger(0,\vec{y};\vec{p},t_x;U) &= \sum_{\vec{x}} e^{-i\vec{p}\cdot\vec{x}} G^{\dagger P}(x,0;U)\gamma^5 G^{\dagger E}(y,x;U). \end{aligned} \tag{2.110}$$

The extended propagator can be calculated be considering the result of operating on the extended propagator by the fermion matrix (equation 2.72).

$$\begin{aligned} M_E(z,y;U)S^\dagger(0,y;\vec{p},t_x;U) &= \sum_{\vec{x}} e^{-i\vec{p}\cdot\vec{x}}\gamma^5 G^{P\dagger}(0,x;U)\delta(y,z) \\ &= \gamma^5 G^{P\dagger}(0,x;U)\delta(t_z,t_x)e^{-i\vec{p}\cdot\vec{x}}. \end{aligned} \tag{2.111}$$

This is equation 2.80 with a non-point source. It is only necessary to calculate the extended propagator from one time-slice of the P propagator. The labels

E, A, and P in figure 2.2 now become clear. E refers to the extended quark propagator, A to the active quark propagator, and P to the passive quark, as it takes no part in the weak decay.

If the hermiticity relation is used on *both* G^P and G^E, equation 2.109 becomes

$$C^{\mu}_{3pt}(\vec{p},t_x,\vec{q},t_y)_{B\to A} = \sum_{\vec{x},\vec{y}} e^{-i(\vec{p}\cdot\vec{x}+\vec{q}\cdot\vec{y})} \frac{1}{\mathcal{Z}}\int [dU]\mathrm{Tr}\left\{G^{P\dagger}(0,x;U)\gamma^5 G^{E\dagger}(x,y;U)\gamma^5\gamma^{\mu}G^{A}(0,y;U)\right\} e^{-S_g}. \tag{2.112}$$

substituting the expression for the extended propagator in equation 2.112

$$C^{\mu}_{3pt}(\vec{p},t_x,\vec{q},t_y) = \left\langle \sum_{\vec{y}} e^{-i\vec{q}\cdot\vec{y}}\mathrm{Tr}\left\{S^{\dagger}(0,y;\vec{p},t_x;U)\gamma^5\gamma^{\mu}G^{A}(0,y;U)\right\}\right\rangle_U . \tag{2.113}$$

Inserting a complete set of states between operators of equation 2.104 using the lattice completeness relation 2.96 the three-point function can be expressed as

$$\begin{aligned} C^{\mu}_{3pt} &= \sum_{\vec{x}\vec{y},n,m,N,M} e^{-i(\vec{p}\cdot\vec{x}+\vec{q}\cdot\vec{y})}\frac{1}{2E_N(\vec{k}_n)L^3}\frac{1}{2E_M(\vec{k}_m)L^3}\times \\ &\quad \left\langle 0\left|\Omega_B(x)\right|N,\vec{k}_n\right\rangle\left\langle N,\vec{k}_n\left|J^{\dagger\mu}(y)\right|M,\vec{k}_m\right\rangle\left\langle M,\vec{k}_m\left|\Omega^{\dagger}_A(0)\right|0\right\rangle . \end{aligned} \tag{2.114}$$

Again using the translation operator, χ, 2.98

$$\begin{aligned} \Rightarrow C^{\mu}_{3pt} &= \sum_{\vec{x}\vec{y},n,m,N,M} e^{-i\vec{p}\cdot\vec{x}-i\vec{q}\cdot\vec{y}}\frac{1}{2E_N(\vec{k}_n)L^3}\frac{1}{2E_M(\vec{k}_m)L^3}\times \\ &\quad \left\langle 0\left|e^{\chi}\Omega_B(0)e^{-\chi}\right|N,\vec{k}_n\right\rangle\left\langle N,\vec{k}_n\left|e^{\chi'}J^{\dagger\mu}(0)e^{-\chi'}\right|M,\vec{k}_m\right\rangle \\ &\quad \times\left\langle M,\vec{k}_m\left|\Omega^{\dagger}_A(0)\right|0\right\rangle \\ &= \sum_{\vec{x}\vec{y},n,m,N,M} \frac{i(\vec{k}_m-\vec{k}_n-\vec{q})\cdot\vec{y}}e^{-iE_m t_y}\frac{e^{i(\vec{k}_n-\vec{p})\cdot\vec{x}}e^{iE_N(t_y-t_x)}}{2E_N(\vec{k}_n)L^3}\frac{}{2E_M(\vec{k}_m)L^3}\times \\ &\quad \left\langle 0\left|\Omega_B(0)\right|N,\vec{k}_n\right\rangle\left\langle N,\vec{k}_n\left|J^{\dagger\mu}(0)\right|M,\vec{k}_m\right\rangle\left\langle M,\vec{k}_m\left|\Omega^{\dagger}_A(0)\right|0\right\rangle . \end{aligned} \tag{2.115}$$

The lattice delta function defined by 2.100, gives

$$\begin{aligned} C^{\mu}_{3pt} &= \sum_{N,M}\frac{e^{-iE_M t_y}}{2E_M}\frac{e^{-iE_N(t_x-t_y)}}{2E_N}\left\langle 0\left|\Omega_B(0)\right|N,\vec{p}\right\rangle\times \\ &\quad \left\langle N,\vec{p}\left|J^{\dagger\mu}(0)\right|M,\vec{p}-\vec{q}\right\rangle\left\langle M,\vec{p}-\vec{q}\left|\Omega^{\dagger}_A(0)\right|0\right\rangle . \end{aligned} \tag{2.116}$$

Again considering the correlation function in Euclidean space with the replacement $\tau \to it$. In the limit in which $t_y \to \infty$ and $(t_x - t_y) \to \infty$ only the groundstate contribution survives. i.e.

$$\begin{aligned} C^{\mu}_{3pt} &= \frac{e^{-E_A(\vec{p}-\vec{q})t_y}}{2E_A(\vec{p}-\vec{q})} Z_A(\vec{p}-\vec{q}) \frac{e^{-E_B(\vec{p})(t_x-t_y)}}{2E_B(\vec{p})} Z_B(\vec{p}) \\ &\quad \times \left\langle B,\vec{p}\left|J^{\dagger\mu}(0)\right|\bar{A},(\vec{p}-\vec{q})\right\rangle, \end{aligned} \tag{2.117}$$

where the Z's are the matrix elements of the interpolating operators by equation 2.87. Let the momentum of state A be $\vec{k}$, defining $\vec{k}$ as $\vec{k} \equiv \vec{p} - \vec{q}$. The matrix element in equation 2.117 is not the matrix element in equation 1.56 which defines the form factors, but its adjoint. For the vector current between two pseudoscalar states, the matrix element is Hermitian. i.e.

$$\begin{aligned} \left(\left\langle B,\vec{p}\left|J^{\dagger\mu}(0)\right|\bar{A},\vec{k}\right\rangle\right)^{\dagger} &= \left\langle A,\vec{k}\left|\left(J^{\dagger\mu}(0)\right)^{\dagger}\right|\bar{B},\vec{p}\right\rangle \\ &= \left\langle A,\vec{k}\left|J^{\mu}(0)\right|\bar{B},\vec{p}\right\rangle. \end{aligned} \tag{2.118}$$

2.7 Smearing

The simplest meson operator one can write down is the local product 2.88 of quark fields. It is certainly not the only operator. In general, a meson operator can be written as

$$\Omega(\vec{x},t) = \bar{\psi}(\vec{x},t) \sum_{\vec{y}} \Upsilon(\vec{x}-\vec{y})\psi(\vec{y},t) \tag{2.119}$$

This property can be used to try and improve the signal from the data by, for instance, increasing the overlap of the operator with the groundstate wavefunction by setting Υ to a function which approximates the groundstate. This is known as *smearing*. In this calculation two types of smearing were used, *Fuzzing* [27] and *Boyling* [28].

2.7.1 Fuzzing

The main source of contamination to the groundstate amplitude will come from the first excited state. By increasing the groundstate amplitude relative to the

first excited state amplitude an operator can be constructed that more efficiently singles out the groundstate. Fuzzing is a method for constructing a hadronic operator non-local in both the fermion and gauge fields. The simple picture of the meson operator is of the quark and anti-quark separated by a distance R joined by a colour flux tube.

The gluon flux tubes are constructed by fuzzing [29] each link operator by combining it with the spatial staples, that is

$$U_\mu(x) \to U_\mu^F(x) = \mathcal{P}\left\{ cU_\mu(x) + \sum_{\nu\neq\mu} U_\nu(x)U_\mu(x+\nu)U_\nu^\dagger(x+\mu) \right\}. \qquad (2.120)$$

However, $SU(3)$ is not closed under addition, so $\mathcal{P}$ projects the operator back onto $SU(3)$; A matrix $\mathcal{O}$ can be projected onto $U \in SU(3)$ by iteratively maximising $\mathbf{R}\mathrm{Tr}(\mathcal{O}U^\dagger)$ using a Cabibbo-Marinari approach. In this calculation $c = 2$ is chosen and the fuzzing repeated 5 times over the whole lattice.

Meson operators can now be constructed with one of the fermion fields fuzzed

$$\Omega_F(\vec{x}, t, R; U) = \sum_i \bar{\psi}(\vec{x} + \vec{R}_i, t)M(\vec{R}_i, \vec{x}, t, U)\Gamma\psi(\vec{x}, t) \qquad (2.121)$$

where the sum over i is the sum over the 6 spatial directions and M is the product of the fuzzed links of length R

$$M(\vec{R}_i, \vec{x}, t, U) = \prod_{n=0}^{N-1} U_i^F(x + ni) \; ; \; N = R/a. \qquad (2.122)$$

So the purely local operator at x is replaced by a spatial average of the fermion fields at distance R from x joined by the fuzzed gauge fields.

In practice, it is actually fuzzed quark propagators that are computed. Defined here is a sink fuzzed propagator

$$G_F(\vec{x}, t, R, 0; U) = \left\langle \sum_i \psi(\vec{x} + \vec{R}_i, t)M(\vec{R}_i, \vec{x}, t, U)\bar{\psi}(0,0) \right\rangle. \qquad (2.123)$$

This is computationally advantageous as once calculated, it is no more expensive to construct correlation functions with fuzzed propagators than it is with purely local ones. With a combination of purely local and fuzzed operators, it is possible to extract efficiently both the groundstate and the first excited state. The R parameter can then be tuned such that the hadronic operator has no contribution from the first excited state.

2.7.2 Boyling

The motivation for Boyling comes from the observation that for systems containing heavy quarks, the mass of the heavy quark is much greater than typical momentum scales, Λ_{QCD}, associated with light degrees of freedom. This suggests non-relativistic behaviour for the heavy quark, see section 3. In particular this implies that the gluonic degrees of freedom can be approximated by a potential. This suggests that the physical states of hadrons can be approximated by non-relativistic wavefunctions, particularly those that factorize into radial and orbital parts. Consider the overlap of the smearing function Υ with the physical wavefunction $\psi(x)$

$$C_{mn} = \int_{R^3} \psi_m^\star(\vec{x})\Upsilon_n(\vec{x},0)d^3x. \tag{2.124}$$

Choosing the smearing function to be of the non-space filling form, i.e. the Domain of the function is a subspace of x,

$$\Upsilon_n(\vec{x},0) = \sum_{r=0}^{N} r^2\phi_n(r)\sum_{i=1}^{6}\delta(\vec{x}+\vec{r}_i) \tag{2.125}$$

where the sum over i is over the 6 forward and backward spatial directions and N is typically half the lattice size. Then the overlap is

$$\begin{aligned} C_{mn} &= \int_{R^3} \psi_m^\star(\vec{x})\Upsilon_n(\vec{x},0)d^3x \\ &= \sum_{r=0}^{N} r^2\psi_m^\star(r)\phi_n(r) \\ \lim_{a\to 0} &\int_0^\infty r^2\psi_m^\star(r)\phi_n(r)dr \\ &\simeq \delta_{mn} \end{aligned} \tag{2.126}$$

By choosing ϕ_n to approximate ψ_n, approximate orthogonality can be established.

The generalisation to include colour is

$$\psi(x) \to \psi'(x) = \sum_{r=0}^{N}\left(r+\frac{1}{2}\right)^2\phi_n(x)\sum_{i=1}^{6}\left[\prod_{n=0}^{r-1}U_i(x+ni)\right]\psi(x+\vec{r}_i) \tag{2.127}$$

where again the sum over i is over the six forward and backward spatial directions. The gauge link variables U are the fuzzed links described in section 2.7.1. This choice of smearing function has two main advantages. Firstly, the form of $\phi_n(x)$

can still be freely chosen, and thus can be chosen to efficiently project out the radially excited state without the need for gauge fixing. Secondly, equation 2.127 is gauge invariant but is still relatively cheap to implement computationally as it is non-space filling.

One particular choice of ϕ is the hydrogenic wavefunctions given by

$$h_n(r) \propto e^{-\tilde{r}} L_n(\tilde{r}) \tag{2.128}$$

with

$$\tilde{r} = \frac{r}{(n+1)r_0}, \tag{2.129}$$

where r_0 is the Bohr radius and $L_n(\tilde{r})$ are the *Laguerre* polynomials

$$L_n(x) = \frac{e^x}{n!}\frac{d^n}{x^n}\left(x^n e^{-x}\right) \tag{2.130}$$

Suppose the physical wavefunction ψ is hydrogenic with Bohr radius r_ψ. The trial smearing hydrogenic wavefunctions ϕ has Bohr radius r_ϕ. Consider the overlap between the physical ground state, and the trial radially excited state.

$$\begin{aligned} c_{10} &= \int r^2 \psi_0(r)\phi_1(r)dr \\ &\propto \int r^2 \left(1 - \frac{r}{2r_\phi}\right) e^{-\frac{r}{r_\psi}} e^{-\frac{r}{2r_\phi}} dr \\ &= \int r^2 e^{-\frac{r}{\rho}} dr - \frac{1}{2r_\phi}\int r^3 e^{-\frac{r}{\rho}} dr \\ &= \rho^3\left[\Gamma(3) - \frac{\rho}{2r_\phi}\Gamma(4)\right] \\ &\simeq 2\rho^3 \frac{\Delta_r}{r_\phi} \end{aligned} \tag{2.131}$$

where $\rho = \frac{2r_\phi r_\psi}{r_\phi + 2r_\psi}$ and the last step is true for a small $\Delta_r = r_\phi - r_\psi$. So the overlap between the physical ground state and the trial first excited state is proportional to the difference in the Bohr radii. Also note that

$$\begin{aligned} r_\phi > r_\psi &\Rightarrow c_{mn} > 0 \\ r_\phi < r_\psi &\Rightarrow c_{mn} < 0. \end{aligned} \tag{2.132}$$

The change in sign can be used to tune the Bohr radius of the smearing function to orthogonalise the trial excited state to the groundstate. The physical wavefunctions are not hydrogenic in form. However for reasonable physical ground

states one should still see the same behaviour in the overlap when going from small to large Bohr radius. In general, because of the non-hydrogenic form of the wave functions one choice of the Bohr radius will not simultaneously minimise c_{10} and c_{01}. An optimal radius for ground and excited states is chosen.

2.8 Statistical Analysis

The expectation value of some operator can be estimated by an average over an ensemble of gauge configurations (equation 2.77). Consider an ensemble of correlation functions $\{C_i(t)\ , i = 1, \cdots, N\}$. The mean value is given by

$$\bar{C}(t) = \frac{1}{N}\sum_{i=1}^{N} C_i(t) \tag{2.133}$$

where N is the number of configurations. The variance of the sample is given by

$$\sigma_s^2 = \frac{1}{N-1}\sum_{i=1}^{N}\left[C_i(t) - \bar{C}(t)\right]^2 \tag{2.134}$$

and the variance of the mean is σ_s^2/N.

The large t behaviour of the correlation function can be parameterised by some functional form in terms of a set of parameters $\{\zeta_n\}$ (e.g. equations 2.102 and 2.117). However, in general it is not possible to measure the $\{\zeta_n\}$ on each configuration and so calculate the mean and variance as above. The statistical uncertainties in these fitted parameters are estimated using a resampling technique known as bootstrap [30].

In the bootstrap sampling technique, N_B sub-ensembles of N configurations (including repetitions) are randomly selected from the set of N configurations. The mean of each sub-ensemble is then

$$\bar{C}^B(t) = \frac{1}{N}\sum_{j=1}^{N} C_j^B(t) \tag{2.135}$$

The parameters $\{\zeta_n\}$ can then be fitted to each sub-ensemble. The mean value of ζ_n and its variance can then be estimated.

$$\bar{\zeta}_n^B = \frac{1}{N_B}\sum_{k=1}^{N_B} \zeta_{kn}^B \tag{2.136}$$

and the variance

$$\left(\sigma^B(\zeta_n)\right)^2 = \frac{1}{N_B - 1}\sum_{k=1}^{N_B}\left[\zeta_{kn}^B - \bar{\zeta}_n^B\right]^2. \tag{2.137}$$

The bootstrap sampling method has the advantage of not assuming any form for the distribution of the correlation functions, and so it is more useful to define 68% confidence levels rather than $\sigma^B(\zeta_n)$. The lower interval bound ζ_n^L is defined by 16% probability of

$$\zeta_{kn}^B < \zeta_n^L \tag{2.138}$$

and similarly for the upper bound.

2.8.1 Fitting method

Consider the data set $\bar{y}_i = \{\bar{C}(t_i), C^B(t_i)\}$. This data set is fitted to some functional form $y(t_i, \{\zeta_n\})$. Defining the χ^2 as

$$\chi^2 = \sum_i \frac{1}{\sigma_i^2}\left[\bar{y}_i - y(t_i, \{\zeta_n\})\right]^2. \tag{2.139}$$

The parameters $\{\zeta_n\}$ are then chosen to minimise the χ^2, that is maximise the probability of the fit. This is known as a least χ^2 squares fit. In general, the data on different time-slices are highly correlated. Define χ^2 for data on different time-slices,

$$\chi^2 = \sum_{ij}\left[\bar{y}_i - y(t_i, \{\zeta_n\})\right]\Omega_{ij}^{-1}\left[\bar{y}_j - y(t_j, \{\zeta_n\})\right] \tag{2.140}$$

where Ω_{ij} is the covariance matrix

$$\Omega_{ij} = \frac{1}{N(N-1)}\sum_{m=1}^{N}(y_i^m - \bar{y}_i)(y_j^m - \bar{y}_j). \tag{2.141}$$

The covariance matrix reduces to the variance for the diagonal elements. In practice, the *correlation* matrix, Φ, defined by

$$\Phi_{ij} = \frac{\Omega_{ij}}{\sigma_i \sigma_j} \tag{2.142}$$

is used as it is found to be more stable. The mean values, and the covariance matrix for each parameter are evaluated using equations 2.136 and 2.137. This

is a correlated fit. The minimisation of χ^2 is implemented using the *Marquardt-Levenberg* algorithm [31].

For correlated fits $\chi^2/dof \sim 1$ (degree of freedom) signifies a very good fit. Another useful quantity is the Q value. It is the probability that the value of χ^2 the minimisation returns exceeds a particular χ^2 by chance. The Q value is determined by the incomplete gamma function,

$$Q(a,x) = \frac{\Gamma(a,x)}{\Gamma(a)} \tag{2.143}$$

In this case the Q value evaluated for $a = N/2$ and $x = \chi^2/2$ where N is the number of degrees of freedom. It assumes that the data is normally distributed.If this is not the case then Q values down to $\mathcal{O}(10^{-3})$ do not necessarily signify a bad fit.

Chapter 3

Heavy Quark Symmetry

Consider a hadron containing a heavy quark. The typical momentum transfer in QCD is $\mathcal{O}(\Lambda_{\rm QCD})$. For a sufficiently heavy quark, $M_Q \gg \Lambda_{\rm QCD}$, the non-perturbative light degrees of freedom, the so called 'brown muck' of glue and light quarks become independent of the heavy quark mass. In the static limit, $M_Q \to \infty$, the heavy quark defines the centre of mass of the hadron. In this frame of reference the heavy quark acts as a static source of colour at the origin. The spin of the heavy quark also decouples from the light degrees of freedom. This $SU(2N_f)$ symmetry (N_f is the number of heavy flavours) can be used to construct an effective theory [32, 33, 34, 35].

3.1 Heavy Quark Effective Theory

Consider a hadron containing a heavy quark such that the light degrees of freedom carry much less four-momentum than the mass of the heavy quark. The heavy quark is nearly on-shell, and so the four-momentum is,

$$P^\mu = m_Q v^\mu + r^\mu, \tag{3.1}$$

where r^μ is small compared to m_Q and v^μ is the four-velocity. The heavy quark propagator $G(P)$ is

$$G(P) = \frac{i(\not{P}_Q + m_Q)}{P_Q^2 - m_Q^2}. \tag{3.2}$$

In the heavy quark limit, the quark propagator becomes

$$G(P) = \frac{i(1+\not{v})}{2v\cdot r} + \mathcal{O}(\frac{r}{m_Q}), \tag{3.3}$$

and

$$\mathcal{P}_+ = \frac{1}{2}(1+\not{v}), \tag{3.4}$$

where P_+ is the positive energy projection operator. Now consider a Dirac matrix between two projection operators,

$$\begin{aligned} \mathcal{P}_+\gamma^\mu\mathcal{P}_+ &= \frac{1}{2}\mathcal{P}_+(\gamma^\mu + \gamma^\mu\not{v}) \\ &= \frac{1}{2}\mathcal{P}_+(2v^\mu + (1-\not{v})\gamma^\mu). \end{aligned} \tag{3.5}$$

However,

$$\mathcal{P}_- = \frac{1}{2}(1-\not{v}), \tag{3.6}$$

and

$$\mathcal{P}_+\mathcal{P}_- = 0. \tag{3.7}$$

This implies

$$\begin{aligned} \mathcal{P}_+\gamma^\mu\mathcal{P}_+ &= \mathcal{P}_+v^\mu \\ &= \mathcal{P}_+\mathcal{P}_+v^\mu \\ &= \mathcal{P}_+v^\mu\mathcal{P}_+. \end{aligned} \tag{3.8}$$

The effective theory can now be constructed from these elements.

Consider the Lagrangian for heavy quarks,

$$\mathcal{L} = \bar{Q}(i\not{D} - m_Q)Q. \tag{3.9}$$

Using an on-shell approximation for the fermion field,

$$Q = e^{-im_Qv\cdot x}h_v, \tag{3.10}$$

substituting this into the Lagrangian gives

$$\mathcal{L} = \bar{h}_v\left\{m_Q(\not{v}-1) + i\not{D}\right\}h_v. \tag{3.11}$$

Now

$$\mathcal{P}_+h_v = \tfrac{1}{2}(\not{v}+1)h_v = h_v \tag{3.12}$$

as

$$\not{v} h_v = h_v, \tag{3.13}$$

by the Dirac equation. The heavy quark Lagrangian is then

$$\mathcal{L} = \bar{h}_v i \not{D} h_v. \tag{3.14}$$

Again using equation 3.12 and 3.8 the heavy quark Lagrangian becomes

$$\begin{aligned} \mathcal{L} &= \bar{h}_v \mathcal{P}_+ i \not{D} \mathcal{P}_+ h_v \\ &= \bar{h}_v i v \cdot D h_v. \end{aligned} \tag{3.15}$$

There is no spin, or mass dependence in this Lagrangian and so there is an $SU(2N_f)$ symmetry.

In the case where $m_Q \not\to \infty$ HQET can be expressed as a power series in $1/m_Q$.

$$\mathcal{L}_{\text{HQET}} = \mathcal{L}_0 + \mathcal{L}_1. \tag{3.16}$$

To $\mathcal{O}(1/m_Q)$ there are two dimension 5 operators which can be added, a heavy quark kinetic term and a colour magnetic moment term,

$$\mathcal{L}_1 = \frac{1}{2m_Q} \bar{h}_v (iD)^2 h_v + \frac{C(m_Q, \alpha_s)}{4m_Q} \bar{h}_v i\sigma^{\mu\nu} \left[D^\mu, D^\nu\right] h_v \tag{3.17}$$

where the coefficient C has to be calculated perturbatively.

3.2 Matrix Elements

It is convenient in HQET to work with meson states that are normalised to be independent of their mass. That is for a state Ω

$$|\Omega(v)\rangle = \frac{1}{\sqrt{m_\Omega}} |\Omega(p)\rangle. \tag{3.18}$$

The conventional, relativistic normalisation,

$$\langle \Omega(p') | \Omega(p) \rangle = 2E\delta^3(\vec{p} - \vec{p}'), \tag{3.19}$$

becomes

$$\langle \Omega(v') | \Omega(v) \rangle = 2\frac{E}{m_\Omega} \delta^3(\vec{p} - \vec{p}'). \tag{3.20}$$

The advantage of this is that the mass independent normalised states can be thought of as eigenstates of the effective Lagrangian 3.15.

In the effective theory, any current operator can be expanded in terms of local operators of the effective theory [36, 37]

$$J^\mu = \bar{q}\gamma^\mu Q = C_1(\frac{m_Q}{\mu})\bar{q}\gamma^\mu h_v + C_2(\frac{m_Q}{\mu})\bar{q}v^\mu h_v + \mathcal{O}(\frac{1}{m_Q}) \tag{3.21}$$

where the expansion of the axial current can be obtained by replacing $\bar{q}$ with $-\bar{q}\gamma^5$. The coefficients $C(\frac{m_Q}{\mu})$ contain all the short distance physics and so are perturbative quantities at leading order in renormalisation group improved perturbation theory [38],

$$\begin{aligned} C_1(\frac{m_Q}{\mu}) &= \left(\frac{\alpha_s(\mu)}{\alpha_s(m_Q)}\right)^{2/\beta_0} \\ C_2(\frac{m_Q}{\mu}) &= 0 \end{aligned} \tag{3.22}$$

where β_0 is the one loop beta function,

$$\beta_0 = 11 - 2/3N_f. \tag{3.23}$$

The matrix element and form factors from equation 1.56 can now be written as [39]

$$\sqrt{m_B}\langle\pi(k)|\bar{\psi}_l\gamma^\mu\psi_H|B(v)\rangle = f_+(q^2)\left[m_B v + k - \Delta_{m^2} q\right]^\mu + f_0(q^2)\Delta_{m^2}q^\mu \tag{3.24}$$

where Δ_{m^2} is defined in equation 1.57.

In HQET it is more natural to work with the four velocity of the heavy meson. Defining a new kinematic variable related to q^2 by,

$$v\cdot k = \frac{m_B^2 + m_\pi^2 - q^2}{2m_B}. \tag{3.25}$$

The matrix element can now be parameterised by form factors which are a function of this new kinematic variable.

$$\langle\pi(k)|\bar{\psi}_l\gamma^\mu\psi_H|B(v)\rangle = 2[f_1(v\cdot k)v^\mu + f_2(v\cdot k)\hat{k}^\mu], \tag{3.26}$$

where

$$\hat{k}^\mu = \frac{k^\mu}{v\cdot k}. \tag{3.27}$$

From equation 3.26 and equation 3.24 the relationship between the form factors can be found. Equating terms proportional to v^μ,

$$2f_1(v\cdot k) = f_+(q^2)(1-\Delta_{m^2})\sqrt{m_B} + f_0(q^2)\sqrt{m_B}, \tag{3.28}$$

and equating terms proportional to $\hat{k}^\mu$,

$$2f_2(v\cdot k) = \frac{f_+(q^2)}{\sqrt{m_B}}(1+\Delta_{m^2})v\cdot k - \frac{f_0(q^2)}{\sqrt{m_B}}\Delta_{m^2}v\cdot k \tag{3.29}$$

Using the expressions for Δ_{m^2} and $v\cdot k$.

$$\begin{aligned} f_+(q^2) &= \sqrt{m_B}\left\{\frac{f_1(v\cdot k)}{m_B} + \frac{f_2(v\cdot k)}{v\cdot k}\right\} \\ f_0(q^2) &= \frac{2}{\sqrt{m_B}}\frac{m_B^2}{m_B^2-m_\pi^2}\Bigg\{[f_1(v\cdot k)+f_2(v\cdot k)] \\ &\quad -\frac{v\cdot k}{m_B}\left[f_1(v\cdot k)+\hat{k}^2 f_2(v\cdot k)\right]\Bigg\}. \end{aligned} \tag{3.30}$$

In the heavy quark limit ($m_b \to \infty$) the functions $f_1(v\cdot k)$ and $f_2(v\cdot k)$ become independent of m_b, apart from logarithmic matching dependence given by equation 3.22. In this limit equation 3.30 implies the scaling relations [40]

$$f_+ \sim \sqrt{m_B} \quad \text{and} \quad f_0 \sim 1/\sqrt{m_B}, \tag{3.31}$$

assuming $v\cdot k$ does not scale with m_B.

3.2.1 Pseudoscalar Decay Constant

A similar argument to the one employed above can be used to obtain the scaling of the pseudoscalar decay constant. Re-writing equation 1.61 with mass independent normalisation,

$$\begin{aligned} \sqrt{m_B}\langle 0|A^\mu|B(\vec{v})\rangle &= m_B v^\mu f_B \\ \Rightarrow \langle 0|A^\mu|B(\vec{v})\rangle &= v^\mu\sqrt{m_B}f_B \end{aligned} \tag{3.32}$$

In the case of the form factors, new form factors were constructed, that were functions of a more 'natural' variable, $v\cdot k$. However, f_B is a constant, so this

is not necessary. In the limit in which $m_b \to \infty$, the quantity $\sqrt{m_B} f_B$ becomes independent of the heavy quark mass. This implies the scaling relation [41]

$$f_B \sim 1/\sqrt{m_B}. \tag{3.33}$$

In the effective theory, mesons containing a heavy quark can be represented by covariant tensor wavefunctions [36, 42], determined by the Lorentz transformations and HQS. The ground state pseudoscalar and vector meson states can be written as

$$\mathcal{B}(v) = \frac{\not{v}+1}{2}\begin{cases} -\gamma^5; \mathrm{Ps} \\ \not{\epsilon}; \mathrm{V} \end{cases} \tag{3.34}$$

So the matrix element for the pseudoscalar decay constant can be written as [43],

$$\left\langle 0\left|\bar{\psi}_l \gamma^5 \gamma^\mu h_v\right| B(\vec{v})\right\rangle = \frac{F(\mu)}{2}\mathrm{Tr}\{\gamma^5\gamma^\mu \mathcal{B}(\vec{v})\}, \tag{3.35}$$

where the low energy parameter $F(\mu)$ is defined as

$$C_1(\mu)F(\mu) = f_B\sqrt{m_B}. \tag{3.36}$$

Again $C_1(\mu)$ is defined in equation 3.22.

3.3 HQET In The Soft Pion Limit

One of the major successes of HQET is in deriving relations between various matrix elements. Relevant to this thesis are the soft pion relations [44, 39] between $f_0(q^2)$ at maximum momentum transfer and the ratio of the heavy and light pseudoscalar decay constants f_B/f_π.

Consider the weak matrix element 3.24, writing the current, and the interpolating operators of equation 2.87 in terms of the heavy quark velocity field h_v of equation 3.10,

$$\langle \pi(k)|\bar{\psi}_l \gamma^\mu h_v|B(v)\rangle \sim -\langle 0|\bar{\psi}'_l \gamma^5 \psi_l \bar{\psi}_l \gamma^\mu h_v \bar{h}_v \gamma^5 \psi'_l|0\rangle. \tag{3.37}$$

This can be evaluated using the *Wick Contraction* of time ordered products,

$$\langle \pi(k)|\bar{\psi}_l \gamma^\mu h_v|B(v)\rangle \sim \mathrm{Tr}\Big\{G_{l'}\gamma^5 G_l \gamma^\mu G_H \gamma^5\Big\}. \tag{3.38}$$

From equation 3.3 the heavy quark propagator can be written, up to some overall constant as

$$G_H = \frac{\not{v}+1}{2}. \tag{3.39}$$

Again the matrix element can be written as the trace over such wavefunctions, that is at leading order in HQET

$$\langle \pi(k)|\bar{\psi}_l \Gamma h_v|B(v)\rangle = -\mathrm{Tr}\Big\{\Upsilon(v\cdot k)\Gamma \mathcal{B}(v)\Big\}. \tag{3.40}$$

The matrix $\Upsilon(v\cdot k)$ must transform like a pseudoscalar, and contains information about the light quark propagators. The most general decomposition is

$$\Upsilon(v\cdot k) = \gamma^5\Big[A(v\cdot k,\mu) + \hat{\not{k}} B(v\cdot k,\mu)\Big]. \tag{3.41}$$

These universal functions depend on the kinematic variable $v\cdot k$ and the scale μ at which the HQET operators are renormalised, but not on the heavy quark mass. These functions A and B are the equivalent of the Isgur-Wise function of heavy to heavy transitions.

Evaluating the traces and comparing equations 3.26 and 3.40 it can be seen that

$$\begin{aligned} f_1(v\cdot k) &= C_1(\mu)A(v\cdot k,\mu) = \hat{A}(v\cdot k) \\ f_2(v\cdot k) &= C_1(\mu)B(v\cdot k,\mu) = \hat{B}(v\cdot k), \end{aligned} \tag{3.42}$$

where the $C_1(\mu)$ coefficient is given by 3.22.

Now consider the form factors in equation 3.30, at leading order in HQET (i.e. no $1/m_b$ corrections)

$$\begin{aligned} f_+(q^2) &= \frac{\sqrt{m_B}}{v\cdot k}\hat{B}(v\cdot k) \\ f_0(q^2) &= \frac{2}{\sqrt{m_B}}\Big(\hat{A}(v\cdot k) + \hat{B}(v\cdot k)\Big). \end{aligned} \tag{3.43}$$

3.3.1 Soft Pion Relations In The Chiral Limit

The PCAC relation [45], relates the divergence of the axial current to the pion field,

$$\partial^\mu A_\mu(x) = f_\pi m_\pi^2 \pi^+(x), \tag{3.44}$$

where $\pi^+(x)$ is the pion field. The LSZ reduction formula can be be used to express the matrix element of a local operator $\mathcal{O}(0)$ as,

$$\Big\langle \pi(\vec{k})\Big|\mathcal{O}(0)\Big|B(\vec{v})\Big\rangle = i\int d^4x e^{ik\cdot x}(m_\pi^2 - k^2)\Big\langle 0\Big|\mathcal{T}\Big(\pi^+(x)\mathcal{O}(0)\Big)\Big|B(\vec{v})\Big\rangle. \quad (3.45)$$

The PCAC relation 3.44 can be used to substitute for the pion field.

$$\Big\langle \pi(\vec{k})\Big|\mathcal{O}(0)\Big|B(\vec{v})\Big\rangle = i\int d^4x e^{ik\cdot x}\frac{(m_\pi^2 - k^2)}{f_\pi m_\pi^2}\Big\langle 0\Big|\mathcal{T}\Big(\partial^\mu A_\mu(x)\mathcal{O}(0)\Big)\Big|B(\vec{v})\Big\rangle. \quad (3.46)$$

The derivative can be extracted from the time ordered product using the following relation,

$$\begin{aligned}\partial^\mu\Big\langle\alpha\Big|\mathcal{T}\Big\{A^\mu(x)\mathcal{O}(0)\Big\}\Big|\beta\Big\rangle &= \Big\langle\alpha\Big|\mathcal{T}\Big\{\partial^\mu A^\mu(x)\mathcal{O}(0)\Big\}\Big|\beta\Big\rangle \\ &\quad +\delta(x_0-0)\Big\langle\alpha\Big|\Big[A^0(x),\mathcal{O}(0)\Big]\Big|\beta\Big\rangle. \quad (3.47)\end{aligned}$$

Integrating by parts gives,

$$\begin{aligned}\Big\langle \pi(\vec{k})\Big|\mathcal{O}(0)\Big|B(\vec{v})\Big\rangle &= \frac{(m_\pi^2 - k^2)}{f_\pi m_\pi^2}\Big\{i\int d^4x e^{ik\cdot x}k^\mu\Big\langle 0\Big|\mathcal{T}\Big(A_\mu(x)\mathcal{O}(0)\Big)\Big|B(\vec{v})\Big\rangle \\ &\quad -i\Big\langle 0\Big|\Big[Q_5,\mathcal{O}(0)\Big]\Big|B(\vec{v})\Big\rangle\Big\}, \quad (3.48)\end{aligned}$$

where Q^5 denotes the axial charge,

$$Q^5 = \int d^3x d^\dagger\gamma^5 u. \quad (3.49)$$

Performing the Wick contraction, the operator $\mathcal{O}$ becomes,

$$\Big\langle 0\Big|\Big[Q^5,\mathcal{O}(0)\Big]\Big|B(\vec{v})\Big\rangle = \Big\langle 0\Big|\mathcal{O}'(0)\Big|B(\vec{v})\Big\rangle \quad (3.50)$$

where $\mathcal{O}'(0)$ is obtained by replacing $\bar{u}$ with $\bar{d}(-\gamma^5)$.

In the limit where $k^\mu \to 0$, assuming the matrix element does not vary much between its on-shell value and its value as the momentum vanishes, the first term in equation 3.48 is saturated with states degenerate with the ground state. In the case of $B \to \pi$ transitions, to leading order in HQET this state is the$B^\star$ meson. In this limit, equation 3.48 becomes

$$\begin{aligned}&\Big\langle \pi(\vec{k})\Big|\mathcal{O}(0)\Big|B(\vec{v})\Big\rangle = \\ &\frac{1}{f_\pi}\Big\{ -i\langle 0|\mathcal{O}'(0)|B(\vec{v})\rangle + \lim_{k\to 0}\int d^4x e^{ik\cdot x}\Big\langle 0\Big|\mathcal{T}\Big(k\cdot A(x)\mathcal{O}(0)\Big)\Big|B(\vec{v})\Big\rangle\Big\}. \quad (3.51)\end{aligned}$$

The matrix element of the first term on the right hand side of equation 3.51 is given by equation 3.35. The second term in equation 3.51 requires the coupling of two heavy mesons to the axial current. Figure 3.1 shows the diagram $B \to B^{\star}\pi$. The black boxes show the matrix elements, and the circled cross is the $BB^{\star}\pi$ coupling, g [44]. Defining the matrix element for such a coupling as,

$$\Big\langle B'(v,k)\Big|k\cdot A\Big|B(v,0)\Big\rangle = g(v\cdot k)\mathrm{Tr}\Big\{\gamma^5 \hat{\not{k}}\bar{\mathcal{B}}'(v)\mathcal{B}(v)\Big\}, \tag{3.52}$$

where

$$\lim_{k\to 0} g(v\cdot k) = g(0) \equiv g. \tag{3.53}$$

Inserting a complete set of states, the second term in equation 3.51 can be written,

$$\sum_{B'}\Big\langle 0\Big|\bar{\psi}_l\Gamma h_v\Big|B'(v)\Big\rangle\frac{i}{2v\cdot(-k)}\Big\langle B'(v)\Big|k\cdot A\Big|B(v)\Big\rangle = \frac{F(\mu)g(v\cdot k)}{4v\cdot k}\sum_{B'}\mathrm{Tr}\Big\{\Gamma\mathcal{B}'(v)\Big\}\mathrm{Tr}\Big\{\gamma^5\hat{\not{k}}\bar{\mathcal{B}}'(v)\mathcal{B}(v)\Big\}. \tag{3.54}$$

The product of two traces can be combined into one trace by the following identity,

$$\sum_{B'=\mathrm{Ps,V}}\mathrm{Tr}\Big\{X\mathcal{B}'(v)\Big\}\mathrm{Tr}\Big\{\gamma^5\hat{\not{k}}\bar{\mathcal{B}}'(v)\mathcal{B}(v)\Big\} = -2\mathrm{Tr}\Big\{\gamma^5(\not{k}-v\cdot k)X\mathcal{B}(v)\Big\}, \tag{3.55}$$

which is valid for any Dirac matrix X, with summation over polarisations if B' is a vector.

Figure 3.1: Feynman diagram for the coupling $B \to B^{\star}\pi$.

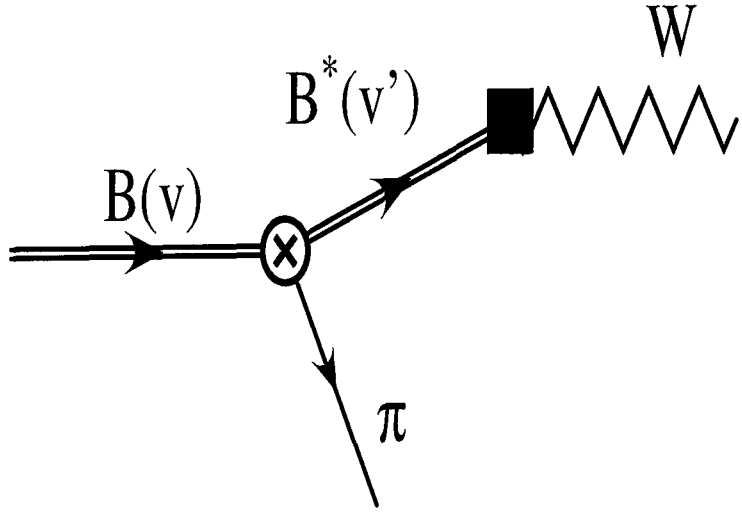

Combining this identity with equations 3.40, 3.51 and 3.54,

$$\lim_{k\to 0}\mathrm{Tr}\Big\{\gamma^5\Big[A(v\cdot k,\mu)+\hat{\not{k}}B(v\cdot k,\mu)\Big]\Gamma\mathcal{B}(v)\Big\}=$$
$$\frac{F(\mu)}{2f_\pi}\Bigg[\mathrm{Tr}\Big\{\gamma^5\Gamma\mathcal{B}(v)\Big\}+\lim_{k\to 0}g(v\cdot k)\mathrm{Tr}\Big\{\gamma^5(\hat{\not{k}}-1)\Gamma\mathcal{B}(v)\Big\}\Bigg]. \qquad (3.56)$$

From this values for A and B can be read off in the soft pion limit,

$$A(0,\mu)=\frac{F(\mu)}{2f_\pi}(1-g),\qquad B(0,\mu)=\frac{F(\mu)}{2f_\pi}g. \qquad (3.57)$$

Including the logarithmic matching factor, equation 3.22,

$$\hat{A}(0)=\frac{\hat{F}}{2f_\pi}(1-g),\qquad \hat{B}(0)=\frac{\hat{F}}{2f_\pi}g. \qquad (3.58)$$

In the soft pion limit, in which the mass of the pion also vanishes, q^2 is simply the mass of the heavy meson squared, q^2_{max}. Substituting for $\hat{A}$ and $\hat{B}$ in equation 3.43, in the soft pion limit, to leading order in HQET,

$$\begin{aligned}\lim_{k\to 0}f_+(q^2) &= \frac{m_B}{2(v\cdot k)}\frac{f_B}{f_\pi}g_{BB^*\pi}\\ f_0(q^2_{\mathrm{max}}) &= \frac{f_B}{f_\pi}.\end{aligned} \qquad (3.59)$$

These relations still hold at sub-leading order in HQET [39].

3.4 Vector Decay Constant

The vector decay constant 1.62 can also be parameterised in HQET [46]. In particular the ratio of the matrix elements can be considered. In this case it is necessary to compute the matching coefficients to next-to-leading order in perturbation theory [38] as they are identical at leading order. The matrix elements for the decay constants, to leading order in HQET are

$$\Big\langle 0\Big|\bar{\psi}_l\Gamma\psi_Q\Big|B(v)\Big\rangle=\frac{F(\mu)}{2}\mathrm{Tr}\{\Gamma\mathcal{B}(v)\} \qquad (3.60)$$

as before. The matching can be written as

$$\left[C_1(\mu)+\frac{(1+4d_m)}{4}C_2(\mu)\right]F(\mu)=f_M\sqrt{M_M} \qquad (3.61)$$

where $d_P = 3$ and $d_V = -1$. However, at NLO, C_2 is non-zero,

$$\begin{aligned} C_1(\mu) &= \left(\frac{\alpha_s(\mu)}{\alpha_s(m_Q)}\right)^{\frac{2}{\beta_0}} \left\{1 + \mathcal{F}(\alpha_s, \beta_0) - \frac{4}{3}\frac{\alpha_s(m_Q)}{\pi}\right\} \\ C_2(\mu) &= \left(\frac{\alpha_s(\mu)}{\alpha_s(m_Q)}\right)^{\frac{2}{\beta_0}} \frac{2}{3}\frac{\alpha_s(m_Q)}{\pi} \end{aligned} \tag{3.62}$$

where $\mathcal{F}$ is some function of the coupling and beta functions. Thus, for the ratio of the matrix elements, the matching can be written as,

$$\begin{aligned} \frac{C_1 + C_2}{C_1} &= \frac{1 + \mathcal{F}(\alpha_s, \beta_0) - \frac{2}{3}\frac{\alpha_s(m_Q)}{\pi}}{1 + \mathcal{F}(\alpha_s, \beta_0) - \frac{4}{3}\frac{\alpha_s(m_Q)}{\pi}} \\ &= \frac{[1 + \mathcal{F}(\alpha_s, \beta_0)]\left[1 - \frac{2}{3}\frac{\alpha_s(m_Q)}{\pi} + \cdots\right]}{[1 + \mathcal{F}(\alpha_s, \beta_0)]\left[1 - \frac{4}{3}\frac{\alpha_s(m_Q)}{\pi} + \cdots\right]} \\ &= 1 + \frac{2}{3}\frac{\alpha_s(m_Q)}{\pi} + \cdots \end{aligned} \tag{3.63}$$

Defining the quantity U in term of the ratio of the pseudoscalar and vector matrix elements

$$U(M) = \frac{\langle 0 | A^\mu | P(v) \rangle}{\langle 0 | V^\mu | V(\epsilon, v) \rangle} = \frac{f_V f_P}{M}\left\{1 + \frac{2}{3}\frac{\alpha_s(m_Q)}{\pi} + \mathcal{O}(\frac{1}{m_Q})\right\} \tag{3.64}$$

where M is the spin averaged mass

$$M = \frac{3M_V + M_P}{4}. \tag{3.65}$$

Chapter 4

Results for D mesons

4.1 Simulation Details

The simulation was performed using 216 gauge configurations on a $24^3 \times 48$ lattice at $\beta = 6.2$. The gauge configurations were generated by the UKQCD Collaboration using the standard Wilson gauge action on the T3D at EPCC at the University of Edinburgh using a combination of the over-relaxed algorithm [47, 48] and the Cabibbo-Marinari algorithm [49] with periodic boundary conditions.

Table 4.1: List of Propagators used in simulation. Source refers to smearing type. L=local, F=Fuzzed, and B=Boyled. a is the lattice spacing.

propagator	κ's	source
light	0.1346, 0.1351, 0.1353	L, F($r = 8a$)
heavy	0.1200, 0.1233, 0.1266 0.1299	B ($R_0 = 3.0a$)
extended $t_x = 28$	0.1200, 0.1233, 0.1266, 0.1299	B $\vec{p} = 0$, $\kappa_l = 0.1346$ $\vec{p} = 1$, $\kappa_l = 0.1346$ $\vec{p} = 0$, $\kappa_l = 0.1351$ $\vec{p} = 1$, $\kappa_; = 0.1351$

Three light propagators were generated by the UKQCD collaboration on each configuration using the non-perturbatively improved Sheikholeslami-Wohlert ac-

Table 4.2: Momentum channels for three-point function $\vec{p} = 0$ in lattice units of $12/a\pi$.

chan	$\vec{q}$	chan	$\vec{q}$	chan	$\vec{q}$	$\lvert\vec{q}\rvert$
1	(0, 0, 0)					0
2	(-1, 0, 0)	3	(0,-1, 0)	4	(0, 0,-1)	$\sqrt{1}$
5	(-1,-1, 0)	6	(-1, 0,-1)	7	(0,-1,-1)	$\sqrt{2}$
8	(-1, 1, 0)	9	(1, 0,-1)	10	(0,-1, 1)	
11	(-1,-1,-1)	12	(1,-1,-1)	13	(1,-1, 1)	$\sqrt{3}$
14	(-1,-1, 1)					
15	(-2, 0, 0)	16	(0,-2, 0)	17	(0, 0,-2)	$\sqrt{4}$

Table 4.3: Momentum channels for three-point function $\vec{p} = (1,0,0)$ in lattice units of $12/a\pi$

chan	$\vec{q}$	$\vec{k}$	chan	$\vec{q}$	$\vec{k}$	$\lvert\vec{q}\rvert$	$\lvert\vec{k}\rvert$
1	(-1, 0, 0)	(0, 0, 0)				$\sqrt{1}$	0
2	(0, 0, 0)	(1, 0, 0)				0	$\sqrt{1}$
3	(-2, 0, 0)	(-1, 0, 0)				$\sqrt{4}$	$\sqrt{1}$
4	(-1, 1, 0)	(0, 1, 0)	5	(-1,-1, 0)	(0,-1, 0)	$\sqrt{2}$	$\sqrt{1}$
6	(-1, 0, 1)	(0, 0, 1)	7	(-1, 0,-1)	(0, 0,-1)		
8	(0, 1, 0)	(1, 1, 0)	9	(0, 0, 1)	(1, 0, 1)	$\sqrt{1}$	$\sqrt{2}$
10	(0,-1, 0)	(1,-1, 0)	11	(0, 0,-1)	(1, 0,-1)		
12	(-1, 1, 1)	(0, 1, 1)	13	(-1, 1,-1)	(0, 1,-1)	$\sqrt{3}$	$\sqrt{2}$
14	(-1,-1, 1)	(0,-1, 1)	15	(-1,-1,-1)	(0,-1,-1)		
16	(0, 1, 1)	(1, 1, 1)	17	(0,-1, 1)	(1,-1, 1)	$\sqrt{2}$	$\sqrt{3}$
18	(0, 1,-1)	(1, 1,-1)	19	(0,-1,-1)	(1,-1,-1)		
20	(1, 0, 0)	(2, 0, 0)				$\sqrt{1}$	$\sqrt{4}$

tion using the BiCGstab algorithm [50]. The extended and heavy propagators were generated by myself using UKQCD time on the T3D. They were also calculated using the non-perturbatively improved Sheikholeslami-Wohlert action and the BiCGstab algorithm. 16 extended and 4 heavy propagators were generated

Table 4.4: Operators of the three-point function

N^0_-	Γ^C	Γ^S	N^0_-	Γ^C	Γ^S	N^0_-	Γ^C	Γ^S
1	γ^1	γ^5	27	$\gamma^1\gamma^5$	γ^1	55	σ^{14}	γ^1
2	γ^2	γ^5	28	$\gamma^1\gamma^5$	γ^2	56	σ^{14}	γ^2
3	γ^3	γ^5	29	$\gamma^1\gamma^5$	γ^3	57	σ^{14}	γ^3
4	γ^4	γ^5	30	$\gamma^1\gamma^5$	γ^4	58	σ^{14}	γ^4
5	σ^{34}	γ^5	31	$\gamma^2\gamma^5$	γ^1	59	σ^{13}	γ^1
6	σ^{24}	γ^5	32	$\gamma^2\gamma^5$	γ^2	60	σ^{13}	γ^2
7	σ^{23}	γ^5	33	$\gamma^2\gamma^5$	γ^3	61	σ^{13}	γ^3
8	σ^{14}	γ^5	34	$\gamma^2\gamma^5$	γ^4	62	σ^{13}	γ^4
9	σ^{13}	γ^5	35	$\gamma^3\gamma^5$	γ^1	63	σ^{12}	γ^1
10	σ^{12}	γ^5	36	$\gamma^3\gamma^5$	γ^2	64	σ^{12}	γ^2
11	γ^1	γ^1	37	$\gamma^3\gamma^5$	γ^3	65	σ^{12}	γ^3
12	γ^1	γ^2	38	$\gamma^3\gamma^5$	γ^4	66	σ^{12}	γ^4
13	γ^1	γ^3	39	$\gamma^4\gamma^5$	γ^1	67	$\mathbf{1}$	γ^1
14	γ^1	γ^4	40	$\gamma^4\gamma^5$	γ^2	68	$\mathbf{1}$	γ^2
15	γ^2	γ^1	41	$\gamma^4\gamma^5$	γ^3	69	$\mathbf{1}$	γ^3
16	γ^2	γ^2	42	$\gamma^4\gamma^5$	γ^4	70	$\mathbf{1}$	γ^4
17	γ^2	γ^3	43	σ^{34}	γ^1	71	γ^5	γ^1
18	γ^2	γ^4	44	σ^{34}	γ^2	72	γ^5	γ^2
19	γ^3	γ^1	45	σ^{34}	γ^3	73	γ^5	γ^3
20	γ^3	γ^2	46	σ^{34}	γ^4	74	γ^5	γ^4
21	γ^3	γ^3	47	σ^{24}	γ^1			
22	γ^3	γ^4	48	σ^{24}	γ^2			
23	γ^4	γ^1	49	σ^{24}	γ^3			
24	γ^4	γ^2	50	σ^{24}	γ^4			
25	γ^4	γ^3	51	σ^{23}	γ^1			
26	γ^4	γ^4	52	σ^{23}	γ^2			
			53	σ^{23}	γ^2			
			54	σ^{23}	γ^3			

on each configuration. See Table 4.1.

The light-light two-point correlation functions were calculated on the T3D by the UKQCD collaboration. The number of operators totals 36, including all the operators necessary for the measuring the ground state masses of the pseudoscalar, vector and scalar mesons and the following matrix elements;

$$\left\langle 0\middle|P_S\middle|P_S\right\rangle,\ \left\langle 0\middle|A^\mu\middle|P_S\right\rangle,\ \left\langle 0\middle|V^\mu\middle|V\right\rangle,$$

and for 11 different momentum channels with modulii;

$$|\vec{p}| = 0, \sqrt{1}, \sqrt{2}, \sqrt{3}, \sqrt{4}, \tag{4.1}$$

in lattice units of $12/a\pi$. The heavy-light two-point correlation functions were generated by myself with the same number of operators and momentum channels, as were the heavy-heavy two-point functions.

The three-point correlation functions were also generated by myself using UKQCD time in the T3D. The number of operators totals 74, see table 4.4, including all the operators necessary for the calculation of the following matrix elements, as well as operators necessary to improve the currents (equation 2.57);

$$\left\langle P_S\middle|V^\mu\middle|P_S\right\rangle,\ \left\langle V\middle|(V-A)^\mu\middle|P_S\right\rangle,\ \left\langle V\middle|\sigma^{\mu\nu}\middle|P_S\right\rangle.$$

The number of momentum channels is 17 for the $\vec{p}=0$ three-point function and 20 for the $\vec{p}=1$, tables 4.2 and 4.3. In this thesis results are only presented for the matrix elements of the pseudoscalar to pseudoscalar improved vector current. That is channels 1-10 in table 4.4.

The improvement coefficient c_V in equation 2.57 has been calculated to 1-loop in perturbation theory [51] by the Alpha collaboration.

$$c_V = -0.01225 g_0^2 \times C_F + \mathcal{O}(g_0^4), \tag{4.2}$$

where $C_F = (N^2-1)/2N$ for $SU(N)$. At $\beta = 6.2$ this implies

$$c_V = -0.015806. \tag{4.3}$$

The Alpha collaboration has presented preliminary results for a non-perturbative calculation of c_V [52].

$$\Rightarrow c_V^{\mathrm{NP}} \sim -0.2. \tag{4.4}$$

This is an order of magnitude larger. As this unexpectedly large result is preliminary, the 1-loop perturbative value of c_V is used.

The improved current equation 2.57 can be written with the derivative of the tensor as the four-momentum. That is

$$V_\mu^{(I)} = V_\mu + c_V \hat{q}_\nu T_{\mu\nu}. \tag{4.5}$$

where $\hat{q}_\nu$ is the momentum transfer in lattice units which can be calculated from the two-point functions.

4.2 The Extension Time Slice

The time dimension on the lattice has periodic boundary conditions. That is to say the time slice 0 is the same as time slice 48. By considering the symmetry properties of the correlation functions under time reversal (equation 2.85) and periodic boundary conditions, it can be shown that, for instance two point functions are symmetric about the mid-point of the lattice. An averaging of the two halves of the lattice, known as folding, can be employed to reduce statistical noise.

There are two sources of contamination to the signal for a particular channel of a correlation function. Firstly, contamination can come from higher excited states, that is, from equation 2.102, if the time is not sufficiently large, then the higher excited exponentials can spoil the asymptotic behaviour. This can be controlled by ensuring that the operators are separated by large times and the use of smearing to improve the signal. The second source of contamination which is important for three-point functions comes from different time orderings. Recalling the definition of the three-point function equation, 2.104, it involves the time ordered product of operators. This correlation function has contributions from the matrix element of interest, but also potentially from different orderings of the operators, in particular the correlation function has a contribution from the matrix element;

$$C^\mu_{3\mathrm{pt}(y>x>0)} \propto \left\langle 0 \middle| \Omega_A(0)\Omega_B(x)V^\mu(y) \middle| 0 \right\rangle. \tag{4.6}$$

Figure 4.1: The time dimension on the lattice

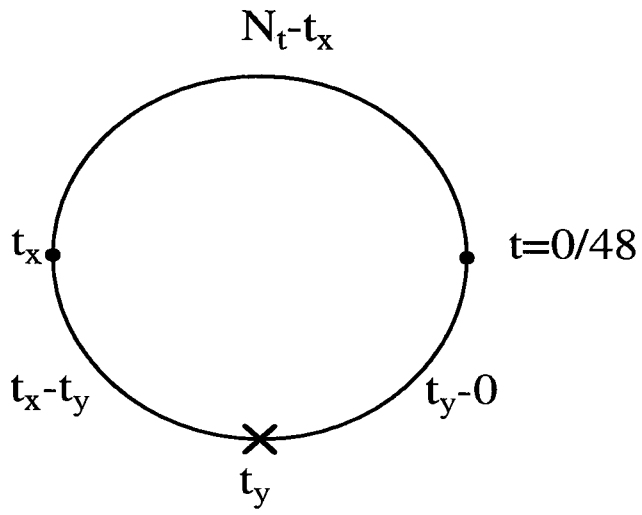

In order to examine these two systematic sources of contamination of the matrix element, it was decided to move the extension time slice from, $t_x = 24$, the mid-point of the lattice. The extension point $t_x = 28$ (or equivalently $t_x = 20$) was chosen. This means the correlation function can no longer be folded, but the fore and back sides of the lattice can be compared to examine these effects.

An analytical estimate of the different time orderings can be made by comparing the equations for the asymptotic behaviour of the two-point 2.102, and the three-point 2.117 correlation functions. Defining the ratio, R,

$$\begin{aligned} R^{\mu}(\vec{p}, t_x, \vec{k}, t_y)_{B\to A} &= \frac{C^{\mu}_{3pt}(\vec{p}, t_x, \vec{k}, t_y)_{B\to A}}{C_{2\mathrm{pt}}(\vec{p}, t_x - t_y)_B \; C_{2\mathrm{pt}}(\vec{k}, t_y)_A} \\ &= \frac{\frac{e^{-E_A(\vec{k})t_y}}{2E_A(\vec{k})} Z_A(\vec{k}) \frac{e^{-E_B(\vec{p})(t_x - t_y)}}{2E_B(\vec{p})} Z_B(\vec{p}) \left\langle A, \vec{k} \middle| V^{\mu} \middle| B, \vec{p} \right\rangle}{\frac{e^{-E_B(\vec{p})(t_x - t_y)}}{2E_B(\vec{p})} Z^2_B(\vec{B}) \frac{e^{-E_A(\vec{k})(t_y)}}{2E_A(\vec{k})} Z^2_A(\vec{A})}. \end{aligned} \quad (4.7)$$

All the time dependence cancels leaving only a ratio of matrix elements

$$R^{\mu}(\vec{p}, t_x, \vec{k}, t_y)_{B\to A} = \frac{\left\langle A, \vec{k} \middle| V^{\mu} \middle| B, \vec{p} \right\rangle}{Z_A(\vec{k}) Z_B(\vec{p})}. \quad (4.8)$$

The contribution to the above ratio from other time orderings can also be calculated. By considering Figure 4.1, it can be seen that $\left| V, \vec{p} \right\rangle$ propagates from

t_y to t_x and that $\left\langle A, \vec{k}\right|$ propagates from t_x to N_t.

$$\begin{aligned} R^{\mu}(\vec{p}, t_x, \vec{k}, t_y)_{V\to A} &= \frac{C^{\mu}_{3\mathrm{pt}}(\vec{p}, t_x, \vec{k}, t_y)_{V\to A}}{C_{2\mathrm{pt}}(\vec{p}, t_x - t_y)_B \; C_{2\mathrm{pt}}(\vec{k}, t_y)_A} \\ &= \frac{\frac{e^{-E_A(\vec{k})(N_t - t_x)}}{2E_A(\vec{k})} Z_A(\vec{k}) \frac{e^{-E_V(\vec{p})(t_x - t_y)}}{2E_V(\vec{p})} Z_V(\vec{p}) \left\langle A, \vec{k}\right|\Omega^{\dagger}_B\left|V, \vec{p}\right\rangle}{\frac{e^{-E_B(\vec{p})(t_x - t_y)}}{2E_B(\vec{p})} Z^2_B(\vec{p}) \frac{e^{-E_A(\vec{k})t_y}}{2E_A(\vec{k})} Z^2_A(\vec{k})} \end{aligned} \tag{4.9}$$

In this case not all the time dependence cancels,

$$\begin{aligned} R^{\mu}(\vec{p}, t_x, \vec{k}, t_y)_{V\to A} &= e^{-(E_V(\vec{p}) - E_B(\vec{p}))(t_x - t_y)} e^{-E_A(\vec{k})(N_t - t_y - t_x)} \\ &\times \frac{E_B(\vec{p})}{E_V(\vec{p})} \frac{\left\langle A, \vec{k}\right|\Omega^{\dagger}_B\left|V, \vec{p}\right\rangle Z_V(\vec{k})}{Z^2_B(\vec{p}) Z_A(\vec{k})}. \end{aligned} \tag{4.10}$$

Assuming the ratio of matrix elements has the same order of magnitude as in equation 4.8, it is clear that the different time orderings are suppressed by some function of the masses of the states. The kappa values used in this simulation roughly correspond to that of charm and strange. This means that the exponential suppression factor can be evaluated. The experimental values of the masses for the K, D_s and $D^{\star}_s$ [53] in GeV are:

$$m_K = 0.497 \quad m_{D_s} = 1.986 \quad m_{D^{\star}_s} = 2.112. \tag{4.11}$$

These masses can be re-written in lattice units, where $a^{-1} = 2.64\mathrm{GeV}$ and is set from m_ρ [54, 55]. An estimate of the suppression factor (sf) on different time slices can be made. With the extension point at $t_x = 28$ c.f. the suppression factor at time slices $t = 16$ and $t = 38$.

$$\begin{aligned} sf(t_y = 16) &\sim \mathcal{O}(25\%) \\ sf(t_y = 38) &\sim \mathcal{O}(3\%) \end{aligned} \tag{4.12}$$

This analysis seems to agree with the data. Figure 4.2 shows the ratio of three-point to two-point correlation functions, and it can be clearly seen that the data on the fore side of the lattice has large uncertainties, whereas the ratios for $t_y > t_x$ show reasonable plateaux. This also seems to suggest that either the contamination from excited states is small, or cancelled by the two-point functions. All the proceeding analysis is done with $t_y > t_x$. Equivalently this can be thought of as analysing the data with $t_x = 20$.

Figure 4.2: The ratios for (a) temporal and (b) spatial parts of the ratio R^μ, 4.7 $\kappa_A = 0.1353$, $\kappa_P = 0.1351$, and $\kappa_E = 0.1233$ and $\vec{p} = \vec{k} = (1,0,0)$.

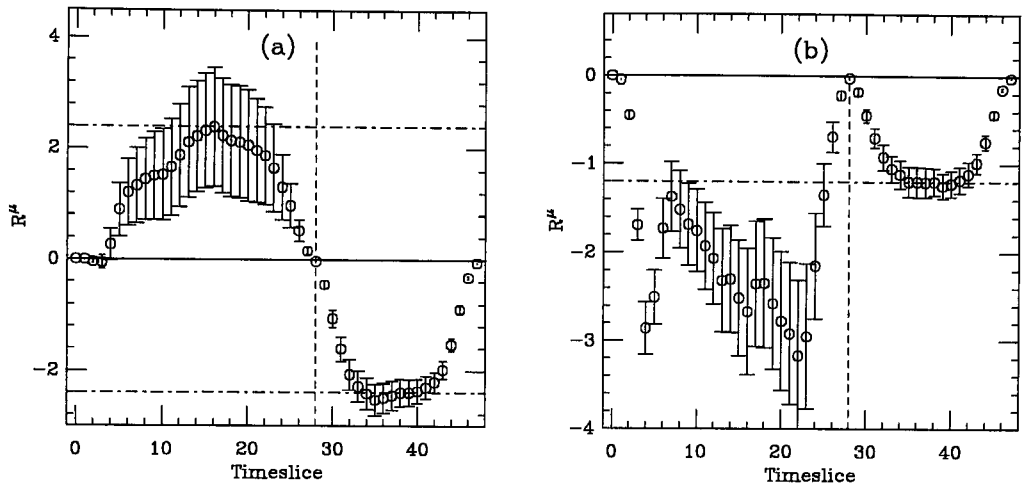

4.3 Measuring Z_V^{eff}

Matrix elements of currents measured on the lattice must be renormalised to compare with continuum values. Considering the equations for renormalised, improved currents 2.57, 2.63 and the parameterisation of the matrix element 1.56, then the renormalised matrix element can be written.

$$Z_V(1+b_V am_q)\Big\langle B(\vec{p})\Big|V^\mu\Big|A(\vec{k})\Big\rangle_{\text{latt}} = f_+(q^2)(k+p-q\Delta_{m^2})^\mu + f_0(q^2)q^\mu\Delta_{m^2} \quad (4.13)$$

where Δ_{m^2} is defined in equation 1.56. An effective renormalisation constant can be defined.

$$Z_V^{\text{eff}} = Z_V(1 + b_V am_q) \quad (4.14)$$

Consider the forward degenerate matrix element of the temporal component of the vector current. That is, the initial and final states are the same and at zero momentum transfer,

$$Z_V^{\text{eff}}\Big\langle D(0)\Big|V^4\Big|D(0)\Big\rangle_{\text{latt}} = f_+(0)(p^4 + k^4). \quad (4.15)$$

For a degenerate transition, the form factor of the forward matrix element is defined to be one, and so

$$Z_V^{\text{eff}} = \frac{2M_D}{\left\langle D(0)\middle|V^4\middle|D(0)\right\rangle_{\text{latt}}}. \tag{4.16}$$

Figure 4.3: (a) The ratio, R_{Z_V} for $\kappa_H = 0.1200$ and $\kappa_P = 0.1346$. (b) Z_V^{eff} vs. mass. The horizontal lines are the Alpha values and the $\kappa_P = 0.1351$ points are offset to the right.

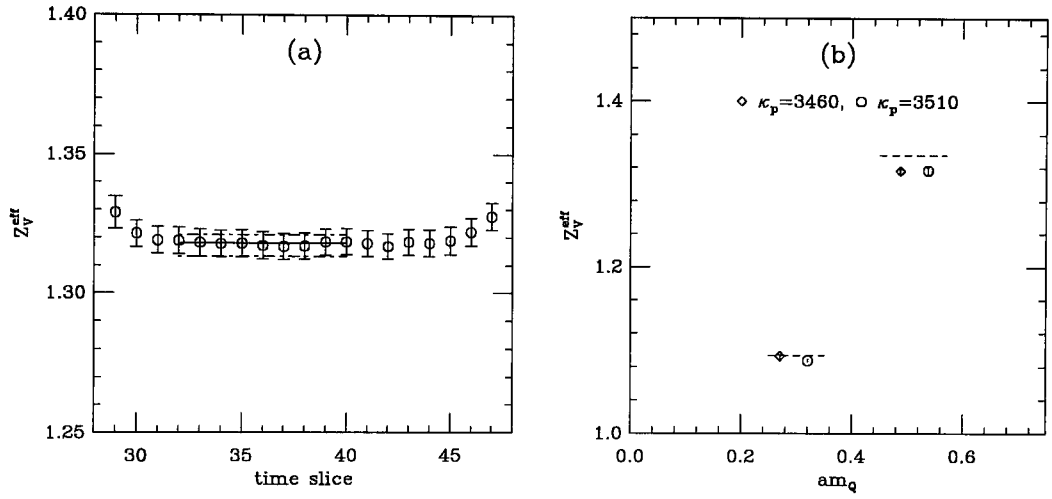

This matrix element is easily calculated by taking the ratio

$$\begin{aligned} R_{Z_V} &= \frac{C_{2\text{pt}}(t=t_x)}{C^4_{3\text{pt}}(t_x,t_y)_{(A=B)}} \\ &= \frac{e^{-M_D t_x}}{2M_D} Z_D^2 \frac{4M_D^2}{e^{-M_D(t_x-t_y)} Z_D e^{-M_D(t_y)} Z_D} \frac{1}{\left\langle D(0)\middle|V^4\middle|D(0)\right\rangle} \\ &= \frac{2M_D}{\left\langle D(0)\middle|V^4\middle|D(0)\right\rangle}. \end{aligned} \tag{4.17}$$

This can be compared with a value for Z_V^{eff} calculated from the Alpha Collaborations results for Z_V and b_V [26],

$$\begin{aligned} Z_V &= \frac{1 - 0.7663g^2 + 0.0488g^4}{1 - 0.6369g^2} \\ b_V &= \frac{1 - 0.7613g^2 + 0.0012g^4 - 0.1136g^6}{1 - 0.9145g^2} \end{aligned} \tag{4.18}$$

Figure 4.3(a) shows Z_V^{eff} evaluated from the ratio of two-point to three-point correlation functions for each time slice. This can only be done for $T > t_x = 28$, equivalent to $T < t_x = 20$, due to the periodic boundary conditions of the lattice. i.e. $C_{2\text{pt}}(t = 28) = C_{2\text{pt}}(t = 20)$. As can be seen from the figure, all time dependence cancels out giving a very clean signal. Figure 4.3(b) shows Z_V^{eff}'s variation with mass for the four different kappa combinations. There is excellent agreement between the Alpha predictions and the measured values.

4.4 Two-Point Correlation Functions

Recalling equation 2.102, and the periodic boundary conditions on the lattice, the asymptotic form of the two-point function can be parameterised by

$$C(t) = A\left[e^{-Et} + e^{-E(T-t)}\right], \tag{4.19}$$

where $T = 48$, E is the energy of the state and the second term is the *backward* propagating meson. The amplitude A is then,

$$A = \frac{Z^2}{2E}, \tag{4.20}$$

where Z is given by equation 2.103.

These parameters are fitted to the two-point correlation functions, as described in section 2.8. In order to ascertain the range of time slices on which the asymptotic form is valid, the effective mass is defined as

$$M_{\text{eff}}(t) = \ln\left[\frac{C(t_n)}{C(t_{n+1})}\right]. \tag{4.21}$$

Considering the effective mass as a function of time slice, it will become constant when the time is sufficiently large that ground state dominates the exponentials. Figure 4.4 shows the effective mass plotted against time slice for pseudoscalar mesons. The horizontal line is the mass fitted between time slices 8 to 22 for the light-light meson and between 12-22 for the heavy-light, as there are plateaux for the effective mass in these ranges.

The notation used to denote the smearing combinations is as follows. F stands for Fuzzed, B for Boyled and L for local. For a particular correlation function,

Figure 4.4: Effective mass plots, (a) $\kappa_1 = \kappa_2 = 0.1346$ FF, LL (b) $\kappa_H = 0.1233$, $\kappa_L = 0.1346$ BB, LL

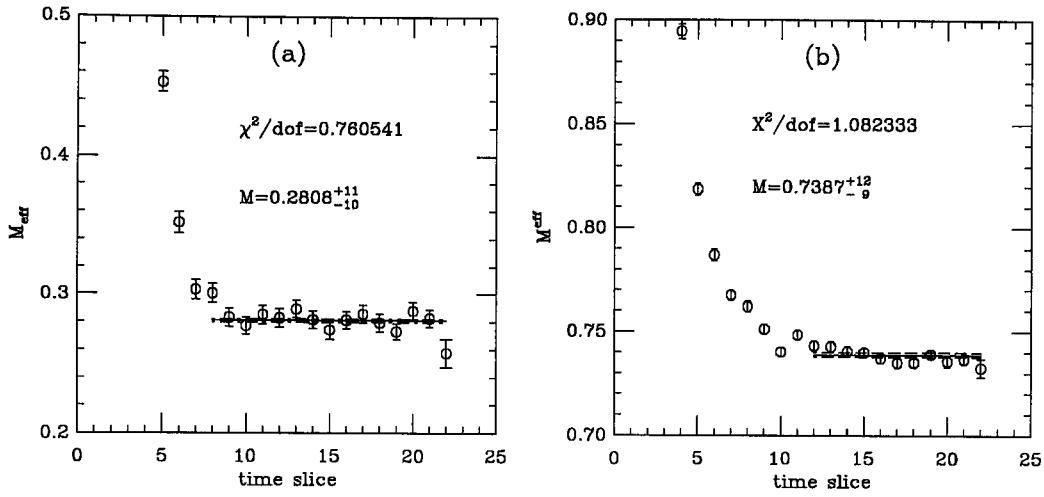

the notation is $Source_1 Sink_1, Source_2, Sink_2$, where the subscripts refer to the propagators.

4.4.1 The Chiral Limit and Charm Mass

The pseudoscalar mesons are used in lattice QCD to define the kappa values which correspond to the quark masses. In this calculation three kappa values need to be defined for 'physical' quark masses. They are;

$$\begin{aligned} \kappa_{\text{crit}} &\longleftrightarrow m_u = m_d = 0 \\ \kappa_s &\longleftrightarrow m_s \\ \kappa_c &\longleftrightarrow m_c, \end{aligned}$$

where the subscript s stands for strange and c for charm.

As previously discussed, algorithms fail to converge when trying to invert the fermion matrix with a really light quark mass, and so the calculation is done with several light kappas around strange which are then extrapolated to the *chiral limit*. There are many ways to define this limit. However in this thesis only the simplest is considered. The chiral limit is defined at vanishing pseudoscalar

Figure 4.5: Linear Chiral Extrapolation of Light Pseudoscalar Meson

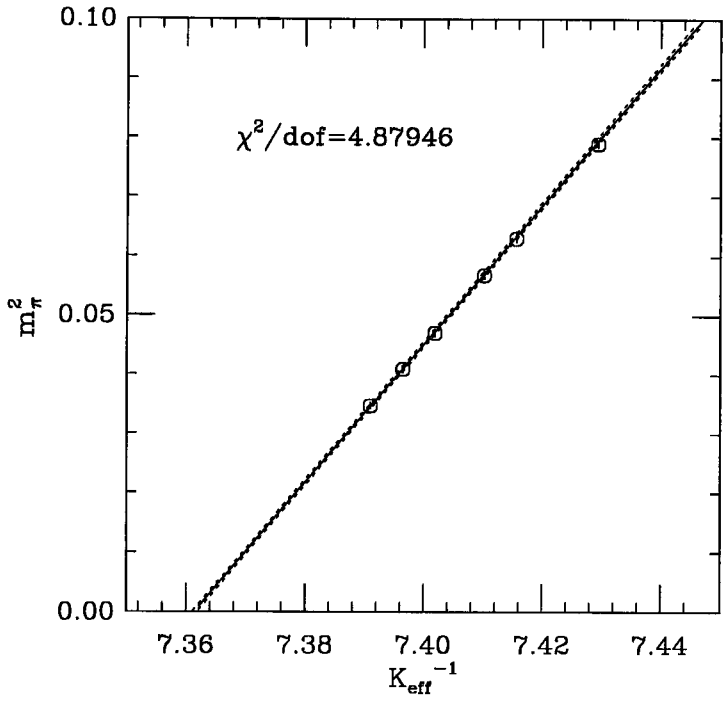

meson mass. PCAC [45] suggests the following dependence of pseudoscalar mass on quark mass,

$$M_{PS}^2 \propto m_q. \tag{4.22}$$

Thus $\kappa_{\rm crit}$ is defined as the kappa value for which the pseudoscalar mass vanishes. The data in Figure 4.5 can be found in table B.1 and is fitted to the form

$$\begin{aligned} m_\pi^2 &= a + b\left(\frac{1}{\kappa_1} + \frac{1}{\kappa_2}\right) \\ &= a + b\frac{2}{\kappa_{\rm eff}}. \end{aligned} \tag{4.23}$$

The results are;

$$a = -8.592^{+49}_{-73} \quad b = 1.167^{+10}_{-7}. \tag{4.24}$$

and

$$\kappa_{\rm crit} = 0.135844^{+7}_{-8}. \tag{4.25}$$

This fit has a rather large χ^2. However, a more extensive investigation of the chiral behaviour in [55, 56] on the same data results in a consistent value for $\kappa_{\rm crit}$ with a variety functional forms.

The value for kappa strange can be defined from several quantities. In this thesis, the pseudoscalar meson K is chosen. Once again using the ρ mass to set the lattice spacing, this gives a value for kappa strange,

$$\kappa_s = 0.134746^{+9}_{-7}. \tag{4.26}$$

Again this is consistent with previous UKQCD results using more sophisticated analysis. This is very close to one of the simulation kappas, $\kappa_l = 0.1346$.

For the heavy-light pseudoscalar meson there is no theoretical motivation for the form of the extrapolation. In this calculation there are only three light kappas, so this suggests as a first attempt a linear extrapolation in the meson mass. In fact there is only a small dependence of m_{PS} on the light quark mass, so a linear fit works rather well.

Figure 4.6: (a) Chiral extrapolation of heavy-light PS meson, $\kappa_H = 0.1233$. (b) heavy-light PS meson dependence on quark mass.

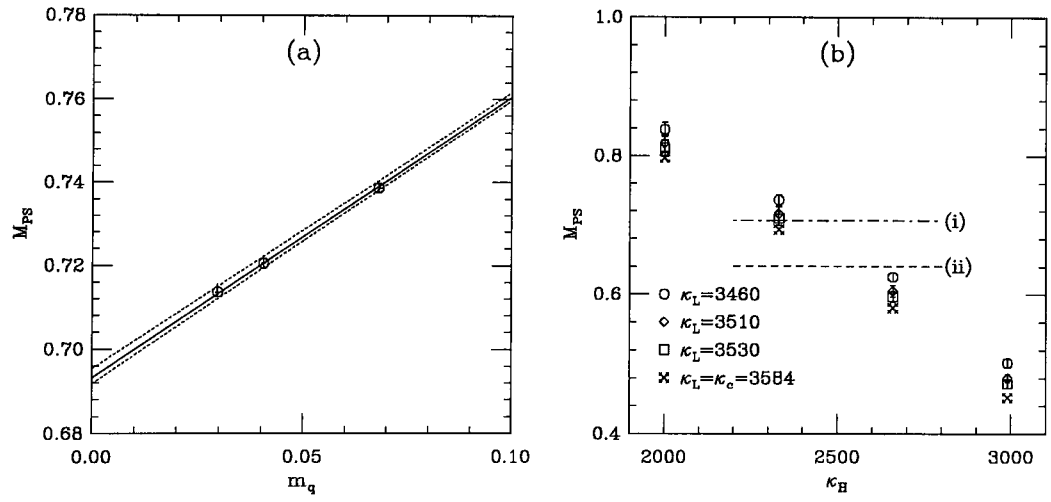

Figure 4.6(a) shows the linear chiral extrapolation. It is clear that this is a reasonable fit. Figure 4.6(b) shows the values of all 12 heavy-light pseudoscalar meson masses. The data is listed in table B.2. Also plotted are the 4 chirally extrapolated values of the meson mass, which have the same valence quark content as m_{D^0}. These masses are listed in table B.5. Experimentally [53] $m_{D^0} = 1.8645$Gev. Line (i) is the D^0 mass in lattice units with the lattice

spacing defined by ρ mass. Line (ii) has the lattice spacing defined by r_0, [57] $a^{-1} = 2.913\text{GeV}$. As can be seen, line (i) is very close to the chirally extrapolated value of the pseudoscalar mass with $\kappa_H = 0.1233$. In this thesis the value of κ which corresponds to the charm mass, k_c, will be taken to be

$$\kappa_c = 0.1233. \tag{4.27}$$

4.4.2 Vectors and Scalars

In order to fully analyse the momentum dependence of the form factors, it is necessary to analyse the scalar and vector heavy-light mesons, see section 4.6 for details The operator for the vector meson is

$$\Omega_V^\mu(x) = \bar{\psi}(x)\gamma^\mu\psi(x). \tag{4.28}$$

The situation for vectors is slightly complicated for vectors by the polarisation vector ϵ. The matrix element of the operator is

$$\left\langle 0\middle|\Omega_V^\mu(0)\middle|V_j(\epsilon,\vec{p})\right\rangle = \epsilon_j^\mu Z_V(\vec{p}) \tag{4.29}$$

where $Z_V(\vec{p})$ is the vector meson amplitude. Considering the polarisation sum for a massive vector meson

$$\sum_j \epsilon_j^\mu \epsilon_j^\nu = -\delta^{\mu\nu} + \frac{p^\mu p^\nu}{m^2}, \tag{4.30}$$

and the large time behaviour the two-point correlation function can be written as

$$C^{\mu\nu}(\vec{p},t) = \left(-\delta^{\mu\nu} + \frac{p^\mu p^\nu}{m^2}\right)\frac{e^{-E_V(\vec{p})t}}{2E_V(\vec{p})}\left|Z_V(\vec{p})\right|^2. \tag{4.31}$$

The polarisation averaged correlation function can then be defined as

$$C(\vec{p},t) = -3\frac{e^{-E_V(\vec{p})t}}{2E_V(\vec{p})}\left|Z_V(\vec{p})\right|^2, \tag{4.32}$$

for a Euclidean metric and the on-shell condition. This differs from the pseudoscalar correlation function equation 2.102 by the factor -3. Only the spatial components of the vector current are considered as they have a non-zero overlap with the vector state at zero momentum. The operator for the scalar is

$$\Omega_S(x) = \bar{\psi}(x)\psi(x). \tag{4.33}$$

Figure 4.7: Effective Mass Plots (a) $J^P = 1^-$ and $\kappa_H = 0.1233$, $\kappa_L = 0.1346$, BB, LL. (b) $J^P = 0^+$ and $\kappa_H = 0.1233$, $\kappa_L = 0.1351$, BB, LL. Both fitted 12-22.

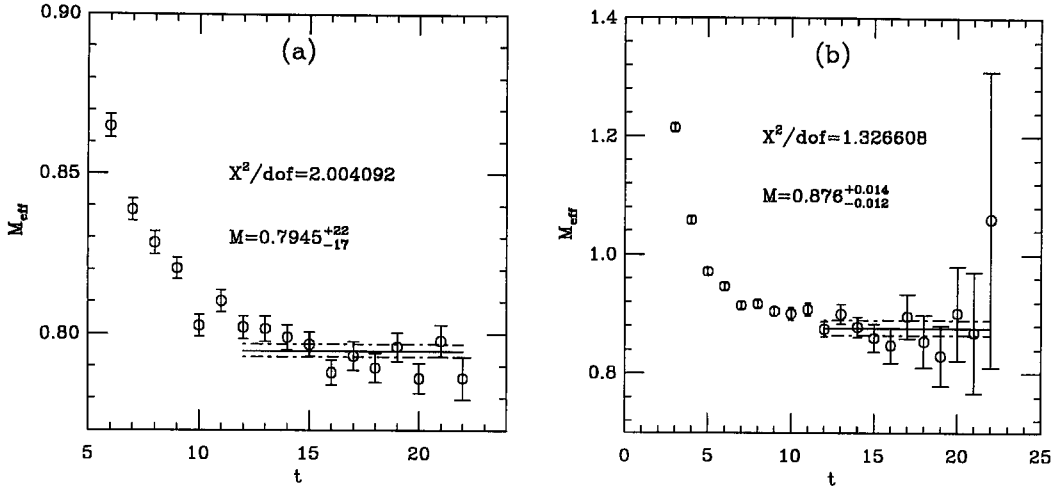

The fit ranges for these states is also determined from effective mass plots.

The fitted masses and amplitudes and the results of their chiral extrapolations are displayed in tables B.3 - B.5.

4.5 Extracting the Form Factors

The form factors of a particular matrix element can be extracted from the data using the ratio defined in equation 4.7. All of the time dependence cancels leaving a ratio of matrix elements. The product of two matrix elements in the denominator can be extracted from the two-point correlation functions. The momentum of the initial state D meson is fixed to be either $\vec{p} = (0,0,0)$ or $\vec{p} = (1,0,0)$, but in order to reduce statistical noise, all equivalent momentum channels of the light state are averaged over. This leaves 6 momentum channels that have initial and final state momentum less than or equal to one, shown in table 4.5.

The form factors are simultaneously fitted to the temporal and spatial components of the ratio of correlation function. All the kinetic factors can be calculated

Table 4.5: Momentum channels, in units of $\frac{\pi}{12a}$

chan	$\vec{p}$	$\vec{k}$	$\vec{q} = \vec{k} - \vec{p}$
1	(0, 0, 0)	(0, 0, 0)	(0, 0, 0)
2	(0, 0, 0)	(1, 0, 0)	(1, 0, 0)
3	(1, 0, 0)	(1, 0, 0)	(0, 0, 0)
4	(1, 0, 0)	(0, 0, 0)	(-1, 0, 0)
5	(1, 0, 0)	(0, 1, 0)	(-1, 1, 0)
6	(1, 0, 0)	(-1, 0, 0)	(-2, 0, 0)

from the masses of the two-point functions. The dispersion relation,

$$E^2(\vec{p}^2) = m^2 + \vec{p}^2 \tag{4.34}$$

is used to calculate the energies of the initial and final state. States with higher momentum than one rapidly become very noisy, and whilst the dispersion relation could be used to calculate the energy from the mass, it could suffer from large violations coming from discretisation errors.

The ratios are plotted as a function of time to see in what range the data can be fitted to a plateau. The spatial and temporal ratios are plotted in figure 4.8(a). There is a reasonable plateau for both spatial and temporal components on time slices 8-11. This is the fit range used for all the form factors except for channel 4 and channel 1 the forward matrix element. In figure 4.8(b) the temporal component momentum channel 4 is shown for all times. The back side of the lattice has a slow approach to a plateau. For time slices 40-42 it is approaching the plateau on the fore side. There appears to be no contamination from different time orderings for this channel. This could be explained by the fact that $\left|V^4(0)\right\rangle$ has no overlap with the vector meson state. The fit range for this channel is then 40-42, which corresponds to 12-14 with $t_x = 20$.

In the case of the forward matrix element, the spatial component vanishes, as does the kinetic term for $f_+(q^2)$. $f_0(q^2)$ is fitted to the temporal component only, on time slices 12-16 with the extension point at $t_x = 28$. The results of these fits are listed in tables C.1 - C.24.

Figure 4.8: Ratios for $\kappa_P = 0.1351$,$\kappa_A = 0.1353$ and $\kappa_H = 0.1233$. (a) Temporal and spatial components for $\vec{p} = (1,0,0)$, $\vec{k} = (1,0,0)$. (b) Ratio at all times for the temporal component of $\vec{p} = (1,0,0)$, $\vec{k} = (0,0,0)$.

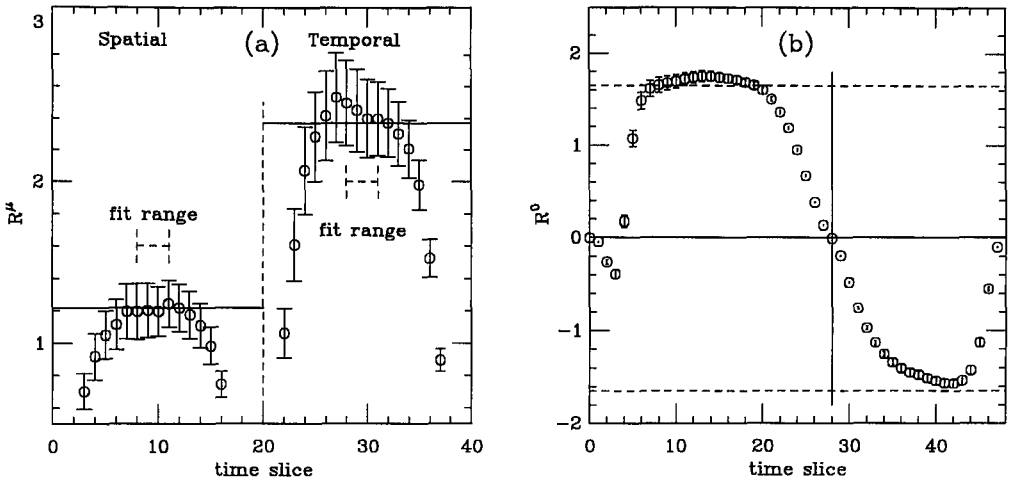

4.5.1 Chiral extrapolations of the Form Factors

Unlike the case of the pseudoscalar mesons, there is no field theoretic input like PCAC to suggest the dependence of the form factor on the light quark mass. However, a reasonable assumption is that the form factor behaves like a constant plus some small variation through the dependence of initial and final states on the light quark mass.

$$F(q^2) = \alpha + \beta \frac{\partial}{\partial m_q}(M_H) + \gamma \frac{\partial}{\partial m_q}(M_L), \tag{4.35}$$

where F is either form factor. From the discussion above particularly figure 4.5 and figure 4.6, this implies that

$$F(q^2) = \alpha + \beta \frac{\Delta M_H(\kappa_c, \kappa_P)}{M_H(\kappa_c, \kappa_{\rm crit})} + \gamma \left(\frac{\Delta M_L(\kappa_P, \kappa_A)}{M_L(\kappa_{\rm crit})} \right)^2 \tag{4.36}$$

and so

$$F(q^2) = \alpha + \beta \left(\frac{1}{\kappa_P} - \frac{1}{\kappa_{\rm crit}} \right) + \gamma \left(\frac{1}{\kappa_P} + \frac{1}{\kappa_A} - \frac{2}{\kappa_{\rm crit}} \right). \tag{4.37}$$

Note that this is an extrapolation in *two* variables, κ_P and κ_A, or

$$F(q^2) = \alpha + \beta m_P + \gamma m_{\rm eff} \tag{4.38}$$

where $m_{\rm eff}$ is the effective quark mass of the light pseudoscalar state.

Figure 4.9: Chiral extrapolation of (a) $f_0^2(q^2)$ channel 1 and (b)$f_+(q^2)$ channel 2.

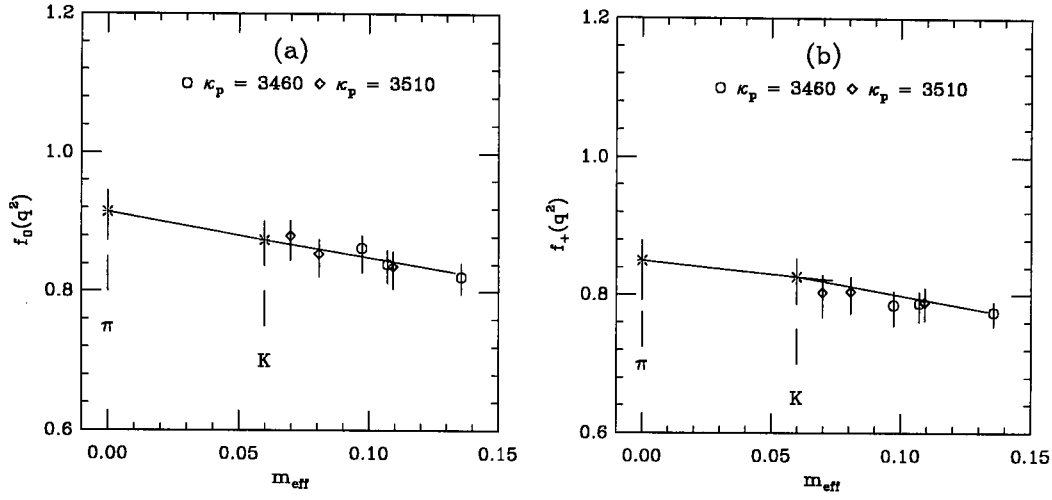

In figure 4.9 the chiral extrapolations are shown for two channels. Note that in figure 4.9(b) there are in fact two lines. This is because the figure is a projection of a two dimensional extrapolation onto the plane $m_P = m_{\rm eff}$. For $D \to K$, the data is extrapolated to

$$\begin{aligned} m_P &\to 0 \\ m_{\rm eff} &\to (m|M_{PS} = M_K), \end{aligned} \tag{4.39}$$

and for $D \to \pi$

$$m_P = m_{\rm eff} \to 0. \tag{4.40}$$

The results of these extrapolations are listed in table 4.6 and table 4.7

It should be noted that in previous UKQCD publications [58, 59] the form of the chiral extrapolation included an extra term. This term is proportional to the change in the light pseudoscalar mass, so equation 4.36 becomes,

$$F(q^2) = \alpha + \beta \frac{\Delta M_H(\kappa_c, \kappa_P)}{M_H(\kappa_c, \kappa_{\rm crit})} + \gamma \left(\frac{\Delta M_L(\kappa_P, \kappa_A)}{M_L(\kappa_{\rm crit})} \right)^2 + \delta \left(\frac{\Delta M_L(\kappa_P, \kappa_A)}{M_L(\kappa_{\rm crit})} \right). \tag{4.41}$$

This implies a term proportional to $(m_{\rm eff})^{1/2}$, equation 4.38 becomes

$$F(q^2) = \alpha + \beta m_P + \gamma m_{\rm eff} + \delta m_{\rm eff}^{\frac{1}{2}}. \tag{4.42}$$

Table 4.6: Chiral extrapolations of $f_+(q^2)$.

mom	$D \to K$	q^2	$D \to \pi$	q^2	χ^2/dof	Q
2	0.826^{+26}_{-40}	0.069^{+2}_{-1}	0.849^{+30}_{-57}	0.118^{+2}_{-1}	0.74838/3	0.86177
3	1.125^{+110}_{-160}	0.176^{+1}_{-1}	1.212^{+14}_{-19}	0.230^{+2}_{-1}	3.3736/3	0.33753
4	1.321^{+51}_{-69}	0.238^{+2}_{-1}	1.534^{+61}_{-87}	0.481^{+3}_{-2}	12.4013/3	0.006128
5	0.754^{+51}_{-83}	0.039^{+2}_{-1}	0.795^{+64}_{-102}	0.093^{+2}_{-1}	1.35883/3	0.715213
5	0.647^{+46}_{-63}	-0.098^{+2}_{-1}	0.673^{+53}_{-71}	-0.046^{+2}_{-1}	1.78304/3	0.618633

Table 4.7: Chiral extrapolations for $f_0(q^2)$.

mom	$D \to K$	q^2	$D \to \pi$	q^2	χ^2/dof	Q
1	0.874^{+27}_{-36}	0.256^{+2}_{-1}	0.914^{+31}_{-41}	0.481^{+3}_{-2}	8.43457/3	0.037835
2	0.764^{+22}_{-38}	0.069^{+2}_{-1}	0.744^{+28}_{-51}	0.118^{+2}_{-1}	1.22597/3	0.746782
3	0.933^{+94}_{-135}	0.176^{+2}_{-1}	1.008^{+105}_{-152}	0.230^{+2}_{-1}	4.78305/3	0.18839
4	0.972^{+22}_{-35}	0.238^{+2}_{-1}	0.992^{+28}_{-42}	0.481^{+3}_{-2}	3.53059/3	0.316816
5	0.703^{+51}_{-73}	0.039^{+2}_{-1}	0.694^{+62}_{-87}	0.093^{+2}_{-1}	1.19947/3	0.753132
6	0.704^{+49}_{-70}	-0.098^{+2}_{-1}	0.718^{+60}_{-78}	-0.045^{+2}_{-1}	1.78959/3	0.617203

This was motivated by writing down the most general form possible. This term makes very little difference for the results for $D \to K$, which can be seen by comparing the results in [58]. However for $D \to \pi$ the derivative of this term diverges

$$\lim_{m_{\text{eff}} \to 0} \frac{\partial}{\partial\, m_{\text{eff}}} \left(m_{\text{eff}}^{1/2} \right) \to \infty. \tag{4.43}$$

This divergence can cause very rapid changes in the form factor as the chiral limit is approached. This behaviour is not consistent with the original ansatz for the chiral behaviour. There are also no terms proportional to M_{PS} in chiral perturbation theory, from which the light quark mass dependence of the light pseudoscalar is modelled. The linear extrapolation is the only one considered in this thesis.

4.6 Pole Mass Dominance Models

The results presented thus far are calculated from first principles. The form factors have been calculated as functions of q^2. One of the motivations for calculating the form factors on the lattice is to test model-dependent assumptions. In particular lattice data can be compared to pole dominance models [60, 61, 62]. They suggest the following forms for the momentum dependence of the form factors,

$$f_+(q^2) = \frac{f_+(0)}{1 - q^2/m_{1^-}^2} \quad , \quad f_0(q^2) = \frac{f_0(0)}{1 - q^2/m_{0^+}^2}, \tag{4.44}$$

where m_{J^P} denotes the mass of a $\bar{s}c$ ($\bar{d}c$) meson for the decay $D \to K$ (π) with spin J and parity P. This model of the momentum dependence does have limitations, for instance the value of the form factor will vary very rapidly with q^2 near the end point.

In order to fit these models to the lattice data, two different fits were tried. Firstly the form factor at zero momentum transfer and the mass of the pole are fitted to the data. This is fit A. Secondly the form factor at zero momentum transfer is fitted to the data and the mass of the pole fixed to be that as measured by the two-point functions (table B.5). Both fits are uncorrelated.

Figure 4.10: Pole mass fits fits for (a) $f_+^K(q^2)$ (b) $f_0^K(q^2)$. The solid line is fit A, the dotted line fit B. The burst points are the fitted values of $f(0)$.

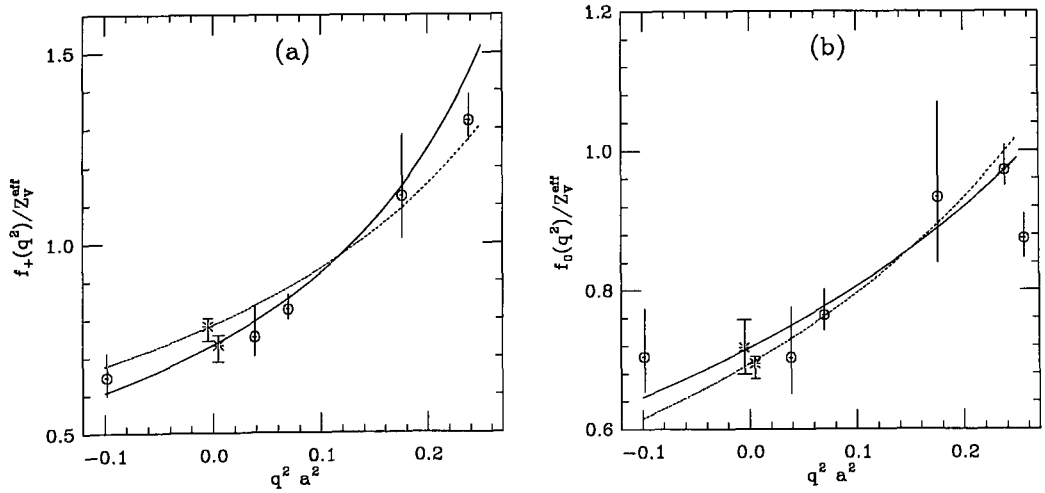

Table 4.8: Fits To Pole Mass Dominance Model For $D \to K$

fit	$f^+(0)$	$m_{1^-}^{cs}$	$\chi^2/d.o.f$	$f^0(0)$	$m_{0^+}^{cs}$	$\chi^2/d.o.f$
A	0.732^{+26}_{-44}	0.695^{+21}_{-23}	0.470279	0.717^{+40}_{-38}	0.953^{+69}_{-70}	0.436369
B	0.785^{+22}_{-39}	0.789^{+2}_{-2}	1.35071	0.694^{+10}_{-22}	0.884^{+12}_{-10}	0.680222

The momentum dependence for the form factors of the decay $D \to K$ are shown in figure 4.10 and the results of the fit in table 4.8. As can be seen from the figure, the data fits the pole mass dominance model rather well. The two form factor obey the kinematic constraint

$$f_+(0) = f_0(0) \tag{4.45}$$

although the masses for vector poles differ somewhat. For the two parameter fit $f_+(q^2)$ and $f_0(q^2)$ are also in agreement, although for the one parameter fit the agreement is worse.

Converting the lattice masses into physical ones from m_ρ (r^0), for the vector

$$\begin{aligned} D_s^{*+} &= 2.112 \text{ GeV} \\ m_{\text{pole}} &= 1.834^{+55}_{-61}\ (2.022) \text{ GeV} \\ m_{C2pt} &= 2.082^{+5}_{-5}\ (2.295) \text{ GeV}. \end{aligned} \tag{4.46}$$

It can be seen that whilst the pole mass as a free parameter of the fit is not a particularly accurate measure of the mass of the vector, given the uncertainly in the lattice spacing, the mass of the pole is consistent with both the experimental measure of D^{*+} and the mass as measured by the two-point function. The scalar particle does not have an experimentally measured mass, so a similar comparison cannot be done.

The form factors are dimensionless quantities. However, as can be seen from figure 4.6, the variation in the value of the lattice spacing as measured by different quantities results in a different value of κ_c. This can be used to try and estimate some of the systematic errors coming from discretisation. Of course a more reliable estimate would be to compare at different lattice spacings, or even better, at several different lattice spacings, then these effects can be extrapolated

away. The matrix element must also be renormalised and $Z_V^{\rm eff}$ is calculated by taking an average of κ_A and κ_E. For $D \to K$, this implies

$$Z_V^{\rm eff} = Z_V \left(1 + b_V a \frac{1}{2}(m_c + m_s)\right) = 1.021. \tag{4.47}$$

Taking these factors into account, a variation of up to 6% in the value of the form factor is found. Taking the two-parameter fit as the preferred result for the momentum dependence gives

$$\begin{aligned} f_+^K(0) &= 0.747^{+22}_{-45\ \rm stat}{}^{+45}_{-45\ \rm sys} \\ f_0^K(0) &= 0.731^{+41}_{-39\ \rm stat}{}^{+44}_{-44\ \rm sys}. \end{aligned} \tag{4.48}$$

A similar analysis can be done of the momentum dependence of the form factors for the decay $D \to \pi$. In this case the one parameter fit, where the mass of the pole is fixed to be the same as the mass measured by the two-point function, fails badly. This is because the largest values of of q^2 are rather near the physical poles in equation 4.44. Thus only fit A is shown in figure 4.11. The pole dominance model is still a reasonable description of the momentum dependence. In table 4.9 the results of the fit are shown, as well as the mass as measured by the two-point function.

Figure 4.11: Pole mass fits for (a) $f_+^\pi(q^2)$ (b) $f_0^\pi(q^2)$. The solid line is fit A. The burst points are the fitted values of $f(0)$.

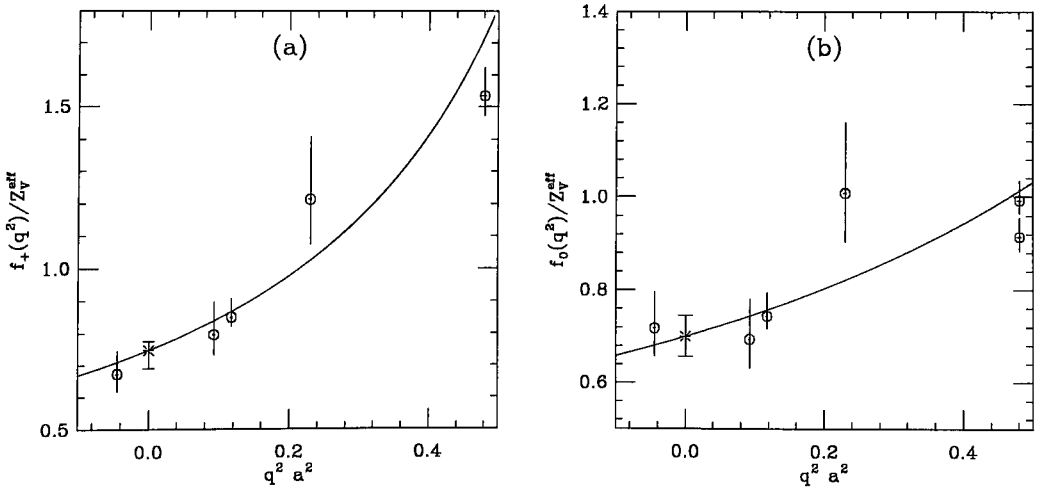

Table 4.9: Fits To Pole Mass Dominance Models For $D \to \pi$

fit	$f^+(0)$	$m_{1^-}^{cd}$	$\chi^2/d.o.f$	$f^0(0)$	$m_{0^+}^{cd}$	$\chi^2/d.o.f$
A	0.747^{+28}_{-56}	0.922^{+23}_{-23}	0.851591	0.700^{+46}_{-44}	1.246^{+85}_{-88}	1.15931
B	N/A	0.752^{+4}_{-3}		N/A	0.840^{+17}_{-15}	

The form factors again obey the kinematic constraint

$$f_+^\pi(0) = f_0^\pi(0), \tag{4.49}$$

within statistical uncertainty. The masses are clearly not in agreement. The growth in the form factor at high q^2 is not sufficiently fast to accommodate a pole of mass as measured by the two-point functions. The pole mass dominance does not model the momentum dependence of the data particularly well. The two-parameter fit will be used to estimate $f(0)$ as from the figures the data can be interpolated to $q^2 = 0$. Again the matrix element must renormalised.

$$Z_V^{\text{eff}} = Z_V \left(1 + b_V a \frac{1}{2}(m_c + m_{\text{crit}})\right) = 1.002. \tag{4.50}$$

Again the systematic uncertainties can be estimated from the different measures of the lattice spacing. However the chiral extrapolations are over a longer range. This suggests a larger systematic uncertainty, of order 10%. This implies

$$\begin{aligned} f_+^\pi(0) &= 0.748^{+22}_{-45\ \text{stat}}\ {}^{+75}_{-75\ \text{sys}} \\ f_0^\pi(0) &= 0.701^{+46}_{-44\ \text{stat}}\ {}^{+70}_{-70\ \text{sys}}. \end{aligned} \tag{4.51}$$

The $SU(3)$ flavour ratio can be computed,

$$\frac{f_+^\pi(0)}{f_+^K(0)} = 1.001^{+42}_{-85} \tag{4.52}$$

where it is believed systematic uncertainties cancel, although uncertainties from the chiral extrapolation could still contribute.

These results can be compared with experiment. Two experiments have results for the semileptonic decays of D mesons. Where two errors are quoted the

first error is statistical, the second systematic. The E687 Collaboration [63, 64] find

$$f_+^K(0) = 0.71^{+3+3}_{-3-3} \tag{4.53}$$

$$m_{\rm pole} = 1.87^{+11+7}_{-\ 8-6}\ \text{GeV} \tag{4.54}$$

$$\left|\frac{f_+^\pi(0)}{f_+^K(0)}\right| = 1.00^{+11+2}_{-11-2}. \tag{4.55}$$

The CLEO Collaboration [65, 66] find

$$f_+^K(0) = 0.77^{+1+4}_{-1-4} \tag{4.56}$$

$$\left|\frac{f_+^\pi(0)}{f_+^K(0)}\right| = 0.99^{+8}_{-8}, \tag{4.57}$$

where the mass of the pole in $f_+^K(q^2)$ is assumed to be $D_s^{\star+}$.

This calculation is in excellent agreement with both sets of results.

4.7 The Pseudoscalar Decay Constant

The pseudoscalar decay constant, defined by equation 1.61, is calculated by considering the time component of the current at zero momentum. The pseudoscalar decay constant is then defined by

$$\left\langle 0\middle|A_4(0)\middle|P(0)\right\rangle = M_P f_P. \tag{4.58}$$

This matrix element is calculated by considering the ratio of two-point correlation functions. Define the ratio,

$$\frac{C_{AP}^{LS}(t)}{C_{PP}^{SS}(t)} = \frac{\sum_{\vec{x}} e^{-i\vec{p}\cdot\vec{x}}\left\langle 0\middle|A_4^L(x)P^{\dagger S}(0)\middle|0\right\rangle}{\sum_{\vec{x}} e^{-i\vec{p}\cdot\vec{x}}\left\langle 0\middle|P^S(x)P^{\dagger S}(0)\middle|0\right\rangle}. \tag{4.59}$$

The superscripts refer to the smearing, and the subscripts to the operator in the correlation function. Then considering the asymptotic form of the correlation functions given by equation 2.102, this ratio becomes

$$\frac{C_{AP}^{LS}(t)}{C_{PP}^{SS}(t)} = \frac{\left\langle 0\middle|A_4^L(0)\middle|P(0)\right\rangle}{\left\langle 0\middle|P^S(0)\middle|P(0)\right\rangle}\tanh\left[M_P(T/2-t)\right]. \tag{4.60}$$

The matrix element in the denominator, and the mass M_P can both be fixed from the $C_{PP}^{SS}(t)$ two-point correlation function. The matrix element parameterised by the pseudoscalar decay constant is the only unknown.

The improved axial current, equation 2.57 can also be written with the derivative as a four-momentum, that is

$$Z_A^{\text{eff}}\Big\langle 0\Big|A_4(0) + c_A M_P P(0)\Big|P(0)\Big\rangle_{\text{latt}} = M_P f_P, \tag{4.61}$$

where c_A is defined in equation 2.66 and Z_A^{eff} is defined in equation 2.63

$$Z_A^{\text{eff}} = Z_A(1 + b_A a m_q). \tag{4.62}$$

The Alpha collaboration [26] have calculated Z_A non-perturbatively to be

$$Z_A = \frac{1 - 0.8496g^2 + 0.0610g^4}{1 - 0.7332g^2} \tag{4.63}$$

where $0 \leq g \leq 1$. Unlike b_V, b_A is not known non-perturbatively. In this calculation a 1-loop perturbative estimate for b_A is used [51]

$$b_A = 1 + 0.1522g^2 + \mathcal{O}(g^4). \tag{4.64}$$

The fit range is decided by plotting the ratio of correlation functions against time. In figure 4.12(a) the solid line is the fit to a tanh with the mass fixed to be that measured by $C_{PP}^{SS}(t)$. The fit range is 14-21. The data is deceptively smooth. It would appear that the fit range could be extended. In figure 4.12(b) it can be seen that the data starts to rise, if we consider time slices before 14. If we include time slices 22 and 23 in the fit, they dominate the tanh plot, and the fit is well below the plateau between time slices 14-21. The fits for all κ combination of the heavy-light pseudoscalar decay constants are listed in table C.25.

The pseudoscalar decay constants must be extrapolated to physical quark masses, κ_{crit} and κ_s. There are only three light quark kappas so this suggests a linear chiral extrapolation as with the heavy-light masses. In figure 4.13 the chiral extrapolation is plotted. The χ^2 squared is rather high, but the linear fit appears to work well. The data for the chiral extrapolations is listed in table C.26.

Figure 4.12: The ratio of $C_{AP}^{LS}(t)/C_{PP}^{SS}(t)$ vs time with $\kappa_H = 0.1233$ and $\kappa_L = 0.1346$. The solid line is the tanh M dependence. Plot (a) shows the ratio over all timeslices, plot (b) is a close up of the fit range.

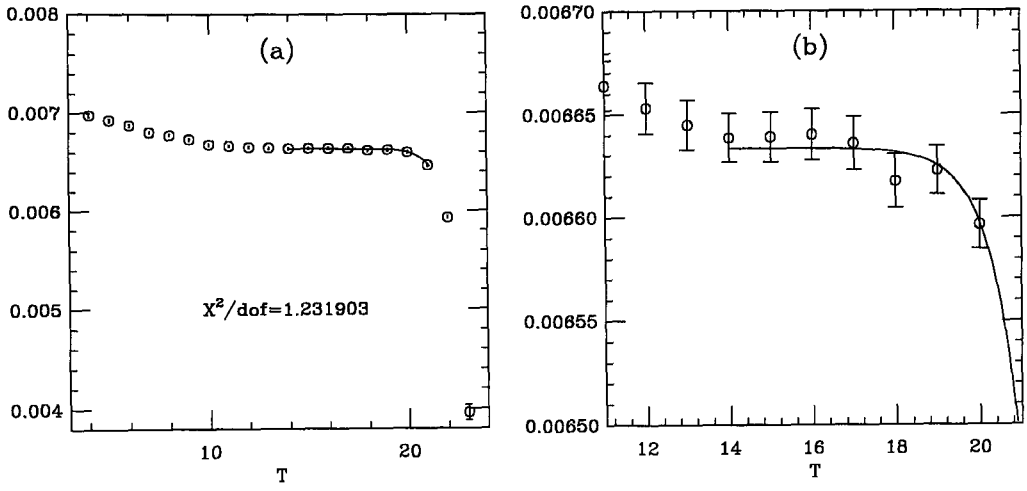

Figure 4.13: Linear chiral extrapolation of the pseudoscalar decay constant, $\kappa_H = 0.1233$.

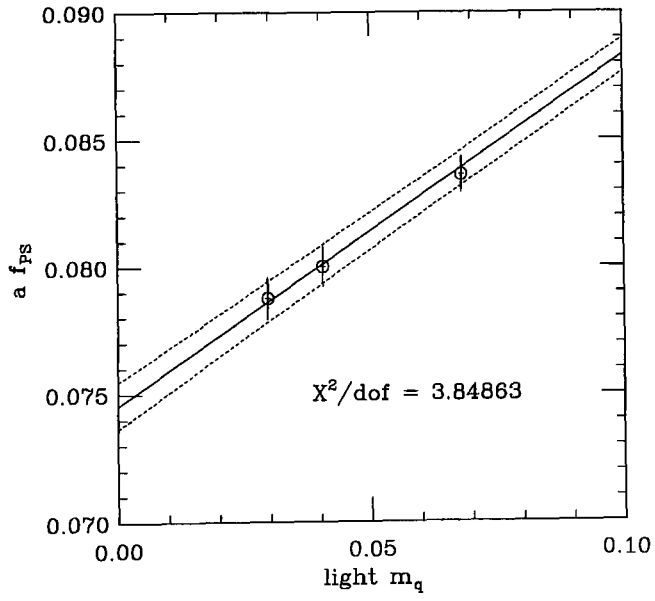

The definition of the lattice spacing will affect the final answer. Once again the lattice spacing is fixed from m_ρ and change in the value of f_P when the lattice spacing is fixed from r_0 is considered an estimate of the systematic error. The results for the pseudoscalar decay constant are

$$f_D = 194^{+2}_{-2\ \text{stat}}\ ^{+19}_{-\ 6\ \text{sys}}\ \text{MeV} \tag{4.65}$$

$$f_{D_s} = 220^{+2}_{-2\ \text{stat}}\ ^{+22}_{-\ 7\ \text{sys}}\ \text{MeV}. \tag{4.66}$$

The $SU(3)$ breaking ratio is then,

$$\frac{f_{D_s}}{f_D} = 1.14^{+3}_{-3}. \tag{4.67}$$

The systematic errors arising from the uncertainty in the lattice spacing are believed to cancel in such a ratio.

Experimental measures of f_D are only recently reported so it is also constructive to compare these results with other calculations. The experimental number quoted for f_{D_s} [67] is

$$f_{D_s} = 254 \pm 31\ \text{MeV}. \tag{4.68}$$

This certainly in agreement with this calculation. There have been many calculations of the pseudoscalar decay constant. Two recent reviews of lattice calculations report on several calculations of the decay constants and quote an 'averaged' figure. The first [68] reports

$$\begin{aligned} f_D &= 191^{+19}_{-28}\ \text{MeV} \\ f_{D_s} &= 206^{+18}_{-28}\ \text{MeV} \\ \frac{f_{D_s}}{f_D} &= 1.08 \pm 8. \end{aligned} \tag{4.69}$$

The second [69] reports

$$\begin{aligned} f_D &= 200 \pm 30\ \text{MeV} \\ f_{D_s} &= 220 \pm 30\ \text{MeV} \\ \frac{f_{D_s}}{f_D} &= 1.10 \pm 8. \end{aligned} \tag{4.70}$$

This calculation lies in the middle of these quoted values. Finally it is worth comparing with a recent calculation [70] which uses the same non-perturbative

action, although they quote a value of b_A slightly different as they have used a boosted coupling. The overall effect is small.

$$\begin{aligned} f_D &= 211 \pm 14^{+\ 0}_{-12}\ \text{MeV} \\ f_{D_s} &= 231 \pm 12^{+6}_{-1}\ \text{MeV} \\ \frac{f_{D_s}}{f_D} &= 1.10 \pm 2. \end{aligned} \tag{4.71}$$

As one would expect, the agreement here is excellent.

4.8 The Vector Decay Constant

The vector decay constant defined in equation 1.62 can be measured on the lattice by considering the ratio of two-point functions with different smearing combinations. Defining this ratio as

$$\frac{C^{LS}_{VV}(t)}{C^{SS}_{VV}(t)} = \frac{\sum_{\vec{x}} e^{-ip\vec{x}} \left\langle 0 \middle| V^L_\mu(x) V^{\dagger S}_\nu(0) \middle| 0 \right\rangle}{\sum_{\vec{x}} e^{-ip\vec{x}} \left\langle 0 \middle| V^S_\mu(x) V^{\dagger S}_\nu(0) \middle| 0 \right\rangle}. \tag{4.72}$$

Only the spatial components are considered as the temporal component has no overlap with the vector state. Considering the asymptotic time behaviour of the correlation functions, the ratio becomes

$$\frac{C^{LS}_{VV}(t)}{C^{SS}_{VV}(t)} = \frac{\sum_j \left\langle 0 \middle| V^j_\mu \middle| V(\epsilon, \vec{p}) \right\rangle \epsilon^j_\nu}{-3Z^S_V}, \tag{4.73}$$

where Z_V is defined in equation 4.29. Inserting the vector decay constant into this expression gives,

$$\frac{C^{LS}_{VV}(t)}{C^{SS}_{VV}(t)} = -\sum_j \epsilon^j_\mu \epsilon^j_\nu \frac{M_V^2}{3Z^S_V f_V}. \tag{4.74}$$

Recalling the massive vector polarisation sum given by equation 4.30, the ratio can be written

$$\frac{C^{LS}_{VV}(t)}{C^{SS}_{VV}(t)} = \frac{M_V^2}{Z^S_V f_V}. \tag{4.75}$$

The vector mass and amplitude can be measured from the two-point functions, leaving f_V as the only unknown.

The vector current must be improved and renormalised. At zero momentum, the improved spatial vector current is given by

$$Z_V^{\rm eff} V_i^{(I)} = Z_V^{\rm eff} \left(V_i + a c_V \partial_4 T_{i4} \right), \tag{4.76}$$

where the derivative can again be written as a four-momentum and c_V is defined in equation 4.3. The renormalisation constant is defined in equation 4.18.

Figure 4.14: The ratio of $C_{VV}^{LS}(t)/C_{PP}^{SS}(t)$ vs time. The line is a fit to a plateau in the range 15-23.

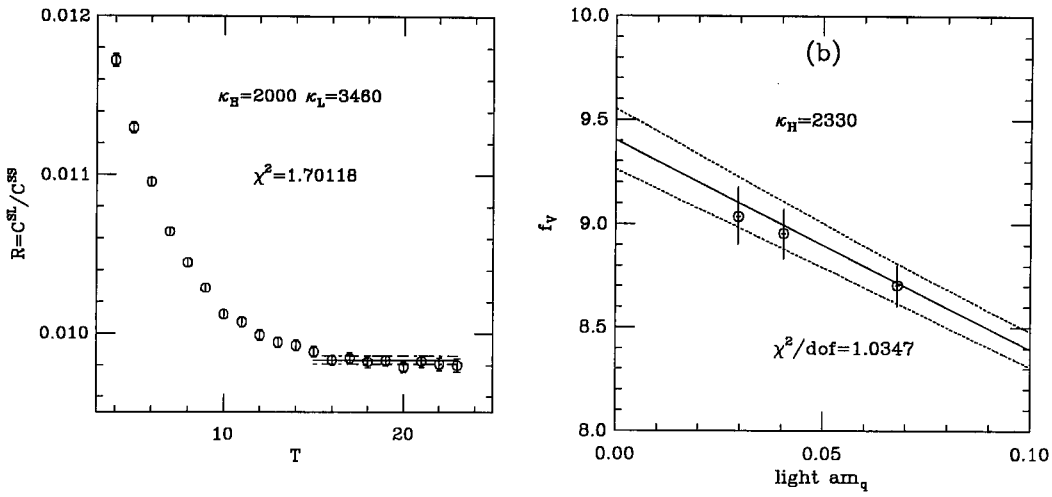

The fit range is determined by examining the time behaviour of the ratio. In figure 4.14(a) the ratio is plotted to see for what range the asymptotic behaviour is valid. The heavy-light vector decay constants for all κ combinations are fitted in the range 15-23 and are listed in table C.27.

The light quark mass dependence of f_V, as with all heavy-light meson quantities is modelled by a linear function. In figure 4.14(b) the chiral extrapolation of f_V is plotted. The fit appears reasonable and χ^2 is close to one. The results for the chiral extrapolation are listed in table C.28.

The same procedure as before of using different measures of the lattice spacing to estimate the systematic errors is used. The value of the charm quark mass is taken to be $\kappa_c = 0.1233$. After applying the renormalisations given by equation

4.47 and equation 4.50 the results are,

$$\begin{aligned} f_{D^\star} &= 9.40^{+15}_{-17\ \text{stat}}{}^{+59}_{-59\ \text{sys}} \\ f_{D_s^\star} &= 8.68^{+\ 9}_{-10\ \text{stat}}{}^{+50}_{-50\ \text{sys}}. \end{aligned} \tag{4.77}$$

The systematic errors here are quite large as the decay constant has a strong dependence on the heavy quark mass (table C.28).

There are only two other calculations with which to compare. A previous UKQCD calculation [71] yields,

$$f_{D^\star} = 9.09^{+41}_{-41\ \text{stat}}{}^{+300}_{-\ 41\ \text{sys}}. \tag{4.78}$$

This result on 60 configurations at $\beta = 6.2$ with the Sheikholeslami-Wohlert action with $c_{SW} = 1$, is in reasonable agreement, even without the large error bars. The other calculation [70], as discussed in the previous section has the same non-perturbative action. They use a different definition of f_V, similar to f_P. Converting their definition to the one used in this calculation, their result is

$$\begin{aligned} f_{D^\star} &= 8.14^{+81}_{-81\ \text{stat}}{}^{+6}_{-0\ \text{sys}} \\ f_{D_s^\star} &= 7.76^{+64}_{-64\ \text{stat}}{}^{+57}_{-0\ \text{sys}}. \end{aligned} \tag{4.79}$$

These results agree within large errors. It is perhaps a little surprising that the central values are not so close, but give the size of the uncertainties, there is still good agreement.

Chapter 5

Results For B mesons

5.1 Form Factors For $B \to \pi$

In order to calculate the form factors at the B meson scale, the form factors are calculated at several different values of κ_H around charm. HQET is then used to motivate the form of the extrapolation to the B meson scale. In equation 3.25 a new kinematic variable, $v \cdot k$, is defined. The scaling of the form factors in equation 3.31 is then motivated *at fixed* $v \cdot k$.

$$\begin{aligned} v \cdot k &= \frac{m_B^2 + m_\pi^2 - q^2}{2m_B} \\ &= \frac{E_B E_\pi - \vec{p} \cdot \vec{k}}{m_B}. \end{aligned} \tag{5.1}$$

If momentum channels with $\vec{p} \cdot \vec{k} = 0$ are chosen then,

$$v \cdot k = E_\pi \left(1 + \frac{\vec{p}^{\,2}}{2m_B^2} + \cdots\right). \tag{5.2}$$

Then $v \cdot k$ is independent of m_B when the heavy quark is at rest and the light meson momentum is fixed. This means that channels 3 and 6 in table 4.5 cannot be used as they have $\vec{p} \cdot \vec{k} \neq 0$. There are two sets of channels that have $\vec{p} \cdot \vec{k} = 0$ and $\left|\vec{k}\right| = \sqrt{2}$ in table 4.2 and table 4.3. These are are very noisy channels, because of the high values of momentum in the final state. They also have lower q^2 than the other channels and so they do not constrain the q^2 behaviour of the

form factors for the decays of D mesons. For this reason they are not included in the analysis of the D decays. The situation is different for the form factors of B decays, as the q^2 is very high after extrapolating to the B scale, so the lower values of q^2 are advantageous.

Table 5.1: Momentum channels for the decays of B mesons. Momenta are in lattice units of $12/a\pi$.

chan	momentum			$v \cdot k$ for κ_H				$(v \cdot k)_{\text{ave}}$	$q^2\|_{m_B}$
	$\vec{p}^{\,2}$	$\vec{q}^{\,2}$	$\vec{k}^{\,2}$	0.1200	0.1233	0.1266	0.1299		
1	0	0	0	0	0	0	0	0	3.99
2	0	1	1	0.262	0.262	0.262	0.262	0.262	2.95
3	0	2	2	0.370	0.370	0.370	0.370	0.370	2.52
4	1	1	0	0	0	0	0	0	3.99
5	1	2	1	0.276	0.280	0.288	0.306	0.288	2.94
6	1	3	2	0.390	0.397	0.408	0.432	0.407	2.51

Table 5.1 shows the values of $v \cdot k$ and q^2 for each momentum channel used. Channels 5 and 6 have a change in the value of $v \cdot k$ which is about 10% over the range of kappa values. This is comparable with the other systematic errors in the calculation from discretisation, quenching etc, so they are included.

The fit ranges of these extra channels have to be chosen carefully due to their noisy nature. Recall from equation 4.7 that in the ratio of the three-point function over the two-point functions all the time dependence cancels once the correlations have reached their asymptotic values, leaving only the ratio of the matrix element in question and matrix elements known from two point functions. Figure 5.1 shows the spatial and temporal ratios for channel 6. It is hard to extract any reliable signal from the spatial component. The temporal component has a peak close to $T = 0$ followed by a 'shoulder'. The fit range is chosen so that the fit is to the shoulder. The initial peak is believed to be a false plateau. This can be seen by considering the behaviour of the light-light two-point function in figure 5.2. It is not clear that the ground state dominates before time slice 9 or 10. This is later than for zero momentum channels. The false peak in the ratio could be coming from contamination due to excited states. For this reason the fit

Figure 5.1: The (a)spatial and (b) temporal ratio for kappa combination $\kappa_H = 2330$, $\kappa_A = \kappa_P = 3460$ momentum channel 6

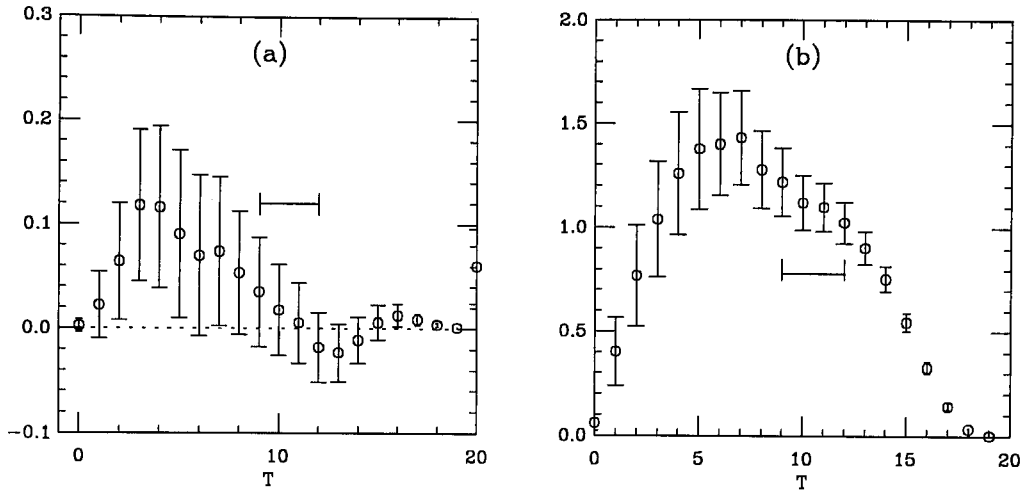

range is chosen to be 9-12 for channels 3 and 6. The results of the fits are listed in table C.7 - table C.24.

Figure 5.2: Effective mass plot for heavy-light pseudoscalar meson. $p^2 = 2$. The solid line is the dispersion relation mass.

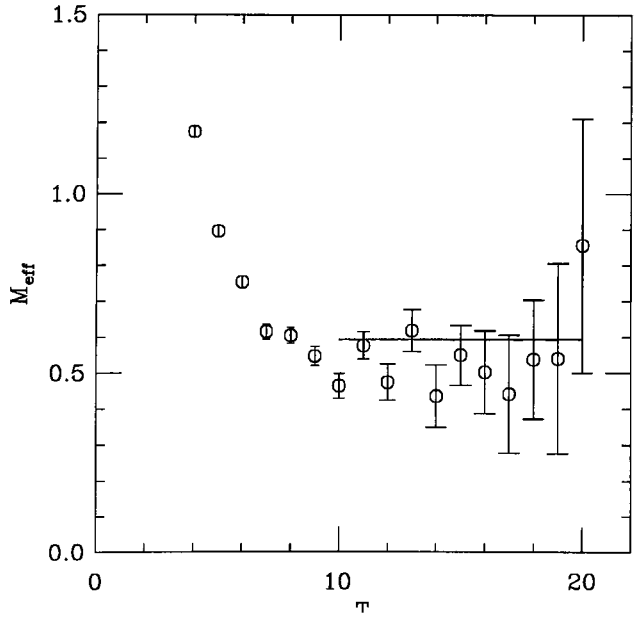

The chiral extrapolations of extra channels proceed as described in section 4.5.1. The results for the chiral extrapolations are displayed in table C.29 to table C.36.

In Chapter 3 the dependence of the matrix elements and form factors on heavy quark mass was discussed. Rather than use the pseudoscalar mass to set the value of κ which corresponds to the mass of the b quark, the extrapolation to the B meson scale is done directly in the inverse of the pseudoscalar mass The physical B meson mass is [53],

$$m_B = 5.2792 \pm 0.0018 \text{ GeV}. \tag{5.3}$$

From equation 3.31, the scaling of the form factors is known. This suggests the following form for the heavy extrapolations at fixed $v \cdot k$

$$\begin{aligned} \frac{C_1(M_P) f_+(q^2)}{\sqrt{M_P}} &= \begin{cases} \gamma_+ \left(1 + \frac{\delta_+}{M_P}\right) & \text{Linear} \\ \gamma_+ \left(1 + \frac{\delta_+}{M_P} + \frac{\epsilon_+}{M_P^2}\right) & \text{Quadratic} \end{cases} \\ C_1(M_P) f_0(q^2) \sqrt{M_P} &= \begin{cases} \gamma_0 \left(1 + \frac{\delta_0}{M_P}\right) & \text{Linear} \\ \gamma_0 \left(1 + \frac{\delta_0}{M_P} + \frac{\epsilon_0}{M_P^2}\right) & \text{Quadratic} \end{cases} \end{aligned} \tag{5.4}$$

where $C_1(M_P)$ is defined in equation 3.22. To one loop, α_s is given by,

$$\alpha_s(M_P) = \frac{4\pi}{\beta_0 \ln(M_P/\Lambda)^2} \tag{5.5}$$

The value of Λ_{QCD} is taken from [72], for four flavours. In the $\bar{M}S$ scheme,

$$\Lambda = 295^{+95}_{-80} \text{ MeV} \tag{5.6}$$

and $\beta_0 = 11$ for quenched QCD. The same reference quotes

$$\Lambda = 210^{+80}_{-65} \text{ MeV} \tag{5.7}$$

for five flavours. If this values is used then the value of C_1 differs by about 2% around the D mass scale. The other uncertainties in the extrapolations are larger than this multiplicative factor.

As previously mentioned the form factors must be renormalised. The value of κ which corresponds to the b quark mass is not known. Therefore the non-perturbative expression for Z_V^{eff} cannot be used. The form factors are therefore

renormalised before the extrapolation. For each heavy kappa, using equation 4.47,

$$Z_V^{\text{eff}} = Z_V \left(1 + b_V a \frac{1}{2} m_H\right). \tag{5.8}$$

The factor of a half comes from taking the average quark mass of the heavy and chiral quark. Then,

$$\begin{aligned} Z_V^{\text{eff}}(\kappa_H = 0.1299) &= 0.887 \\ Z_V^{\text{eff}}(\kappa_H = 0.1266) &= 0.943 \\ Z_V^{\text{eff}}(\kappa_H = 0.1233) &= 1.002 \\ Z_V^{\text{eff}}(\kappa_H = 0.1200) &= 1.064. \end{aligned} \tag{5.9}$$

Table 5.2: $f_+(q^2)$ for $B \to \pi$.

mom	q^2	Linear		Quadratic	
		$f_+(q^2)$	χ^2/dof	$f_+(q^2)$	χ^2/dof
2	2.95149	1.51^{+8}_{-10}	0.00379181/2	1.49^{+21}_{-20}	0.00251162/1
3	2.51780	1.05^{+18}_{-21}	0.0111033/2	1.13^{+40}_{-43}	0.00828925/1
4	3.99848	3.22^{+16}_{-21}	2.85936/2	4.84^{+36}_{-61}	0.321782/1
5	2.94255	1.66^{+16}_{-28}	0.0701752/2	1.89^{+58}_{-41}	0.0249573/1
6	2.50517	1.55^{+37}_{-48}	0.93291/2	3.62^{+100}_{-153}	0.0335135/1

Table 5.3: $f_0(q^2)$ for $B \to \pi$.

mom	q^2	Linear		Quadratic	
		$f_0(q^2)$	χ^2/dof	$f_0(q^2)$	χ^2/dof
1	3.99848	$0.78^{+\ 3}_{-\ 4}$	1/2	$0.74^{+10}_{-\ 5}$	1/1
2	2.95149	$0.55^{+\ 3}_{-\ 4}$	0.0251982/2	$0.56^{+\ 5}_{-\ 6}$	0.0200793/1
3	2.51780	$0.61^{+\ 9}_{-12}$	0.17009/2	0.81^{+18}_{-23}	0.00243446/1
4	3.99848	0.78^{+20}_{-35}	0.999799/2	0.93^{+38}_{-76}	0.0803181/1
5	2.94255	0.55^{+47}_{-58}	0.0475617/2	0.58^{+19}_{-11}	0.0401551/1
6	2.50517	0.74^{+19}_{-26}	0.754674/2	1.85^{+52}_{-79}	0.00616235/1

For each momentum, that is for fixed $v \cdot k$, a linear and a quadratic extrapolation is performed. For all channels except 4 and 7, the results of the linear

and the quadratic extrapolations agree, the quadratic extrapolations giving larger statistical errors. This can be seen in figure 5.3(a) and figure 5.3(b). The extrapolations of $f_+(q^2)$ and $f_0(q^2)$ are plotted. The effect of the quadratic extrapolation is essentially larger error bars. It is harder to extract a signal from the ratios for Channels 4 and 7 (figure 4.8(b) and figure 5.1). This could explain the seemingly different dependence on heavy quark mass. Figure 5.3(c) shows the extrapolation of $f_0(q^2)$ for channel 1. The linear and quadratic fits agree. Figure 5.3(d) shows $f_0(q^2)$ for channel 4. here there is a difference between linear and quadratic which is not large given the size of the errors. Channels 1 and 4 have the same momentum transfer, so the form factors should have the same value. The linear extrapolation of channel 4 agrees with both the linear and quadratic extrapolation of channel 1. Figure 5.3(e) and (f) show the extrapolations for $f_+(q^2)$ for channels 2 and 6. For channel 6 the result of the quadratic extrapolation nearly agrees with the linear due to huge error bars. Channels 2 and 6 also have the same momentum transfer, and so should agree. The linear extrapolation of channel 6 agrees with the linear and quadratic extrapolation of channel 2. The form of the heavy extrapolation is thus chosen to be linear. The results of both linear and quadratic extrapolations are listed in table 5.2 and table 5.3.

Figure 5.3: Extrapolation of Form Factors to the B meson scale. The burst points are the extrapolated data.

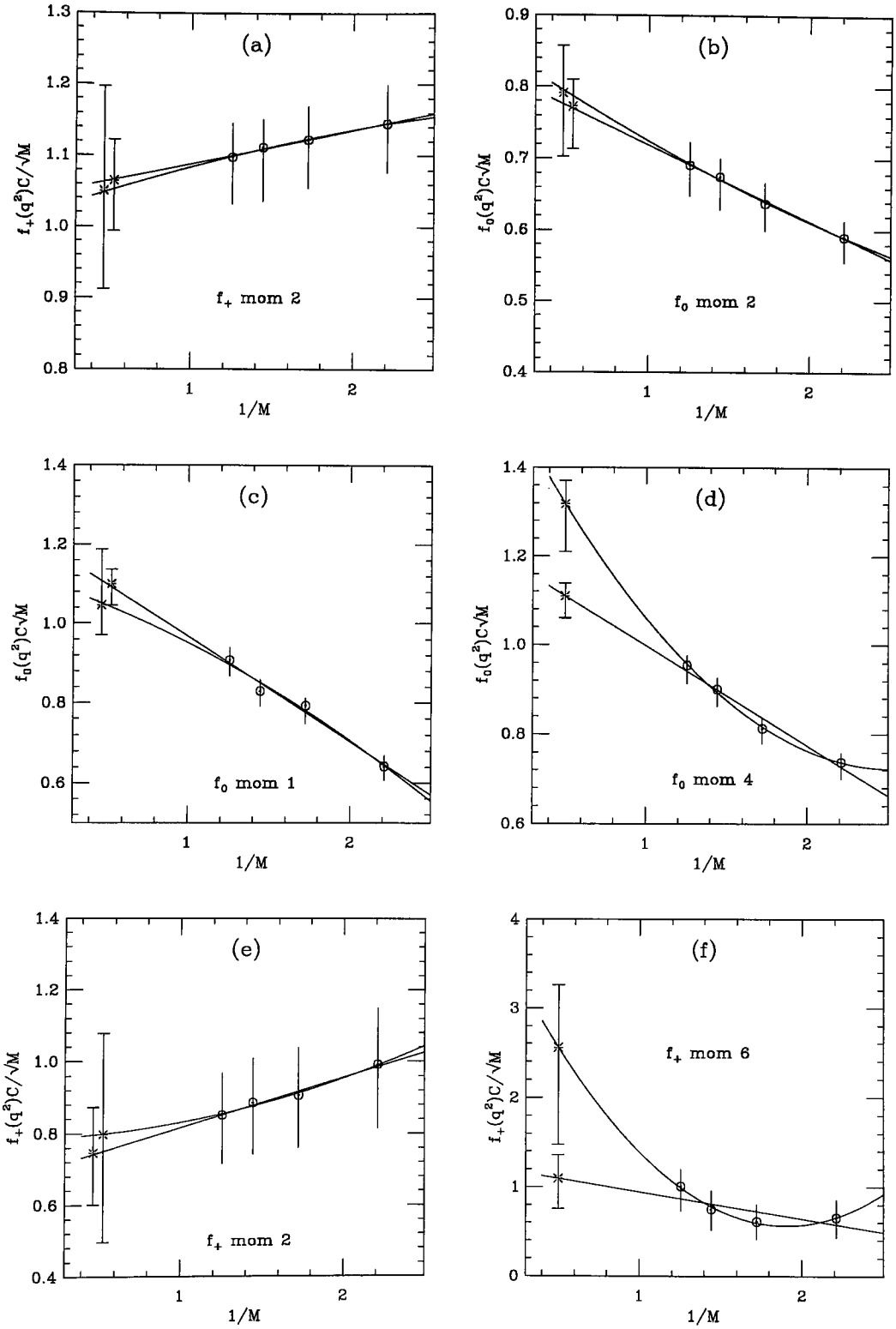

5.2 Momentum Dependence and V_{ub}

In order to try and measure the form factors at $q^2 = 0$ some form of the momentum dependence must be motivated. Pole dominance models can be combined with HQET to suggest the form of the momentum dependence [73].

Pole dominance models suggest

$$f(q^2) = \frac{f(0)}{(1 - q^2/M_f^2)^{n_f}}, \tag{5.10}$$

where f is either f_+ or f_0, n_f is the power of the pole, and M_f is equal to the mass, M, used to scale the form factors plus some $1/M$ correction. That is

$$M_f = M\left(1 + \frac{\alpha_f}{M} + \cdots\right) \tag{5.11}$$

For a large M,

$$\begin{aligned} 1 - q^2_{\max}/M_f^2 &= 1 - \left(\frac{M}{M + \alpha_f}\right)^2 \\ &= 1 - 1 + \frac{2\alpha_f}{M} + \cdots \end{aligned} \tag{5.12}$$

The form factors then have the following behaviour

$$f(q^2) \sim f(0)\left(\frac{M}{\alpha_f}\right)^{n_f}. \tag{5.13}$$

The scaling relations for the form factors, equation 3.31 then imply

$$n_{f_+} = n_{f_0} + 1 \tag{5.14}$$

That is the degree of the pole for $f_+(q^2)$ is one greater than for $f_0(q^2)$, so the momentum dependence is for a pole/constant, dipole/pole for $f_+(q^2)$ and $f_0(q^2)$. The kinematic constraint,

$$f_+(0) = f_0(0) \tag{5.15}$$

can be used to further model the q^2 dependence.

A 'quartic' parameterisation can also be used to model the q^2 behaviour

$$f(q^2) = \frac{f(0)}{1 - \alpha_f q^2/M^2 + \beta_f (q^2/M^2)^2}. \tag{5.16}$$

Here the mass of the pole is fixed to be m_B and $f(0)$, α_f and β_f are free parameters. It also uses the constraint equation 5.15.

Fits to unconstrained pole/constant are shown in figure 5.4(a) and fits to unconstrained dipole/pole are shown in figure 5.4(b). It is clear that the $f_0(q^2)$ has some curvature in q^2 and so the dipole/ pole fits are clearly better. This is born out in the fit results, table 5.4. There is no Q value quoted for the constant fit to $f_0(q^2)$ as this essentially fails to fit the data.

Figure 5.4: Momentum dependence of form factors. (a) $f_+(q^2)$ pole, $f_0(q^2)$ constant, (b) $f_+(q^2)$ dipole, $f_0(q^2)$ pole.

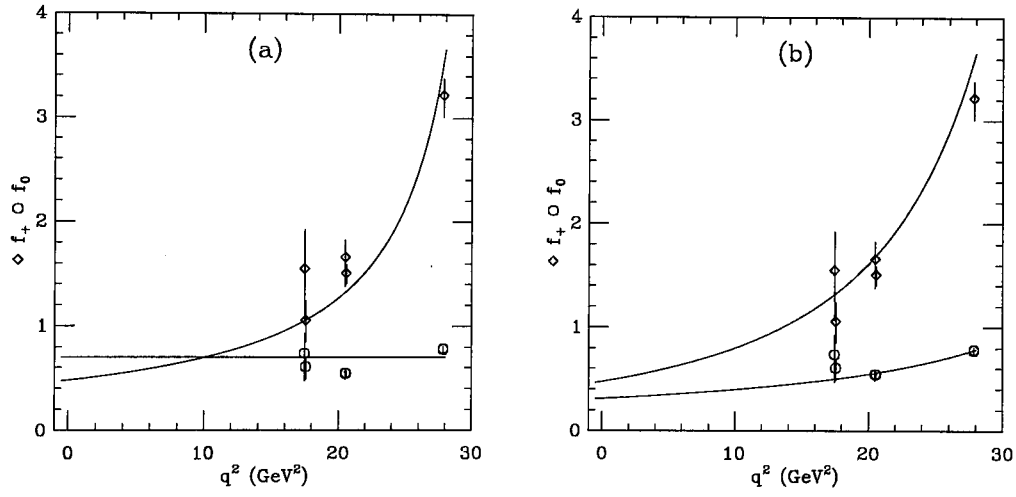

Table 5.4: Fit results for momentum dependence of form factors.

fit type	$f(0)$	M_{f+} GeV	M_{f^0} GeV	χ^2/dof	Q
$f_+(q^2)$ pole	0.481^{+14}_{-9}	5.685^{+3}_{-2}	N/A	3.47046	0.015374
$f_0(q^2)$ const	0.697^{+14}_{-27}	N/A	N/A	11.1618	-
$f_+(q^2)$ dipole	0.427^{+49}_{-59}	6.62^{+14}_{-14}	N/A	0.845067	0.429529
$f_0(q^2)$ pole	0.312^{+37}_{-44}	N/A	6.81^{+33}_{-30}	0.812792	0.486531
pole/const	0.689^{+1}_{-1}	6.177^{+1}_{-1}	N/A	6.70643	-
dipole/pole	0.330^{+41}_{-28}	6.37^{+6}_{-10}	6.96^{+36}_{-20}	1.18478	0.303571

Figure 5.5 shows the constrained fits for (a) pole/constant and (b) dipole/pole. The results are also displayed in table 5.4. The preferred fit is the dipole/pole.

Figure 5.5: Momentum dependence of form factors. (a) $f_+(q^2)$ pole, $f_0(q^2)$ constant, (b) $f_+(q^2)$ dipole, $f_0(q^2)$ pole with $f_0(0) = f_+(0)$.

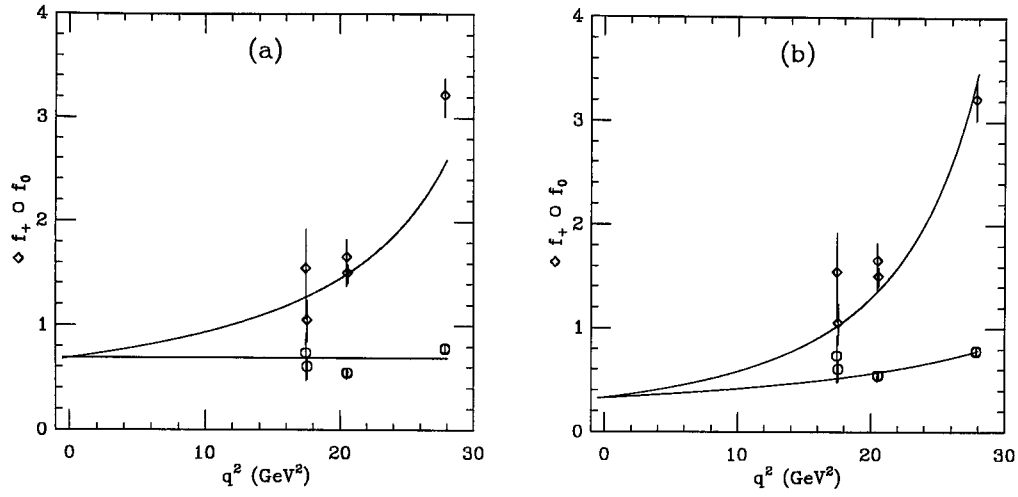

The quartic parameterisation cannot be fitted to the data with the mass fixed at the B meson mass. This can be seen in figure 5.6. The solid lines are the fit to the data. Clearly this does not work well. The B meson mass is significantly smaller than the masses that are free parameters of the pole dominance fits. In [74] Light Cone Sum Rules (LCSR) are used to calculate the form factors for $q^2 < 20$ GeV^2. This data is then fitted to the quartic parameterisation in equation 5.16. The dashed lines in figure 5.6 are the results of this fit. As can be seen, they diverge around $q^2 = 20$ Gev^2.

An estimate of the systematic error can be obtained from the difference between the constrained and unconstrained fits to the dipole/pole for $f_+(q^2)$ and $f_0(q^2)$. The results for the q^2 behaviour of the form factors are then

$$\begin{aligned} f(0) &= 0.33^{+4}_{-3\ \text{stat}}\ ^{+10}_{-\ 2\ \text{sys}} \\ m_{f+} &= 6.37^{+\ 6}_{-10\ \text{stat}}\ ^{+25}_{-25\ \text{sys}}\ \text{GeV} \\ m_{f^0} &= 6.96^{+36}_{-20\ \text{stat}}\ ^{+15}_{-15\ \text{sys}}\ \text{GeV} \end{aligned} \tag{5.17}$$

The decay rate for $B \to \pi$ is given by the expression [75]

$$\Gamma(B \to \pi l^- \nu_l) = \frac{G_F^2 \left|V_{\text{ub}}\right|^2}{192\pi^2 m_B^3} \int_0^{(m_B - m_\pi)^2} dq^2 [\lambda(q^2)]^{3/2} \left|f_+(q^2)\right|^2, \tag{5.18}$$

Figure 5.6: Momentum dependence of form factors, quartic model

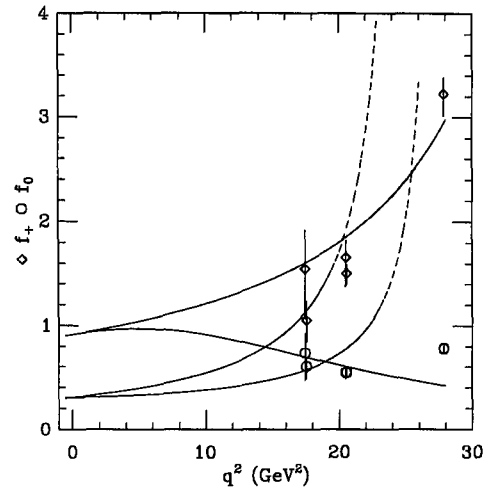

where λ is a kinetic factor given by,

$$\lambda(q^2) = (m_B^2 + m_\pi^2 - q^2)^2 - 4m_B^2 m_\pi^2. \tag{5.19}$$

However, all results have been presented after extrapolating to the chiral limit, $m_\pi \to 0$. This simplies the integral significantly. Whilst the pion has non-zero mass it is certainly small compared to the mass of the B meson, and so any error coming from this procedure is smaller than the other systematic uncertainties in the calculation.

The result for the decay rate is then

$$\frac{\Gamma}{|V_{\rm ub}|^2} = 16.9^{+2.4}_{-1.2\ \rm stat}\ ^{+4.7}_{-1.6\ \rm sys}\ 10^{12}\ \rm s^{-1}. \tag{5.20}$$

This is somewhat larger than a previous UKQCD calculation [73]. However, the previous UKQCD calculation did not extrapolate the light quark masses to the chiral limit. This makes a large difference to the range of q^2 (in lattice units) that the form factors are evaluated on, and this could well account for the discrepancy.

This decay rate has recently been measured. In [53] the branching ratio for $B \to \pi l \nu_l$ is given as

$$Br = 1.8^{+0.6}_{-0.6}\ 10^{-4}, \tag{5.21}$$

and the mean life of

$$\tau(B) = 1.56\ 10^{-12}\ \text{s}. \tag{5.22}$$

By comparing the experimental decay rate with the calculation of the decay rate the value of V_{ub} can be extracted.

$$V_{\text{ub}} = 0.0026^{+1}_{-2\ \text{stat}}\ {}^{+1}_{-3\ \text{sys}}\ {}^{+4}_{-5\ \text{exp}}. \tag{5.23}$$

This compares very well with, but is much more accurate than the world average given in [53] of

$$V_{\text{ub}} = 0.0018 - 0.0045. \tag{5.24}$$

5.3 The Pseudoscalar Decay Constant

In the static limit the scaling of the pseudoscalar decay constant is given by equation 3.33. This suggests that a $1/M_P$ expansion for the extrapolation to the B meson scale is

$$C_1(M_P) f_P \sqrt{M_P} = \begin{cases} \gamma\left(1 + \frac{\delta}{M_P}\right) & \text{Linear} \\ \gamma\left(1 + \frac{\delta}{M_P} + \frac{\epsilon}{M_P^2}\right) & \text{Quadratic} \end{cases} \tag{5.25}$$

where $C_1(M_P)$ is the logarithmic matching factor given in equation 3.22 and equation 5.5. The data for the heavy-light pseudoscalar decay constant is listed in table C.26. As with the form factors the decay constant has to be renormalised before the extrapolation,

$$Z_A^{\text{eff}} = Z_A\left(1 + b_A a \frac{1}{2} m_H\right). \tag{5.26}$$

where Z_A and b_A are determined by the Alpha Collaboration and are given by equation 4.63 and equation 4.64

Figure 5.7 shows the extrapolation of the pseudoscalar decay constant. The statistical uncertainties in f_P are much smaller than those of the form factors. This obviously constrains the fit much more, and a quadratic fit has a smaller χ^2 in table 5.5. This is reinforced by the figure where there is definite curvature in f_P. The quadratic fit and the linear fit disagree by several σ. This is opposite

Figure 5.7: Extrapolation of the pseudoscalar decay constant to the B meson scale. The solid line is a quadratic fit to all points, the dotted line a linear fit to the heaviest three data points. The burst points are at the B meson scale

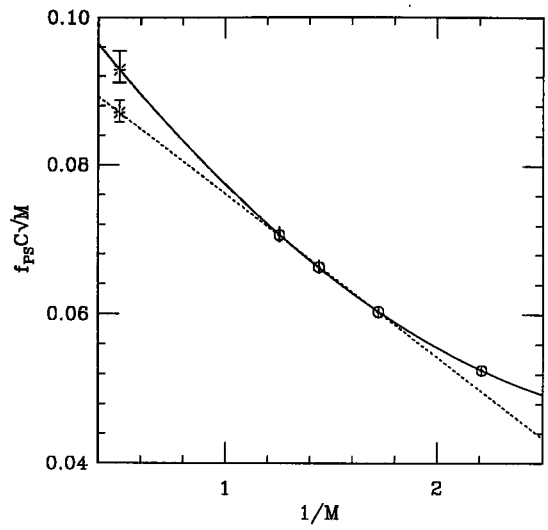

Table 5.5: The pseudoscalar decay constant at the B meson scale

fit	f_B MeV	χ^2/dof	Q
Quadratic	174^{+5}_{-3}	0.0275514/1	0.868168
Linear 4	156^{+3}_{-2}	2.16851/2	0.338154
Linear 3	163^{+3}_{-2}	0.0175467/1	0.894617

to the case for the form factors. The quadratic fit is preferred. The dotted line is a linear fit to the heaviest three data points. The difference can be used to estimate the systematic uncertainty.

The pseudoscalar decay constant for f_{B_s} can be extrapolated in a similar fashion. Figure 5.8 shows f_B and f_{B_s} together. They both have a similar curvature, although f_{B_s} is slowly growing away from f_B. From the figure it can be seen that they have the same dependence on the heavy pseudoscalar mass. The value for f_{B_s} is then

$$f_{B_s} = 208^{+3}_{-2} \text{ MeV} \quad \chi^2/dof = 0.0746877 \quad Q = 0.963345. \tag{5.27}$$

Figure 5.8: Extrapolation of f_B and f_{B_S}. The burst points are the decay constants at the B and B_s mass scale.

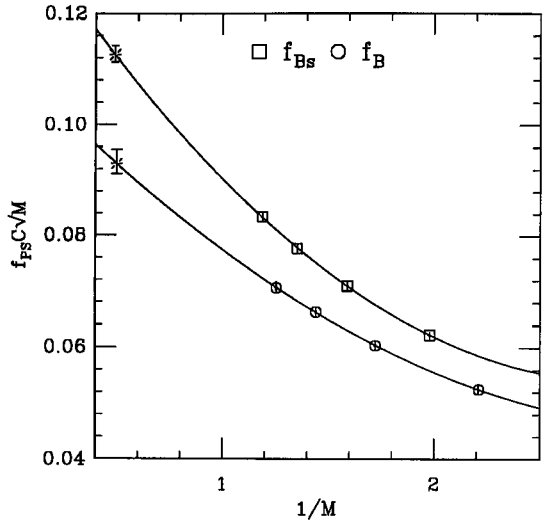

The lattice spacing has been set by m_ρ. Choosing the lattice spacing set by r_0 will give a different result. Using this, as well as the linear fit to the heaviest 3 data point to estimate the systematic uncertainties gives the following results.

$$\begin{aligned} f_B &= 174^{+5}_{-3\ \text{stat}}\ ^{+17}_{-11\ \text{sys}}\ \text{MeV} \\ f_{B_s} &= 208^{+3}_{-2\ \text{stat}}\ ^{+20}_{-13\ \text{sys}}\ \text{MeV}. \end{aligned} \tag{5.28}$$

The $SU(3)$ flavour breaking ratio can then be evaluated.

$$\frac{f_{B_s}}{f_B} = 1.20^{+4}_{-2}. \tag{5.29}$$

These values can be compared with other calculations of f_B. In particular comparison with the same two reviews as quoted in chapter four, the first quoted [68]

$$\begin{aligned} f_B &= 172^{+27}_{-31}\ \text{MeV} \\ \frac{f_{B_s}}{f_B} &= 1.14 \pm 8. \end{aligned} \tag{5.30}$$

and the second [69]

$$f_B = 175 \pm 35\text{MeV}$$

$$\begin{aligned} f_{B_s} &= 195 \pm 35\text{MeV} \\ \frac{f_{B_s}}{f_B} &= 1.14 \pm 8. \end{aligned} \tag{5.31}$$

This calculation is certainly in good agreement with both these reviews. The ratio is slightly higher, but agrees within errors. Again this calculation can be compared with [70],

$$\begin{aligned} f_B &= 179 \pm 19^{+26}_{-9}\text{MeV} \\ f_{B_s} &= 204 \pm 16^{+28}_{-0}\text{MeV} \\ \frac{f_{B_s}}{f_B} &= 1.14 \pm 3^{+0}_{-1}. \end{aligned} \tag{5.32}$$

Again the agreement here is excellent.

5.3.1 The Soft Pion Relation

In chapter three, HQET was used to derive equation 3.59, which should hold at $\mathcal{O}(1/m_b)$. Taking the experimental value for f_π from [53],

$$f_{\pi^0} = 130 \pm 5 \quad f_{\pi^+} = 130.7 \pm 4 \text{ MeV} \tag{5.33}$$

The heavy-light decay constant divided by 130 MeV can then be compared with $f_0(q^2_{\text{max}})$.

In figure 5.9 the heavy extrapolations of both f_B/f_π and f_0 are plotted. It is clear that there is a substantial violation of the soft pion relation. The reason for this is unclear. The value of f_B is a reasonable one and in very good agreement with other calculations. The value of f_π is also reasonably determined. What about f_0? Recall from figure 5.3(d) that it is possible to extrapolate f_0 quadratically. However even this would only give a value of around 1.3 for the quantity plotted, still substantially less than the corresponding f_B/f_π.

Other calculations of the form factors have been made. A preliminary calculation on this data [58] found that the relation held. However, the form of the chiral extrapolation used was flawed. A previous UKQCD calculation of the form factors did not chirally extrapolate the data. Two other recent calculations

Figure 5.9: The Soft Pion Relation for B mesons.

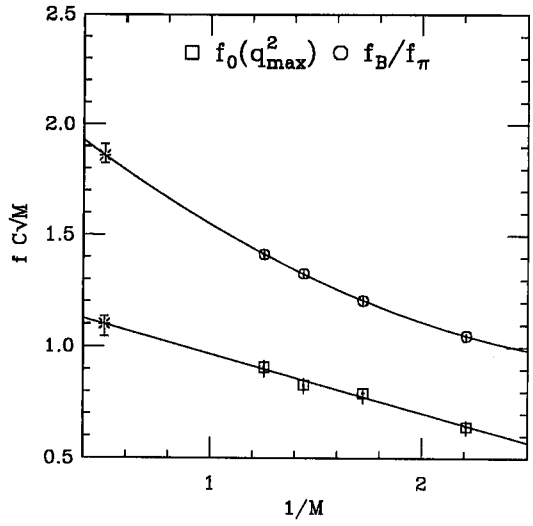

[76, 77] of the form factors and decay constants using different actions and lattice spacings also report large violations of the relation. Possible reasons could be chiral symmetry breaking by the lattice, the systematic uncertainty in the chiral extrapolation, or the breakdown of the soft pion theorem itself in semileptonic decays. Clearly this needs further study.

5.4 The Vector Decay Constant

In chapter three the ratio of the vector and the pseudoscalar decay constants and its scaling with the mass of a heavy meson were defined. Recall equation 3.64,

$$U(M) = \frac{f_V f_P}{M}\left\{1 + \frac{2}{3}\frac{\alpha_s(m_Q)}{\pi} + \mathcal{O}(\frac{1}{m_Q})\right\} \tag{5.34}$$

where M is the spin averaged mass

$$M = \frac{3M_V + M_P}{4}. \tag{5.35}$$

In the static limit $U(\infty) = 1$. To motivate the extrapolation of this quantity, a new variable can be defined.

$$\tilde{U}(M) = \frac{U(M)}{1 + \frac{2}{3}\frac{\alpha_s(m_Q)}{\pi}}. \tag{5.36}$$

Table 5.6: Extrapolation of $U(M)$ to the static limit.

fit	$U(M_B)$	$U(M_\infty)$	χ^2/dof	Q
Linear	0.92^{+2}_{-2}	0.94^{+3}_{-2}	0.204717	0.814878
Quadratic	0.84^{+4}_{-3}	0.77^{+8}_{-7}	0.0531115	0.817735

This is just $U(M)$ divided by the logarithmic corrections where the mass is the spin averaged mass.. The form of the extrapolation is then

$$\tilde{U}(M) = \gamma\left(1 + \frac{\delta}{M} + \frac{\epsilon}{M^2}\right) \tag{5.37}$$

where the ϵ term is dropped for a linear extrapolation.

Figure 5.10: Scaling of U(M)

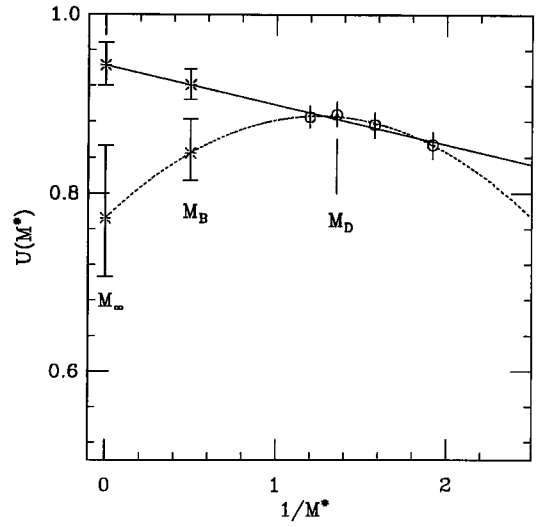

In figure 5.10 both the linear and quadratic extrapolations are shown. The Linear extrapolation is close to the HQS limit of 1. The quadratic fit makes very little difference within the range of the data, but a rather large difference in the static limit. The quadratic fit has rather large errors. Both fits have reasonable χ^2 and Q value. The values of $U(M_B)$ and $U(M_\infty)$ are shown in table 5.6. The linear fit is preferred. The heaviest point has a slight dip in relation to the other points, and it is this that allows negative curvature in the quadratic fit.

The value for $\tilde{U}(M_D)$ is one of the data points and has the value

$$\tilde{U}(M_D) = 0.89^{+1}_{-1} \tag{5.38}$$

Using the figure quoted in equation 5.28, the value of $f_{B^\star}$ can be estimated.

$$f_{B^\star} = 28^{+1}_{-1\ \text{stat}}\ {}^{+3}_{-3\ \text{sys}} \tag{5.39}$$

This central value is from the linear fit and the systematic the difference between the linear and quadratic fit, and the systematic uncertainty in f_B.

These results can again be compared with a previous UKQCD calculation, [71]. The HQS relation is satisfied, for both the linear and quadratic fits. The curvature is positive for their quadratic fit. Quoting the numbers for $\tilde{U}(M)$ for B and D mesons

$$\begin{aligned} \tilde{U}(M_D) &= 0.77^{+2}_{-2} \\ \tilde{U}(M_B) &= 0.93^{+4}_{-3}\ \ (0.96^{+4}_{-5}) \end{aligned} \tag{5.40}$$

where the number in brackets is for the quadratic fit. The value for $\tilde{U}(M_D)$ is significantly lower than for this calculation, but at the B meson scale it is better for the linear fit. The other recent calculation of $f_{B^\star}$, [70], which uses the same action as this calculation sees a similar pattern for the HQS relation, that is negative curvature in the quadratic fit, although the masses are heavier than in this calculation. Converting their definition of f_V to the one used in this calculation gives,

$$f_{B^\star} = 27 \pm 3^{+0.2}_{-4} \tag{5.41}$$

where the first error is statistical and the second systematic. As expected the agreement between the two calculations with the same action is excellent.

Chapter 6

Conclusions

The motivation for this calculation was to reduce the theoretical uncertainties in the CKM matrix elements. The theoretical uncertainties are dominated by non-perturbative strong interaction effects. This thesis demonstrates that lattice gauge theory is an effective tool for the calculation of matrix elements of the semileptonic decays of heavy mesons. One of the least well known CKM matrix elements is $V_{\rm ub}$. The matrix elements relevant to the decay $B \to \pi l \nu_l$ has been calculated. This allows the theoretical decay rate to be computed and compared with experiment. Examining equation 5.23 the statistical uncertainties are around $5-7\%$. The systematic uncertainties are much harder to quantify. Discretisation errors are hard to determine with results for only one lattice spacing and from other calculations systematic errors coming from quenching could be as large as 20%. By varying various quantities this calculation has estimated some of these systematic uncertainties at around 12%. The UKQCD collaboration is currently generating data at a different lattice spacing to try and quantify the a dependence. By far the largest uncertainty in the value of $V_{\rm ub}$ quoted in this thesis comes from experiment, around 20%. This is about to change with measurements from the new B factory experiments. This estimation of $V_{\rm ub}$ compares very well with the 'world average' given in [53]. The aim of this calculation was to reduce the theoretical uncertainties in the extraction of CKM matrix elements. This has been successfully achieved. It is hoped that the decay $B \to \rho l \nu_l$ will constrain $V_{\rm ub}$ further.

It is very important to understand the chiral behaviour of the form factors. The decays of heavy mesons to light mesons are rather violent processes. The momentum 'kick' to the active light quark, and how this affects the remaining light degrees of freedom is certainly a non-perturbative affect. In determining the light hadron spectrum, combinations of 3 light κ's result in 6 effective quark masses in which to extrapolate, usually at zero momentum. In this calculation a flavour symmetry between the active and passive quarks is not assumed. This allows the calculation of the form factors for $D \to Kl\nu_l$. However, the 6 combinations of light κ's then have to be extrapolated in two dimensions to physical quark masses. The data cannot constrain the chiral behaviour to the same degree as the light hadron spectrum. In using a linear dependence of the form factors on the quark mass, the change in the form factor as the chiral limit is approached is small, resulting in the $SU(3)$ flavour breaking ratios for $f_+^\pi(0)/f_+^K(0)$ being close to unity. This agrees very well with experiment. An extra passive kappa would help to examine the chiral behaviour. However this would require an amount of computer time equal to a half what has already been used in generating the three-point correlation functions.

The extrapolation of the form factors to the B meson scale can also contain difficulties. The q^2 of the form factors after the extrapolation are all (relatively) close to $q^2_{\rm max}$ which implies that the mass of the heavy meson dominates $v\cdot k$ and so the value of $v\cdot k$ should not vary greatly. The pseudoscalar decay constant has no ambiguities coming from momentum dependence in either the chiral extrapolation or the scaling to the B meson. The violation of the soft pion theorem is puzzling. Whilst, for instance the renormalisation constant $Z_A^{\rm eff}$ has been calculated with a perturbative value for b_A, the value of f_B/f_π in this calculation is consistent with many other determinations. A quadratic extrapolation in the heavy mass could increase the value of $f_0(q^2_{\rm max})$, but it would have to nearly double to satisfy the soft pion theorem. Other lattice calculations also see large violations of the soft pion theorem. Further study is necessary to determine the cause. Possible reasons include some as yet unknown lattice artifact, a quenching effect or even the break down of the soft pion theorem itself.

The calculation of the form factors, and their momentum dependence allows

the comparison with pole dominance models. This comparison finds the data from this calculation in excellent agreement for $D \to Kl\nu_l$ for both the general behaviour and the masses of the poles. The agreement for $D \to \pi l\nu_l$ is not so good. The masses suggested by pole dominance models are significantly lower than is consistent with these fits. If the chiral behaviour were to increase the value of the form factors at high q^2 then perhaps the comparison would be better. This would boost the value of f_0 before the heavy extrapolation. However, this could spoil the agreement with experiment for the $SU(3)$ flavour breaking ratios described above.

As ever numerical calculations in lattice gauge field theory can always be improved with more data. In this calculation the statistical uncertainties are smaller than the systematic. Calculating the form factors for more quark masses would certainly improve the calculation, this however would be very expensive computationally. As previously mentioned repeating the calculation at several different lattice spacings would allow extrapolation to the continuum limit. Again this is very expensive computationally, however, the UKQCD collaboration is currently generating data at another lattice spacing. There are also other matrix elements that can be calculated from this data set which can be used to further constrain V_{ub}. In particular the form factors for the decay $B \to \rho l\nu_l$ could be calculated. The form factors of the electromagnetic penguin $B \to K^\star\gamma$ should have the same HQS scaling behaviour as the form factors $f_+(q^2)$ and $f_0(q^2)$. Besides being sensitive to new physics, a calculation of the tensor matrix element could be used to check the scaling of the form factors in this calculation. Finally, quenching is potentially a large uncontrolled approximation to full QCD. The UKQCD collaboration is currently generating dynamical fermion gauge configurations. This presents an unparalleled opportunity to calculate these form factors in full QCD.

Appendix A

Grassmann Variables

Consider N anti-commuting Grassmann variables $\{\psi_i\}$ $i = 1, 2, \cdots, N$,

$$\{\psi_i, \psi_j\} = \psi_i\psi_j + \psi_j\psi_i = 0 \tag{A.1}$$

$$\Rightarrow \psi_i^2 = 0 \tag{A.2}$$

and let $f(\psi)$ be some function of the Grassmann variables. Since the Grassmann variables anti-commute, the functions f can only be polynomials of a finite degree

$$f(\psi) = f_0 + \sum_i f_i\psi + \sum_{i\neq j} f_{ij}\psi_i\psi_j + \cdots + f_{12\cdots N}\psi_i\psi_j\cdots\psi_N \tag{A.3}$$

where the f's are complex numbers. Due to the anti-commutation relations there must be two types of differentiation: left and right. The derivative $\partial/\partial\psi_i$ is performed by anti-commuting ψ_i to the left, whence

$$\frac{\partial}{\partial\psi_i}\psi_i = 1. \tag{A.4}$$

Similarly for left differentiation,

$$\psi_i\frac{\overleftarrow{\partial}}{\partial\psi_i} = 1. \tag{A.5}$$

For instance

$$\frac{\partial}{\partial\psi_i}\psi_j\psi_i = -\psi_j = \psi_i\psi_j\frac{\overleftarrow{\partial}}{\partial\psi_i} \tag{A.6}$$

The integration of functions of Grassmann variables is defined by

$$\begin{aligned} \int d\psi_i &= 0 \\ \int d\psi_i \psi_i &= 1 \end{aligned} \tag{A.7}$$

wher the integration measures $\{d\psi_j\}$ anti-commute with themselves and $\{\psi_i\}$

$$\{\psi_i, d\psi_j\} = \{d\psi, d\psi_j\} = 0 \ \forall i, j. \tag{A.8}$$

This results in the peculiar property of Grassmann variables, that differentiation and integration have the same result.

$$\int d\psi_i f(\psi) = \frac{\partial f(\psi)}{\partial \psi_i}. \tag{A.9}$$

Now consider the generalisation to N *pairs* of independent Grassmann variables $\{\bar{\psi}_i, \psi_i\}$ $i = 1, 2, \cdots, N$. In particular consider the following integral, important in quantum field theory,

$$I[M] = \int \prod_{k=1}^{N} [d\bar{\psi}_k d\psi_k] e^{-\sum_{i,j=1}^{N} \bar{\psi}_i M_{ij} \psi_j}. \tag{A.10}$$

Writing the integrand as

$$e^{-\sum_{i,j=1}^{N} \bar{\psi}_i M_{ij} \psi_j} = \prod_{i=1}^{N} e^{-\bar{\psi}_i \sum_{j=1}^{N} M_{ij} \psi_j}. \tag{A.11}$$

Expanding the exponential yields

$$e^{-\sum_{i,j=1}^{N} \bar{\psi}_i M_{ij} \psi_j} = \prod_{i=1}^{N} (1 - \bar{\psi}_i \sum_{j=1}^{N} M_{ij} \psi_j). \tag{A.12}$$

By applying the integration rules, A.7, it can be seen that only term which contributes is the product of all the Grassmann variables.

$$I[M] = \int \prod_{k=1}^{N} d\bar{\psi}_k d\psi_k \prod_{i=1}^{N} \bar{\psi}_i \sum_{j=1}^{N} M_{ij} \psi_j \tag{A.13}$$

Products of Grassmann variables are antisymmetric under exchange of any pair of indices, thus

$$I[M] = \int \prod_{k=1}^{N} d\bar{\psi}_k d\psi_k \psi_k \bar{\psi}_k \sum_{j_1 \cdots j_N} \epsilon_{j_1 \cdots j_N} M_{1 j_1} \cdots M_{N j_N} \tag{A.14}$$

where $\epsilon_{j_1 \cdots j_N}$ is the N-dimensional antisymmetric tensor. Recalling the definition of the determinant of a matrix

$$\det M = \sum_{j_1 \cdots j_N} \epsilon_{j_1 \cdots j_N} M_{1 j_1} \cdots M_{N j_N}. \tag{A.15}$$

Thus obtaining

$$I[M] = \int \prod_{k=1}^{N} [d\bar{\psi}_k d\psi_k] e^{-\sum_{i,j=1}^{N} \bar{\psi}_i M_{ij} \psi_j} = \det M. \tag{A.16}$$

Now consider the generating functional

$$Z[\bar{\eta}, \eta] = \int \prod_{k=1}^{N} [d\bar{\psi}_k d\psi_k] e^{-\sum_{i,j}^{N} \bar{\psi}_i M_{ij} \psi_j + \sum_i (\bar{\psi}_i \eta_i + \bar{\eta}_i \psi_i)} \tag{A.17}$$

where $\bar{\eta}$ and η are anti-commuting sources. By redefining the Grassmann variables,

$$\begin{aligned} \psi_i' &= \psi_i - \sum_k M_{ik}^{-1} \eta_K \\ \bar{\psi}_i' &= \bar{\psi}_i - \sum_k \bar{\eta}_k M_{ik}^{-1} \end{aligned} \tag{A.18}$$

we can re-write equation A.17 as

$$\begin{aligned} Z[\bar{\eta}, \eta] &= \int \prod_{k=1}^{N} [d\bar{\psi}_k d\psi_k] e^{-\sum_{i,j}^{N} \bar{\psi}_i' M_{ij} \psi_j'} e^{\sum_{i,j} \bar{\eta}_i M_{ij}^{-1} \eta_j} \\ &= \det M \; e^{\sum_{i,j} \bar{\eta}_i M_{ij}^{-1} \eta_j}. \end{aligned} \tag{A.19}$$

Applying the rules of differentiation, A.4 and A.5 to the generating functional A.17 and then setting the sources to zero, we have

$$\begin{aligned} &\left[\frac{\partial}{\partial \eta_i} \cdots \frac{\partial}{\partial \eta_n} Z[\bar{\eta}, \eta] \frac{\overleftarrow{\partial}}{\partial \bar{\eta}_i} \cdots \frac{\overleftarrow{\partial}}{\partial \bar{\eta}_n} \right]_{\eta = \bar{\eta} = 0} = \\ &\int [d\bar{\psi} d\psi] \psi_i \cdots \psi_n \bar{\psi}_i \cdots \bar{\psi}_n e^{-\sum_{i,j}^{N} \bar{\psi}_i M_{ij} \psi_j}. \end{aligned} \tag{A.20}$$

By making an expansion of the exponential in A.19 in a similar manner to that of A.11

$$\begin{aligned} Z[\bar{\eta}, \eta] &= \det M \prod_i e^{\bar{\eta}_i \sum_j M_{ij}^{-1} \eta_j} \\ &= \det M \prod_i (1 + \bar{\eta}_i \sum_j M_{ij}^{-1} \eta_j) \end{aligned} \tag{A.21}$$

and applying the rules of differentiation, A.4 and A.5, it can be seen that the only term which contributes after the differentiation in A.20 is the product of all Grassmann variables, so that

$$Z[\bar{\eta},\eta] = \det M \prod_i (\bar{\eta}_i \sum_j M^{-1}_{ij}\eta_j). \tag{A.22}$$

In particular, considering the integral of one pair of Grassmann variables

$$\begin{aligned} \int [d\bar{\psi}d\psi]\psi_i\bar{\psi}_j e^{-\sum_{i,j}^{N}\bar{\psi}_i M_{ij}\psi_j} &= \left[\frac{\partial}{\partial\eta_i} Z[\bar{\eta},\eta]\frac{\overleftarrow{\partial}}{\partial\bar{\eta}_j}\right]_{\eta=\bar{\eta}=0} \\ &= \det M M^{-1}_{ij} \end{aligned} \tag{A.23}$$

where equation A.23 can be generalised to any number of pairs of Grassmann variables.

Appendix B

Meson Spectrum

In the tables that follow are displayed the results to the fits for the meson spectrum. The data in each table are the results of fitting the correlation functions to

$$C(t) = A\left(2e^{-ET/2}\cosh(E(t-T/2))\right) \tag{B.1}$$

where $T = 48$, $E = E(p^2)$, the energy of the state, and A, the amplitude is

$$A = \frac{Z^2}{2E}, \tag{B.2}$$

and Z is the two-point amplitude given by equation 2.103. In this appendix, the abreviation of the kappa value $\kappa\kappa\kappa\kappa$ will be taken to mean $0.1\kappa\kappa\kappa\kappa$. For example $\kappa = 2330$ means $\kappa = 0.1233$.

Table B.1: Light Light Pseudoscalar Mesons. κ_1 is FF, κ_2 are LL, fit range is 8-22

κ_1	κ_2	A	E	χ^2/dof	Q
3460	3460	0.01393^{+22}_{-33}	0.2808^{+12}_{-10}	0.760541	0.703145
3510	3460	0.01471^{+25}_{-40}	0.2509^{+14}_{-11}	0.865043	0.590255
3510	3510	0.01599^{+25}_{-54}	0.2168^{+15}_{-12}	0.835155	0.622795
3530	3460	0.01525^{+26}_{-51}	0.2383^{+15}_{-13}	0.905768	0.546175
3530	3510	0.01694^{+27}_{-67}	0.2022^{+16}_{-13}	0.855999	0.600096
3530	3530	0.01816^{+33}_{-81}	0.1862^{+16}_{-14}	0.84415	0.613

Table B.2: Heavy Light Pseudoscalar Mesons. Heavies are BB, Lights are LL, fit range is 12-22

κ_H	κ_L	A	E	χ^2/dof	Q
2000	3460	53.9^{+10}_{-9}	0.8405^{+14}_{-9}	1.09799	0.360133
	3510	50.8^{+12}_{-10}	0.8231^{+18}_{-12}	1.01715	0.423150
	3530	49.9^{+13}_{-11}	0.8165^{+21}_{-13}	0.92469	0.502024
2330	3460	58.7^{+10}_{-10}	0.7387^{+12}_{-9}	1.08233	0.371857
	3510	55.4^{+13}_{-11}	0.7205^{+16}_{-11}	0.93334	0.494381
	3530	54.5^{+13}_{-12}	0.7136^{+18}_{-12}	0.8123	0.604815
2660	3460	64.2^{+11}_{-10}	0.6284^{+11}_{-8}	1.16498	0.312677
	3510	60.9^{+13}_{-12}	0.6091^{+14}_{-10}	0.95453	0.475875
	3530	59.9^{+14}_{-14}	0.6017^{+16}_{-12}	0.79017	0.625511
2990	3460	70.3^{+12}_{-14}	0.5051^{+11}_{-9}	1.27592	0.244029
	3530	67.2^{+13}_{-16}	0.4840^{+13}_{-10}	1.07040	0.380956
	3530	66.4^{+14}_{-18}	0.4758^{+14}_{-11}	0.86976	0.551583

Table B.3: Heavy Light Vector Mesons. Heavies are BB, Lights are LL, fit range is 12-22

κ_H	κ_L	A	E	χ^2/dof	Q
2000	3460	33.3^{+9}_{-8}	0.8887^{+23}_{-17}	1.86344	0.0524253
	3510	31.0^{+10}_{-9}	0.8726^{+29}_{-22}	1.44828	0.16105
	3530	30.2^{+12}_{-10}	0.8667^{+35}_{-29}	1.24573	0.261485
2330	3460	34.8^{+10}_{-9}	0.7945^{+22}_{-17}	2.00409	0.0347487
	3510	32.4^{+11}_{-10}	0.7785^{+29}_{-22}	1.57727	0.115542
	3530	31.7^{+12}_{-11}	0.7727^{+34}_{-26}	1.35869	0.200746
2660	3460	35.6^{+10}_{-8}	0.6944^{+22}_{-18}	2.22583	0.0177129
	3510	33.3^{+11}_{-10}	0.6783^{+27}_{-23}	1.79956	0.0628993
	3530	32.6^{+13}_{-12}	0.6727^{+32}_{-27}	1.54442	0.125936
2990	3460	35.0^{+10}_{-10}	0.5865^{+22}_{-18}	2.5098	0.0071905
	3510	32.8^{+11}_{-11}	0.5704^{+27}_{-25}	2.10716	0.0254967
	3530	32.2^{+12}_{-12}	0.5648^{+32}_{-30}	1.80523	0.0618984

Table B.4: Heavy Light Scalar Mesons. Heavies are BB, Lights are LL, fit range is 12-22

κ_H	κ_L	A	E	χ^2/dof	Q
2330	3460	-13.3^{+15}_{-19}	0.889^{+11}_{-9}	1.95509	0.0401635
	3510	-14.2^{+19}_{-25}	0.876^{+14}_{-12}	1.32661	0.216743
	3530	-15.2^{+22}_{-33}	0.878^{+17}_{-16}	1.09282	0.363979

Table B.5: Masses (in lattice units) of Heavy-Light Mesons after chiral extrapolation.

J^P		2000	2330	2660	2990
0^-	$\kappa = \kappa_c$	0.7968^{+25}_{-15}	0.6932^{+22}_{-14}	0.5804^{+19}_{-14}	0.4523^{+16}_{-12}
	$\kappa = \kappa_s$	0.8405^{+14}_{-9}	0.7387^{+12}_{-9}	0.6284^{+11}_{-8}	0.5051^{+11}_{-9}
	χ^2/dof	2.68469	3.06916	3.14993	2.43356
1^-	$\kappa = \kappa_c$	0.8469^{+35}_{-29}	0.7525^{+36}_{-30}	0.6515^{+35}_{-31}	0.5438^{+35}_{-32}
	$\kappa = \kappa_s$	0.8887^{+23}_{-17}	0.7945^{+22}_{-17}	0.6944^{+22}_{-18}	0.5865^{+22}_{-18}
	χ^2/dof	1.32046	2.31914	2.76268	3.22384
0^+	$\kappa = \kappa_c$		0.8402^{+170}_{-146}		
	$\kappa = \kappa_s$		0.8844^{+116}_{-100}		
	χ^2/dof		3.72088		

Appendix C

Matrix Elements

This appendix will use the same abbreviation for the κ value as appendix B. Table C.1 to table C.24 show the results of a simultaneous fit for the form factors $f_+(q^2)$ and $f_0(q^2)$ to the spatial and temporal ratios of three-point over two-point correlation functions as defined in equation 4.7. Listed are all eight momentum channels, the six listed in table 4.5 and the two extra channels described in chapter five table 5.1.

Table C.25 to table C.28 show the results of the fits for the pseudoscalar and vector decay constants defined in chapter four and their chiral extrapolations for each heavy κ.

Table C.29 to table C.36 show the results of the chiral extrapolations of the form factors for each heavy κ for the six momentum channels described in table 5.1.

All data is for the unrenormalised matrix elements, apart from table C.27 and table C.28, which list data for the vector decay constant, renormalised by Z_V^{eff}.

Table C.1: $\kappa_a = 3460$, $\kappa_p = 3460$, $\kappa_e = 2000$, $Z_V^{\text{eff}} = 1.08371$.

p^2	q^2	k^2	$f_+(q^2)$	$f_0(q^2)$	q^2	χ^2/dof	Q
0	0	0		0.766^{+18}_{-23}	0.313^{+1}_{-1}	9.48648/6	0.14801
0	1	1	0.783^{+14}_{-23}	0.688^{+12}_{-21}	0.140^{+1}_{-1}	7.84886/6	0.249386
0	2	2	0.649^{+46}_{-56}	0.649^{+49}_{-58}	-0.076^{+1}_{-1}	29.6854/6	4.510e-05
1	0	1	0.963^{+59}_{-70}	0.852^{+36}_{-56}	0.246^{+1}_{-1}	10.6857/6	0.098589
1	1	0	1.284^{+31}_{-43}	0.874^{+15}_{-22}	0.291^{+2}_{-1}	5.28637/4	0.259156
1	2	1	0.786^{+30}_{-44}	0.687^{+21}_{-33}	0.109^{+1}_{-1}	8.71542/6	0.190227
1	4	1	0.570^{+26}_{-38}	0.583^{+26}_{-40}	-0.028^{+1}_{-1}	3.18071/6	0.785848
1	3	2	0.690^{+59}_{-82}	0.852^{+79}_{-109}	-0.124^{+1}_{-1}	9.85635/6	0.130833

Table C.2: $\kappa_a = 3510$, $\kappa_p = 3460$, $\kappa_e = 2000$, $Z_V^{\text{eff}} = 1.07606$

p^2	q^2	k^2	$f_+(q^2)$	$f_0(q^2)$	q^2	χ^2/dof	Q
0	0	0		0.788^{+20}_{-25}	0.348^{+2}_{-2}	5.48867/6	0.482828
0	1	1	0.792^{+17}_{-27}	0.674^{+16}_{-23}	0.160^{+1}_{-1}	5.9486/6	0.428973
0	2	2	0.648^{+47}_{-58}	0.653^{+51}_{-60}	-0.070^{+1}_{-1}	17.752/6	0.0068827
1	0	1	1.001^{+74}_{-82}	0.864^{+43}_{-57}	0.268^{+1}_{-1}	10.3802/6	0.109526
1	1	0	1.438^{+36}_{-60}	0.888^{+15}_{-22}	0.328^{+2}_{-2}	9.1348/4	0.0578171
1	2	1	0.794^{+41}_{-52}	0.671^{+27}_{-34}	0.131^{+1}_{-1}	9.1195/6	0.166968
1	4	1	0.592^{+27}_{-42}	0.595^{+27}_{-42}	-0.006^{+1}_{-1}	3.40205/6	0.756952
1	3	2	0.727^{+75}_{-103}	0.889^{+96}_{-141}	-0.116^{+1}_{-1}	8.18152/6	0.225104

Table C.3: $\kappa_a = 3530$, $\kappa_p = 3460$, $\kappa_e = 2000$, $Z_V^{\text{eff}} = 1.07302$.

p^2	q^2	k^2	$f_+(q^2)$	$f_0(q^2)$	q^2	χ^2/dof	Q
0	0	0		0.800^{+19}_{-28}	0.363^{+2}_{-2}	1.33312/6	0.9698
0	1	1	0.813^{+17}_{-34}	0.675^{+16}_{-27}	0.168^{+1}_{-1}	5.78018/6	0.44826
0	2	2	0.638^{+53}_{-59}	0.644^{+54}_{-62}	-0.067^{+1}_{-1}	14.9245/6	0.0208519
1	0	1	1.011^{+85}_{-101}	0.874^{+52}_{-70}	0.277^{+1}_{-1}	9.48666/6	0.148001
1	1	0	1.514^{+45}_{-69}	0.891^{+17}_{-24}	0.344^{+2}_{-2}	11.2658/4	0.0237341
1	2	1	0.798^{+48}_{-62}	0.662^{+31}_{-43}	0.140^{+1}_{-1}	5.4835/6	0.483453
1	4	1	0.607^{+30}_{-47}	0.605^{+30}_{-47}	0.003^{+1}_{-1}	3.8995/6	0.690275
1	3	2	0.739^{+83}_{-120}	0.903^{+108}_{-161}	-0.113^{+1}_{-1}	5.66807/6	0.46138

Table C.4: $\kappa_a = 3460$, $\kappa_p = 3510$, $\kappa_e = 2000$, $Z_V^{\text{eff}} = 1.08371$.

p^2	q^2	k^2	$f_+(q^2)$	$f_0(q^2)$	q^2	χ^2/dof	Q
0	0	0		0.781^{+22}_{-28}	0.328^{+2}_{-2}	6.2685/6	0.393795
0	1	1	0.801^{+18}_{-26}	0.697^{+16}_{-25}	0.144^{+2}_{-1}	9.02227/6	0.172329
0	2	2	0.657^{+56}_{-67}	0.665^{+55}_{-68}	-0.078^{+1}_{-1}	18.2869/6	0.00555393
1	0	1	0.996^{+82}_{-98}	0.833^{+56}_{-72}	0.252^{+2}_{-1}	10.1651/6	0.117867
1	1	0	1.318^{+37}_{-53}	0.887^{+16}_{-24}	0.308^{+2}_{-2}	9.29207/4	0.0541997
1	2	1	0.791^{+44}_{-58}	0.686^{+30}_{-39}	0.114^{+2}_{-1}	5.57944/6	0.471908
1	4	1	0.623^{+33}_{-46}	0.634^{+33}_{-48}	-0.0226^{+2}_{-1}	3.12901/6	0.792489
1	3	2	0.710^{+79}_{-108}	0.895^{+161}_{-150}	-0.125^{+1}_{-1}	10.2056/6	0.116255

Table C.5: $\kappa_a = 3510$, $\kappa_p = 3510$, $\kappa_e = 2000$, $Z_V^{\rm eff} = 1.07606$.

p^2	q^2	k^2	$f_+(q^2)$	$f_0(q^2)$	q^2	χ^2/dof	Q
0	0	0		0.802^{+22}_{-28}	0.368^{+24}_{-18}	3.93872/6	0.68497
0	1	1	0.811^{+23}_{-32}	0.682^{+19}_{-29}	0.165^{+2}_{-2}	7.51794/6	0.275589
0	2	2	0.675^{+61}_{-87}	0.678^{+65}_{-89}	-0.071^{+1}_{-1}	11.2699/6	0.0803852
1	0	1	1.052^{+89}_{-125}	0.850^{+62}_{-85}	0.274^{+2}_{-1}	5.62207/6	0.466827
1	1	0	1.477^{+45}_{-65}	0.898^{+18}_{-30}	0.350^{+2}_{-2}	11.0885/4	0.0255867
1	2	1	0.836^{+53}_{-77}	0.692^{+61}_{-54}	0.137^{+2}_{-1}	4.51726/6	0.607039
1	4	1	0.631^{+23}_{-57}	0.631^{+23}_{-58}	0.000^{+1}_{-1}	2.71537/6	0.843629
1	3	2	0.697^{+98}_{-135}	0.887^{+145}_{-186}	-0.117^{+1}_{-1}	6.72494/6	0.347035

Table C.6: $\kappa_a = 3530$, $\kappa_p = 3510$, $\kappa_e = 2000$, $Z_V^{\rm eff} = 1.07302$.

p^2	q^2	k^2	$f_+(q^2)$	$f_0(q^2)$	q^2	χ^2/dof	Q
0	0	0		0.831^{+21}_{-33}	0.386^{+2}_{-2}	3.79276/6	0.704698
0	1	1	0.823^{+25}_{-38}	0.671^{+22}_{-33}	0.174^{+1}_{-1}	3.31478/6	0.768426
0	2	2	0.662^{+69}_{-77}	0.672^{+85}_{-79}	-0.069^{+1}_{-1}	8.44682/6	0.20716
1	0	1	1.029^{+122}_{-135}	0.864^{+58}_{-106}	0.284^{+2}_{-1}	6.4938/6	0.370202
1	1	0	1.540^{+52}_{-71}	0.904^{+18}_{-28}	0.369^{+3}_{-2}	7.97133/4	0.0926341
1	2	1	0.795^{+73}_{-84}	0.651^{+46}_{-52}	0.147^{+2}_{-1}	5.65146/6	0.463343
1	4	1	0.687^{+30}_{-80}	0.682^{+30}_{-80}	0.001^{+2}_{-1}	2.63772/6	0.852747
1	3	2	0.744^{+97}_{-173}	0.936^{+133}_{-231}	-0.114^{+1}_{-1}	4.96814/6	0.547906

Table C.7: $\kappa_a = 3460$, $\kappa_p = 3460$, $\kappa_e = 2330$, $Z_V^{\text{eff}} = 1.02167$.

p^2	q^2	k^2	$f_+(q^2)$	$f_0(q^2)$	q^2	χ^2/dof	Q
0	0	0		0.821^{+20}_{-24}	0.210^{+1}_{-1}	5.85466/6	0.439667
0	1	1	0.774^{+15}_{-21}	0.728^{+15}_{-21}	0.057^{+1}_{-1}	8.63748/6	0.195016
0	2	2	0.658^{+46}_{-57}	0.647^{+50}_{-55}	-0.116^{+1}_{-1}	30.2428/6	3.534e-05
1	0	1	0.982^{+57}_{-71}	0.919^{+43}_{-59}	0.160^{+1}_{-1}	9.39058/6	0.152774
1	1	0	1.221^{+28}_{-38}	0.923^{+16}_{-24}	0.184^{+1}_{-1}	7.55452/4	0.109329
1	2	1	0.749^{+26}_{-39}	0.725^{+24}_{-36}	0.023^{+1}_{-1}	7.04171/6	0.317007
1	4	1	0.544^{+24}_{-34}	0.604^{+27}_{-40}	-0.114^{+1}_{-1}	3.55279/6	0.736933
1	3	2	0.656^{+53}_{-70}	0.935^{+86}_{-116}	-0.170^{+1}_{-1}	11.3189/6	0.0790055

Table C.8: $\kappa_a = 3510$, $\kappa_p = 3460$, $\kappa_e = 2330$, $Z_V^{\text{eff}} = 1.01402$.

p^2	q^2	k^2	$f_+(q^2)$	$f_0(q^2)$	q^2	χ^2/dof	Q
0	0	0		0.840^{+20}_{-27}	0.238^{+1}_{-1}	5.15078/6	0.524625
0	1	1	0.788^{+16}_{-27}	0.720^{+15}_{-26}	0.073^{+1}_{-1}	5.97173/6	0.426364
0	2	2	0.658^{+45}_{-62}	0.656^{+51}_{-60}	-0.112^{+1}_{-3}	17.621/6	0.00725265
1	0	1	1.022^{+72}_{-87}	0.961^{+43}_{-66}	0.177^{+1}_{-1}	5.93726/6	0.430255
1	1	0	1.338^{+28}_{-44}	0.938^{+16}_{-25}	0.215^{+1}_{-1}	8.5758/4	0.0726227
1	2	1	0.768^{+33}_{-49}	0.722^{+27}_{-42}	0.040^{+1}_{-1}	7.43648/6	0.282359
1	4	1	0.559^{+25}_{-41}	0.614^{+30}_{-44}	-0.097^{+1}_{-1}	2.6757/6	0.848309
1	3	2	0.654^{+63}_{-83}	0.919^{+105}_{-136}	-0.164^{+1}_{-1}	4.33324/6	0.631678

Table C.9: $\kappa_a = 3530$, $\kappa_p = 3460$, $\kappa_e = 2330$, $Z_V^{\rm eff} = 1.01097$.

p^2	q^2	k^2	$f_+(q^2)$	$f_0(q^2)$	q^2	χ^2/dof	Q
0	0	0		0.863^{+18}_{-36}	0.250^{+2}_{-1}	0.300488/6	0.999495
0	1	1	0.785^{+20}_{-30}	0.711^{+18}_{-27}	0.079^{+1}_{-1}	5.92334/6	0.431832
0	2	2	0.645^{+52}_{-62}	0.643^{+55}_{-63}	-0.110^{+1}_{-1}	13.9186/6	0.0305583
1	0	1	1.028^{+85}_{-94}	0.949^{+51}_{-74}	0.185^{+1}_{-1}	5.7192/6	0.455368
1	1	0	1.386^{+34}_{-52}	0.937^{+18}_{-27}	0.229^{+2}_{-2}	9.46677/4	0.0504346
1	2	1	0.783^{+36}_{-56}	0.725^{+29}_{-49}	0.048^{+1}_{-1}	6.01894/6	0.421072
1	4	1	0.561^{+29}_{-41}	0.614^{+31}_{-45}	-0.090^{+1}_{-1}	2.08773/6	0.911456
1	3	2	0.660^{+75}_{-93}	0.932^{+121}_{-150}	-0.162^{+1}_{-1}	3.29223/6	0.771376

Table C.10: $\kappa_a = 3460$, $\kappa_p = 3510$, $\kappa_e = 2330$, $Z_V^{\rm eff} = 1.02167$.

p^2	q^2	k^2	$f_+(q^2)$	$f_0(q^2)$	q^2	χ^2/dof	Q
0	0	0		0.836^{+21}_{-33}	0.221^{+1}_{-1}	3.28743/6	0.772002
0	1	1	0.790^{+19}_{-27}	0.740^{+17}_{-26}	0.060^{+1}_{-1}	6.81561/6	0.338237
0	2	2	0.672^{+58}_{-68}	0.669^{+64}_{-68}	-0.117^{+1}_{-1}	16.1228/6	0.0131097
1	0	1	1.029^{+76}_{-101}	0.931^{+59}_{-86}	0.164^{+1}_{-1}	9.0963/6	0.168234
1	1	0	1.249^{+37}_{-49}	0.929^{+202}_{-28}	0.198^{+2}_{-1}	8.27247/4	0.0820919
1	2	1	0.741^{+37}_{-50}	0.714^{+34}_{-46}	0.026^{+1}_{-1}	6.64026/6	0.3554
1	4	1	0.582^{+31}_{-44}	0.643^{+35}_{-49}	-0.111^{+1}_{-1}	2.4725/6	0.871533
1	3	2	0.626^{+73}_{-103}	0.945^{+124}_{-171}	-0.171^{+1}_{-1}	8.04392/6	0.234903

Table C.11: $\kappa_a = 3510$, $\kappa_p = 3510$, $\kappa_e = 2330$, $Z_V^{\text{eff}} = 1.01402$.

p^2	q^2	k^2	$f_+(q^2)$	$f_0(q^2)$	q^2	χ^2/dof	Q
0	0	0		0.854^{+21}_{-33}	0.254^{+2}_{-1}	6.37521/6	0.382497
0	1	1	0.805^{+21}_{-32}	0.732^{+19}_{-31}	0.076^{+1}_{-1}	4.01969/6	0.674012
0	2	2	0.640^{+67}_{-73}	0.666^{+64}_{-78}	-0.113^{+1}_{-1}	11.8706/6	0.0649194
1	0	1	1.035^{+98}_{-111}	0.915^{+68}_{-93}	0.182^{+1}_{-1}	3.51332/6	0.742196
1	1	0	1.379^{+38}_{-57}	0.939^{+21}_{-31}	0.234^{+2}_{-2}	9.24886/4	0.0551713
1	2	1	0.758^{+45}_{-62}	0.708^{+38}_{-54}	0.045^{+1}_{-1}	6.4172/6	0.378112
1	4	1	0.594^{+36}_{-48}	0.649^{+40}_{-53}	-0.092^{+1}_{-1}	2.18393/6	0.902029
1	3	2	0.640^{+95}_{-11}	0.965^{+164}_{-195}	-0.166^{+1}_{-1}	5.54717/6	0.475774

Table C.12: $\kappa_a = 3530$, $\kappa_p = 3510$, $\kappa_e = 2330$, $Z_V^{\text{eff}} = 1.01097$.

p^2	q^2	k^2	$f_+(q^2)$	$f_0(q^2)$	q^2	χ^2/dof	Q
0	0	0		0.880^{+22}_{-35}	0.269^{+2}_{-1}	2.13514/6	0.906859
0	1	1	0.803^{+25}_{-36}	0.720^{+24}_{-33}	0.083^{+1}_{-1}	5.86007/6	0.439046
0	2	2	0.658^{+63}_{-77}	0.6712^{+71}_{-81}	-0.112^{+1}_{-1}	7.02445/6	0.318592
1	0	1	1.004^{+126}_{-127}	0.931^{+74}_{-95}	0.190^{+1}_{-1}	4.76399/6	0.57442
1	1	0	1.458^{+42}_{-63}	0.960^{+18}_{-30}	0.250^{+2}_{-2}	14.2246/4	0.006612
1	2	1	0.758^{+60}_{-65}	0.700^{+46}_{-56}	0.053^{+1}_{-1}	4.39264/6	0.623700
1	4	1	0.616^{+38}_{-56}	0.671^{+43}_{-60}	-0.084^{+1}_{-1}	3.58254/6	0.732958
1	3	2	0.577^{+155}_{-157}	0.930^{+236}_{-245}	-0.163^{+1}_{-1}	3.33641/6	0.765592

Table C.13: $\kappa_a = 3460$, $\kappa_p = 3460$, $\kappa_e = 2660$, $Z_V^{\rm eff} = 0.962856$.

p^2	q^2	k^2	$f_+(q^2)$	$f_0(q^2)$	q^2	χ^2/dof	Q
0	0	0		0.880^{+20}_{-26}	0.121^{+1}_{-1}	8.2583/6	0.219784
0	1	1	0.771^{+14}_{-23}	0.780^{+15}_{-23}	-0.009^{+1}_{-1}	8.10439/6	0.230555
0	2	2	0.683^{+47}_{-59}	0.633^{+48}_{-539}	-0.136^{+1}_{-1}	29.8365/6	4.2224e-05
1	0	1	0.994^{+64}_{-68}	1.011^{+49}_{-62}	0.088^{+1}_{-1}	8.46896/6	0.205719
1	1	0	1.160^{+24}_{-35}	0.980^{+17}_{-25}	0.091^{+1}_{-1}	6.11581/4	0.190665
1	2	1	0.704^{+24}_{-31}	0.763^{+30}_{-40}	-0.049^{+1}_{-1}	5.60788/6	0.468515
1	4	1	0.514^{+21}_{-34}	0.627^{+27}_{-42}	-0.186^{+1}_{-1}	5.1047/6	0.530457
1	3	2	0.609^{+45}_{-71}	1.074^{+106}_{-158}	-0.198^{+1}_{-1}	11.2482/6	0.081002

Table C.14: $\kappa_a = 3510$, $\kappa_p = 3460$, $\kappa_e = 2660$, $Z_V^{\rm eff} = 0.955207$.

p^2	q^2	k^2	$f_+(q^2)$	$f_0(q^2)$	q^2	χ^2/dof	Q
0	0	0		0.898^{+21}_{-29}	0.142^{+1}_{-1}	4.95478/6	0.549626
0	1	1	0.776^{+16}_{-26}	0.774^{+16}_{-27}	0.002^{+1}_{-1}	7.60469/6	0.268518
0	2	2	0.637^{+53}_{-64}	0.614^{+55}_{-59}	-0.135^{+1}_{-1}	19.1743/6	0.003879
1	0	1	1.061^{+68}_{-96}	1.051^{+53}_{-69}	0.101^{+1}_{-1}	7.7516/6	0.256873
1	1	0	1.235^{+27}_{-36}	0.984^{+18}_{-26}	0.116^{+1}_{-1}	8.55191/4	0.0733294
1	2	1	0.705^{+29}_{-39}	0.751^{+35}_{-45}	-0.036^{+1}_{-1}	7.14537/6	0.307613
1	4	1	0.515^{+22}_{-39}	0.633^{+29}_{-48}	-0.173^{+1}_{-1}	2.67443/6	0.848458
1	3	2	0.589^{+56}_{-72}	0.983^{+121}_{-142}	-0.196^{+1}_{-1}	5.50874/6	0.480401

Table C.15: $\kappa_a = 3530$, $\kappa_p = 3460$, $\kappa_e = 2660$, $Z_V^{\rm eff} = 0.952163$.

p^2	q^2	k^2	$f_+(q^2)$	$f_0(q^2)$	q^2	χ^2/dof	Q
0	0	0		0.916^{+22}_{-33}	0.152^{+1}_{-1}	1.88957/6	0.929569
0	1	1	0.771^{+18}_{-28}	0.763^{+18}_{-27}	0.007^{+1}_{-1}	6.1987/6	0.401304
0	2	2	0.658^{+51}_{-63}	0.627^{+56}_{-62}	-0.134^{+1}_{-1}	13.6536/6	0.0337541
1	0	1	1.030^{+95}_{-97}	1.059^{+56}_{-78}	0.107^{+1}_{-1}	5.05494/6	0.536786
1	1	0	1.303^{+28}_{-47}	0.999^{+17}_{-28}	0.127^{+1}_{-1}	8.47961/4	0.0755077
1	2	1	0.724^{+28}_{-50}	0.768^{+33}_{-58}	-0.030^{+1}_{-1}	3.94609/6	0.683972
1	4	1	0.519^{+25}_{-40}	0.638^{+30}_{-49}	-0.167^{+1}_{-1}	2.68245/6	0.847516
1	3	2	0.593^{+63}_{-88}	1.017^{+134}_{-187}	-0.194^{+1}_{-1}	3.59128/6	0.731789

Table C.16: $\kappa_a = 3460$, $\kappa_p = 3510$, $\kappa_e = 2660$, $Z_V^{\rm eff} = 0.962856$.

p^2	q^2	k^2	$f_+(q^2)$	$f_0(q^2)$	q^2	χ^2/dof	Q
0	0	0		0.887^{+24}_{-33}	0.129^{+1}_{-1}	6.98499/6	0.322238
0	1	1	0.781^{+19}_{-272}	0.789^{+19}_{-27}	-0.008^{+1}_{-1}	7.10223/6	0.311496
0	2	2	0.689^{+56}_{-67}	0.668^{+64}_{-66}	-0.136^{+1}_{-1}	15.1462/6	0.0191495
1	0	1	1.073^{+78}_{-99}	1.061^{+63}_{-98}	0.091^{+1}_{-1}	7.13596/6	0.308456
1	1	0	1.179^{+32}_{-44}	0.982^{+21}_{-30}	0.102^{+1}_{-1}	7.63631/4	0.105847
1	2	1	0.703^{+29}_{-44}	0.756^{+39}_{-50}	-0.047^{+1}_{-1}	2.49817/6	0.868673
1	4	1	0.548^{+29}_{-44}	0.669^{+37}_{-52}	-0.184^{+1}_{-1}	3.43425/6	0.752696
1	3	2	0.567^{+62}_{-89}	1.068^{+142}_{-193}	-0.199^{+1}_{-1}	7.36821/6	0.288133

Table C.17: $\kappa_a = 3510$, $\kappa_p = 3510$, $\kappa_e = 2660$, $Z_V^{\rm eff} = 0.955207$.

p^2	q^2	k^2	$f_+(q^2)$	$f_0(q^2)$	q^2	χ^2/dof	Q
0	0	0		0.926^{+19}_{-37}	0.154^{+1}_{-1}	1.47819/6	0.96093
0	1	1	0.779^{+21}_{-32}	0.775^{+22}_{-33}	0.004^{+1}_{-1}	4.73772/6	0.577865
0	2	2	0.671^{+62}_{-72}	0.654^{+68}_{-78}	-0.135^{+1}_{-1}	10.3961/6	0.108933
1	0	1	1.067^{+98}_{-111}	1.040^{+84}_{-104}	0.104^{+1}_{-1}	4.22814/6	0.645833
1	1	0	1.286^{+31}_{-48}	1.000^{+20}_{-32}	0.131^{+1}_{-1}	11.9947/4	0.0173907
1	2	1	0.725^{+38}_{-54}	0.771^{+43}_{-617}	-0.033^{+1}_{-1}	4.38225/6	0.625095
1	4	1	0.556^{+31}_{-47}	0.680^{+39}_{-57}	-0.170^{+1}_{-1}	2.57504/6	0.859977
1	3	2	0.569^{+80}_{-101}	1.049^{+172}_{-217}	-0.196^{+1}_{-1}	3.59846/6	0.730827

Table C.18: $\kappa_a = 3530$, $\kappa_p = 3510$, $\kappa_e = 2660$, $Z_V^{\rm eff} = 0.952163$.

p^2	q^2	k^2	$f_+(q^2)$	$f_0(q^2)$	q^2	χ^2/dof	Q
0	0	0		0.937^{+22}_{-38}	0.166^{+1}_{-1}	3.26794/6	0.774543
0	1	1	0.783^{+23}_{-34}	0.772^{+24}_{-34}	0.009^{+1}_{-1}	4.81181/6	0.568167
0	2	2	0.675^{+65}_{-75}	0.663^{+74}_{-82}	-0.135^{+1}_{-1}	7.86923/6	0.247842
1	0	1	1.074^{+109}_{-139}	1.058^{+76}_{-118}	0.110^{+1}_{-1}	4.61807/6	0.593644
1	1	0	1.341^{+34}_{-54}	1.006^{+21}_{-33}	0.144^{+1}_{-1}	11.2686/4	0.0237053
1	2	1	0.716^{+42}_{-59}	0.753^{+46}_{-68}	-0.027^{+1}_{-1}	4.46141/6	0.614492
1	4	1	0.559^{+34}_{-50}	0.681^{+42}_{-60}	-0.164^{+1}_{-1}	3.22019/6	0.780746
1	3	2	0.562^{+91}_{-108}	1.082^{+178}_{-245}	-0.195^{+1}_{-1}	3.08339/6	0.798311

Table C.19: $\kappa_a = 3460$, $\kappa_p = 3460$, $\kappa_e = 2990$, $Z_V^{\text{eff}} = 0.907034$.

p^2	q^2	k^2	$f_+(q^2)$	$f_0(q^2)$	q^2	χ^2/dof	Q
0	0	0		0.947^{+21}_{-29}	0.050^{+1}_{-1}	8.8349/6	0.183078
0	1	1	0.760^{+15}_{-24}	0.829^{+15}_{-25}	-0.054^{+1}_{-1}	7.88483/6	0.246663
0	2	2	0.712^{+47}_{-63}	0.553^{+53}_{-52}	-0.129^{+1}_{-1}	30.0509/6	3.844e-05
1	0	1	1.069^{+58}_{-73}	1.135^{+55}_{-75}	0.034^{+1}_{-1}	8.83057/6	0.183333
1	1	0	1.062^{+20}_{-30}	1.027^{+19}_{-28}	0.014^{+1}_{-1}	6.68781/4	0.153335
1	2	1	0.650^{+19}_{-29}	0.805^{+37}_{-50}	-0.103^{+1}_{-1}	1.6905/6	0.945853
1	4	1	0.461^{+19}_{-31}	0.638^{+28}_{-43}	-0.240^{+1}_{-1}	4.05386/6	0.669387
1	3	2	0.519^{+41}_{-60}	1.242^{+132}_{-197}	-0.205^{+1}_{-1}	7.54577/6	0.273304

Table C.20: $\kappa_a = 3510$, $\kappa_p = 3460$, $\kappa_e = 2990$, $Z_V^{\text{eff}} = 0.899385$.

p^2	q^2	k^2	$f_+(q^2)$	$f_0(q^2)$	q^2	χ^2/dof	Q
0	0	0		0.963^{+21}_{-32}	0.065^{+1}_{-1}	5.10162/6	0.530847
0	1	1	0.747^{+15}_{-27}	0.820^{+16}_{-28}	-0.048^{+1}_{-1}	6.37703/6	0.382306
0	2	2	0.692^{+50}_{-68}	0.570^{+55}_{-56}	-0.131^{+1}_{-1}	18.8908/6	0.004352
1	0	1	1.108^{+69}_{-96}	1.174^{+65}_{-89}	0.043^{+1}_{-1}	7.08023/6	0.313492
1	1	0	1.128^{+23}_{-37}	1.039^{+20}_{-32}	0.033^{+1}_{-1}	8.78952/4	0.0665814
1	2	1	0.648^{+21}_{-35}	0.800^{+44}_{-58}	-0.094^{+1}_{-1}	3.92662/6	0.686607
1	4	1	0.446^{+21}_{-37}	0.632^{+1}_{-1}	-0.232^{+1}_{-1}	3.90267/6	0.689846
1	3	2	0.489^{+56}_{-69}	1.110^{+159}_{-204}	-0.205^{+1}_{-1}	6.24129/6	0.39671

Table C.21: $\kappa_a = 3530$, $\kappa_p = 3460$, $\kappa_e = 2990$, $Z_V^{\rm eff} = 0.896342$.

p^2	q^2	k^2	$f_+(q^2)$	$f_0(q^2)$	q^2	χ^2/dof	Q
0	0	0		0.979^{+22}_{-33}	0.071^{+1}_{-1}	4.18745/6	0.651326
0	1	1	0.750^{+17}_{-30}	0.825^{+18}_{-30}	-0.046^{+1}_{-1}	6.81731/6	0.338073
0	2	2	0.677^{+53}_{-68}	0.564^{+57}_{-60}	-0.132^{+1}_{-1}	14.0002/6	0.0296342
1	0	1	1.110^{+81}_{-97}	1.219^{+61}_{-97}	0.046^{+1}_{-1}	6.7693/6	0.342711
1	1	0	1.167^{+21}_{-39}	1.051^{+18}_{-31}	0.041^{+1}_{-1}	8.49146/4	0.0751464
1	2	1	0.643^{+24}_{-37}	0.789^{+52}_{-61}	-0.091^{+1}_{-1}	4.34837/6	0.629644
1	4	1	0.452^{+21}_{-38}	0.650^{+32}_{-55}	-0.228^{+1}_{-1}	3.02573/6	0.80561
1	3	2	0.484^{+62}_{-70}	1.100^{+175}_{-213}	-0.206^{+1}_{-1}	3.21587/6	0.781306

Table C.22: $\kappa_a = 3460$, $\kappa_p = 3510$, $\kappa_e = 2990$, $Z_V^{\rm eff} = 0.907034$.

p^2	q^2	k^2	$f_+(q^2)$	$f_0(q^2)$	q^2	χ^2/dof	Q
0	0	0		0.937^{+25}_{-35}	0.055^{+1}_{-1}	8.78107/6	0.18627
0	1	1	0.773^{+18}_{-28}	0.849^{+19}_{-29}	-0.054^{+1}_{-1}	6.85021/6	0.334922
0	2	2	0.720^{+60}_{-73}	0.574^{+68}_{-66}	-0.128^{+1}_{-1}	15.3203/6	0.0179068
1	0	1	1.104^{+79}_{-100}	1.148^{+82}_{-109}	0.035^{+1}_{-1}	8.37494/6	0.2119
1	1	0	1.089^{+23}_{-36}	1.037^{+21}_{-32}	0.022^{+1}_{-1}	11.5063/4	0.0214262
1	2	1	0.652^{+23}_{-39}	0.801^{+49}_{-67}	-0.102^{+1}_{-1}	4.12901/6	0.659223
1	4	1	0.486^{+26}_{-37}	0.677^{+41}_{-50}	-0.239^{+1}_{-1}	3.21467/6	0.781461
1	3	2	0.501^{+57}_{-83}	1.296^{+174}_{-253}	-0.205^{+1}_{-1}	6.70157/6	0.34933

Table C.23: $\kappa_a = 3510$, $\kappa_p = 3510$, $\kappa_e = 2990$, $Z_V^{\text{eff}} = 0.899385$.

p^2	q^2	k^2	$f_+(q^2)$	$f_0(q^2)$	q^2	χ^2/dof	Q
0	0	0		0.972^{+22}_{-38}	0.071^{+1}_{-1}	5.24516/6	0.512776
0	1	1	0.755^{+20}_{-32}	0.834^{+21}_{-34}	-0.048^{+1}_{-1}	5.31347/6	0.504282
0	2	2	0.699^{+65}_{-78}	0.598^{+76}_{-76}	-0.130^{+1}_{-1}	9.87629/6	0.129959
1	0	1	1.134^{+104}_{-122}	1.213^{+85}_{-126}	0.044^{+1}_{-1}	4.72766/6	0.579187
1	1	0	1.157^{+27}_{-44}	1.043^{+21}_{-36}	0.043^{+1}_{-1}	12.0862/4	0.0167214
1	2	1	0.649^{+29}_{-46}	0.797^{+59}_{-77}	-0.093^{+1}_{-1}	4.12208/6	0.66016
1	4	1	0.493^{+67}_{-46}	0.702^{+39}_{-63}	-0.230^{+1}_{-1}	3.88168/6	0.692685
1	3	2	0.484^{+67}_{-90}	1.280^{+196}_{-299}	-0.205^{+1}_{-1}	2.31242/6	0.888842

Table C.24: $\kappa_a = 3530$, $\kappa_p = 3510$, $\kappa_e = 2990$, $Z_V^{\text{eff}} = 0.896342$.

p^2	q^2	k^2	$f_+(q^2)$	$f_0(q^2)$	q^2	χ^2/dof	Q
0	0	0		0.994^{+24}_{-41}	0.0794^{+1}_{-1}	3.6775/6	0.720223
0	1	1	0.759^{+21}_{-36}	0.839^{+22}_{-39}	-0.045^{+1}_{-1}	5.38288/6	0.495724
0	2	2	0.681^{+66}_{-78}	0.589^{+78}_{-82}	-0.131^{+}_{-1}	7.14768/6	0.307406
1	0	1	1.117^{+119}_{-133}	1.228^{+84}_{-137}	0.048^{+1}_{-1}	5.69125/6	0.458649
1	1	0	1.202^{+27}_{-48}	1.056^{+20}_{-37}	0.053^{+1}_{-1}	11.0704/4	0.0257838
1	2	1	0.648^{+35}_{-53}	0.800^{+66}_{-85}	-0.089^{+1}_{-1}	4.07736/6	0.666208
1	4	1	0.494^{+29}_{-49}	0.714^{+40}_{-69}	-0.226^{+1}_{-1}	3.5036/6	0.743491
1	3	2	$0.482^{+0.075}_{-98}$	1.251^{+232}_{-337}	-0.205^{+1}_{-1}	1.79201/6	0.937799

Table C.25: The pseudoscalar decay constant. Fit range is 14-21

κ_H	κ_L	af_P	χ^2/dof	Q
	3460	0.0809^{+7}_{-7}	0.842898	0.536474
2000	3510	0.0774^{+8}_{-7}	0.603387	0.727898
	3530	0.0761^{+9}_{-8}	0.505311	0.804837
	3460	0.0836^{+7}_{-7}	1.2319	0.28616
2330	3510	0.0800^{+8}_{-8}	0.97497	0.440222
	3530	0.0788^{+8}_{-8}	0.823752	0.551207
	3460	0.0858^{+7}_{-7}	2.08967	0.0509875
2660	3510	0.0822^{+7}_{-8}	1.70814	0.114556
	3530	0.0809^{+8}_{-6}	1.3854	0.216075
	3460	0.0860^{+6}_{-7}	3.4354	0.00215311
2990	3510	0.0825^{+7}_{-9}	2.76928	0.0108044
	3530	$0.0812^{+}_{-10}{}^{7}$	2.18274	0.0415301

Table C.26: Chiral extrapolation of heavy-light f_P.

κ_H	af_P	af_P^s	χ^2/dof	Q
2000	0.0712^{+10}_{-9}	0.0809^{+7}_{-7}	3.43583	0.0637964
2330	0.0745^{+9}_{-9}	0.0836^{+7}_{-7}	3.84863	0.0497867
2660	0.0765^{+9}_{-9}	0.0858^{+7}_{-7}	2.93041	0.0869253
2990	$0.0771^{+}_{-10}{}^{8}$	0.0860^{+6}_{-7}	2.29832	0.129514

Table C.27: The vector decay constant. Fit range is 15-23.

κ_H	κ_L^*	f_V	χ^2/dof	Q
2000	3460	9.63^{+11}_{-12}	1.70133	0.092495
	3510	9.96^{+14}_{-14}	1.29772	0.239248
	3530	10.07^{+16}_{-16}	1.20861	0.289037
2330	3460	$8.70^{+\ 9}_{-10}$	1.59199	0.121264
	3510	8.95^{+12}_{-13}	1.25211	0.263846
	3530	9.04^{+14}_{-13}	1.21347	0.286138
2660	3460	$7.71^{+\ 8}_{-\ 8}$	1.4449	0.171983
	3510	7.88^{+10}_{-10}	1.19042	0.300084
	3530	7.93^{+12}_{-11}	1.18876	0.301109
2990	3460	$6.68^{+\ 7}_{-\ 7}$	1.42663	0.179375
	3510	$6.76^{+\ 9}_{-\ 7}$	1.17966	0.306761
	3530	$6.78^{+\ 9}_{-\ 8}$	1.1187	0.346564

Table C.28: Chiral extrapolation of heavy-light f_V.

κ_H	f_V	f_V^s	χ^2/dof	Q
2000	10.51^{+16}_{-17}	9.63^{+11}_{-12}	0.66746	0.413939
2330	9.40^{+15}_{-14}	$8.70^{+\ 9}_{-10}$	1.03477	0.309041
2660	8.21^{+13}_{-12}	$7.71^{+\ 8}_{-\ 8}$	1.14329	0.284959
2990	6.90^{+10}_{-10}	$6.68^{+\ 7}_{-\ 7}$	0.950229	0.329661

Table C.29: $f_+^\pi(q^2)$ for $\kappa_H = 2000$

p^2	q^2	k^2	$f_+(q^2)$	q^2	χ^2/dof	Q
0	1	1	$0.859^{+\ 37}_{-\ 51}$	0.218^{+3}_{-2}	5.05402/3	0.167884
0	2	2	$0.665^{+\ 89}_{-106}$	-0.062^{+1}_{-1}	1.30808/3	0.727216
1	1	0	$1.753^{+\ 66}_{-112}$	0.634^{+4}_{-2}	1.27384/3	0.735354
1	2	1	$0.863^{+\ 83}_{-111}$	0.196^{+3}_{-2}	1.92467/3	0.588188
1	3	2	0.788^{+149}_{-215}	-0.106^{+2}_{-1}	1.02157/3	0.796032

Table C.30: $f_0^\pi(q^2)$ for $\kappa_H = 2000$

p^2	q^2	k^2	$f_0(q^2)$	q^2	χ^2/dof	Q
0	0	0	$0.890^{+\ 29}_{-\ 40}$	0.635^{+4}_{-2}	13.7659/3	0.003242
0	1	1	$0.678^{+\ 32}_{-\ 42}$	0.218^{+3}_{-2}	2.6011/3	0.457296
0	2	2	$0.689^{+\ 90}_{-111}$	-0.062^{+1}_{-1}	0.597728/3	0.896952
1	1	0	$0.936^{+\ 21}_{-\ 39}$	0.635^{+4}_{-2}	0.114332/3	0.990064
1	2	1	$0.663^{+\ 60}_{-\ 69}$	0.196^{+3}_{-2}	2.01523/3	0.569251
1	3	2	1.040^{+196}_{-298}	-0.106^{+2}_{-1}	0.584164/3	0.900048

Table C.31: $f_+^\pi(q^2)$ for $\kappa_H = 2330$

p^2	q^2	k^2	$f_+(q^2)$	q^2	χ^2/dof	Q
0	1	1	$0.849^{+\ 30}_{-\ 57}$	0.118^{+2}_{-1}	0.748379/3	0.86177
0	2	2	$0.676^{+\ 93}_{-110}$	-0.108^{+1}_{-1}	2.24829/3	0.522499
1	1	0	$1.534^{+\ 61}_{-\ 87}$	0.481^{+3}_{-2}	12.4013/3	0.006128
1	2	1	$0.795^{+\ 64}_{-102}$	0.093^{+2}_{-1}	1.35883/3	0.715213
1	3	2	0.572^{+156}_{-175}	-0.158^{+1}_{-1}	0.637297/3	0.887843

Table C.32: $f_0^\pi(q^2)$ for $\kappa_H = 2330$

p^2	q^2	k^2	$f_+(q^2)$	q^2	χ^2/dof	Q
0	0	0	$0.914^{+\ 31}_{-\ 41}$	0.481^{+3}_{-2}	8.43457/3	0.037835
0	1	1	$0.744^{+\ 28}_{-\ 51}$	0.118^{+2}_{-1}	1.22597/3	0.746782
0	2	2	$0.698^{+\ 93}_{-106}$	-0.108^{+1}_{-1}	0.809935/3	0.847089
1	1	0	$0.992^{+\ 28}_{-\ 42}$	0.481^{+3}_{-2}	3.53059/3	0.316816
1	2	1	$0.694^{+\ 62}_{-\ 87}$	0.093^{+2}_{-1}	1.19947/3	0.753132
1	3	2	0.932^{+266}_{-343}	-0.158^{+1}_{-1}	0.835376/3	0.840988

Table C.33: $f_+^\pi(q^2)$ for $\kappa_H = 2660$

p^2	q^2	k^2	$f_+(q^2)$	q^2	χ^2/dof	Q
0	1	1	$0.818^{+\ 33}_{-\ 48}$	0.033^{+1}_{-1}	3.11264/3	0.374582
0	2	2	$0.660^{+\ 95}_{-106}$	-0.134^{+1}_{-1}	2.56828/3	0.463078
1	1	0	$1.406^{+\ 53}_{-\ 73}$	0.337^{+2}_{-2}	13.363/3	0.003914
1	2	1	$0.739^{+\ 40}_{-\ 90}$	0.0035^{+1}_{-1}	1.39931/3	0.705696
1	3	2	0.447^{+136}_{-142}	-0.193^{+1}_{-1}	0.852428/3	0.83689

Table C.34: $f_0^\pi(q^2)$ for $\kappa_H = 2660$

p^2	q^2	k^2	$f_0(q^2)$	q^2	χ^2/dof	Q
0	0	0	$0.996^{+\ 22}_{-\ 55}$	0.337^{+2}_{-2}	15.2682/3	0.001601
0	1	1	$0.801^{+\ 37}_{-\ 48}$	0.033^{+1}_{-1}	2.92055/3	0.404038
0	2	2	0.679^{+105}_{-116}	-0.134^{+1}_{-1}	1.72128/3	0.632213
1	1	0	$1.021^{+\ 30}_{-\ 43}$	0.337^{+2}_{-2}	3.17119/3	0.365977
1	2	1	$0.759^{+\ 62}_{-\ 99}$	0.003^{+1}_{-1}	1.51853/3	0.678
1	3	2	0.925^{+284}_{-323}	-0.193^{+1}_{-1}	2.46406/3	0.481822

Table C.35: $f_+^\pi(q^2)$ for $\kappa_H = 2990$

p^2	q^2	k^2	$f_+(q^2)$	q^2	χ^2/dof	Q
0	1	1	$0.760^{+\ 35}_{-\ 45}$	-0.032^{+1}_{-1}	2.48139/3	0.478663
0	2	2	0.658^{+103}_{-116}	-0.132^{+1}_{-1}	1.07477/3	0.783168
1	1	0	$1.288^{+\ 39}_{-\ 67}$	0.205^{+1}_{-1}	6.16286/3	0.10395
1	2	1	$0.642^{+\ 54}_{-\ 61}$	-0.069^{+1}_{-1}	1.00512/3	0.800013
1	3	2	0.435^{+131}_{-147}	-0.206^{+1}_{-1}	0.385849/3	0.94315

Table C.36: $f_0^\pi(q^2)$ for $\kappa_H = 2990$

p^2	q^2	k^2	$f_+(q^2)$	q^2	χ^2/dof	Q
0	0	0	$0.942^{+\ 40}_{-\ 52}$	0.205^{+1}_{-1}	17.9051/3	0.000460
0	1	1	$0.867^{+\ 32}_{-\ 52}$	-0.032^{+1}_{-1}	3.38677/3	0.335747
0	2	2	0.678^{+104}_{-110}	-0.132^{+1}_{-1}	2.55672/3	0.465127
1	1	0	$1.083^{+\ 29}_{-\ 53}$	0.205^{+1}_{-1}	1.65504/3	0.646975
1	2	1	$0.786^{+\ 89}_{-118}$	-0.069^{+1}_{-1}	1.7771/3	0.619931
1	3	2	1.345^{+379}_{-477}	-0.206^{+1}_{-1}	1.22261/3	0.747588

Bibliography

[1] L. H. Ryder, *Quantum Field Theory* (Cambridge University Press, Cambridge, 1985).

[2] J. F. Donoghue, E. Golowich, and B. R. Holstein, *Dynamics of the Standard Model* (Cambridge University Press, Cambridge, 1992).

[3] D. Perkins, *Introduction to High Energy Physics* (Addison-Wesley, California, 1986).

[4] F. Halzen and D. Martin, *Quarks and Leptons* (John Wiley & Sons, New York, 1984).

[5] Y. Fukuda *et al.*, Phys. Rev. Lett **81**, 1562 (1998).

[6] N. Cabibbo, Phys. Lett. **10**, 531 (1963).

[7] M. Kobayashi and K. Maskawa, Prog. Theor. Phys **49**, 652 (1973).

[8] L. Wolfenstein, Phys. Rev. Lett. **51**, 1945 (1983).

[9] I. Montvay and G. Münster, *Quantum Fields on a Lattice* (Cambridge University Press, Cambridge, 1994).

[10] H. J. Rothe, *Lattice Gauge Theories* (World Scientific, Singapore, 1992).

[11] M. Creutz, *Quarks, gluons and lattices* (Cambridge University Press, Cambridge, 1983).

[12] K. G. Wilson, Phys. Rev. D **10**, 2445 (1974).

[13] M. Lüscher and P. Weisz, Comm. Math. Phys **97**, 59 (1985).

[14] H. B. Nielsen and M. Ninomiya, Nucl. Phys. B **185**, 20 (1981).

[15] J. Kogut and L. Susskind, Phys. Rev. D **11**, 395 (1975).

[16] K. G. Wilson, in *New Phenomena in Subnuclear Physics*, edited by A. Zichichi (Plenum, New York, 1975).

[17] R. Kenway, in *Confinement, Duality, and Non-perturbative Aspects of QCD*, edited by P. van Baal (Plenum Press, New York, 1997).

[18] G. Lepage, in *Confinement, Duality, and Non-perturbative Aspects of QCD*, edited by P. van Baal (Plenum Press, New York, 1997).

[19] P. Weisz, in *Confinement, Duality, and Non-perturbative Aspects of QCD*, edited by P. van Baal (Plenum Press, New York, 1997).

[20] K. Symanzik, in *Mathematical Problems in Theoretical Physics*, edited by R. Schrader *et al.* (Springer, New York, 1982).

[21] K. Symanzik, Nucl. Phys. B **226**, 187 (1983).

[22] B. Sheikholeslami and R. Wohlert, Nucl. Phys. B **259**, 572 (1985).

[23] G.P. Lepage and P.B. Mackenzie, Phys. Rev. D **48**, 2250 (1993).

[24] M. Lüscher, S. Sint, R. Sommer and P. Weisz, Nucl. Phys. B **478**, 365 (1996).

[25] M. Lüscher, S. Sint, R. Sommer, P. Weisz, H. Wittig and U. Wolff, Nucl. Phys. B (Proc. Suppl.) **53**, 905 (1997).

[26] M. Lüscher, S. Sint, R. Sommer, and H. Wittig, Nucl. Phys. B **491**, 344 (1997).

[27] P. Lacock, A. McKerrel, C. Michael, I.M. Stopher and P.W. Stephenson, Phys. Rev. D **51**, 5403 (1995).

[28] P. Boyle, Ph.D. thesis, University of Edinburgh, 1997.

[29] S.J. Perantonis, A. Huntley and C. Michael, Nucl. Phys. B **326**, 544 (1989).

[30] B.Efron, Soc. for Industrial and Applied mathematics (1982).

[31] W.H. Press *et al.*, in *Numerical Recipies in C* (Cambridge Press, Cambridge, 1988).

[32] H. D. Politzer and M. B. Wise, Phys. Lett. B **208**, 504 (1988).

[33] H. Georgi, Phys. Lett. B **240**, 447 (1990).

[34] M. Wise, Heavy Quark Theory, `hep-ph/9411264`.

[35] N. Isgur, in *Phenomenology and Lattice QCD*, edited by G. Kilcup and S. Sharpe (World Scientific, Singapore, 1995).

[36] M. Luke, Phys. Lett. B **152**, 447 (1990).

[37] M. Neubert, Phys. Rep. **245**, 259 (1994).

[38] M. Neubert, Phys. Rev. D **49**, 1542 (1994).

[39] G. Burdman *et al.*, Phys. Rev. D **49**, 2331 (1994).

[40] N. Isgur and M. Wise, Phys. Rev. D **42**, 2388 (1990).

[41] E. Eichten, Nucl. Phys. B (Proc. Suppl.) **4**, 170 (1988).

[42] A. F. Falk, H. Georgi, B. Grinstein, and M. B. Wise, Nucl. Phys. B **343**, 1 (1990).

[43] M. Neubert, Phys. Rev. D **45**, 2451 (1992).

[44] M. Wise, Phys. Rev. D **45**, R2188 (1992).

[45] S. L. Adler and R. Dashen, *Current Algebras and Applications to Particle Physics* (W. A. Benjamin, New York, 1968).

[46] M. Neubert, Phys. Rev. D **46**, 1076 (1992).

[47] M. Creutz, Phys. Rev. D **36**, 2394 (1987).

[48] F. Brown and T. Woch, Phys. Rev. Lett. **58**, 163 (1987).

[49] N. Cabibbo and E. Marinari, Phys. Lett. B **119**, 387 (1982).

[50] S. Pickles, Ph.D. thesis, University of Edinburgh, 1998.

[51] S. Sint and P. Weisz, Nucl. Phys. B **502**, 251 (1997).

[52] M. Guagnelli and R. Sommer, Nucl. Phys. B (Proc. Suppl.) **63A-C**, 886 (1998).

[53] C. Caso *et al.*, Eur. Phys. J. C **3**, 1 (1998).

[54] P. Rowland, Nucl. Phys. B (Proc. Suppl.) **63A-C**, 175 (1998).

[55] P. Rowland, Ph.D. thesis, University of Edinburgh, 1997.

[56] Quenched Light Hadron Spectrum, in preparation, UKQCD Collaboration.

[57] M. Guagnelli, R. Sommer and H. Wittig, `hep-lat/9806005`.

[58] C. Maynard, UKQCD Collaboration, `hep-lat/9809064`, to appear in proceedings of Lattice 98.

[59] UKQCD Collaboration, K.C. Bowler *et al.*, Phys. Rev. D **51**, 4905 (1995).

[60] M. Bauer, B. Stech and M. Wirbel, Z. Phys. C **29**, 627 (1985).

[61] M. Bauer, B. Stech and M. Wirbel, Z. Phys. C **34**, 103 (1987).

[62] M. Bauer and M. Wirbel, Z. Phys. C **42**, 671 (1989).

[63] P.L. Frabetti *et al.*, Phys. Lett. B **364**, 127 (1995).

[64] P.L. Frabetti *et al.*, Phys. Lett. B **382**, 312 (1996).

[65] A. Bean *et al.*, Phys. Lett. B **317**, 647 (1993).

[66] J. Bartelt *et al.*, Phys. Lett. B **405**, 373 (1997).

[67] F. Parodi, P. Roudeau and A. Stocchi, `hep-ph/9802289`.

[68] H. Wittig, Int. J. Mod. Phys. A **12**, 4477 (1997).

[69] J. Flynn and C. Sachrajda, in *Heavy Flavours*, edited by A. Buras and M. Lindner (World Scientific, Singapore, 1997).

[70] D. Becirevic *et al.*, `hep-lat/9811003`.

[71] UKQCD Collaboration, R. M. Baxter *et al.*, Phys. Rev. D **49**, 1594 (1994).

[72] S. Bethke, Nucl. Phys. B (Proc. Suppl.) **54A**, 314 (1997).

[73] UKQCD Collaboration, D.R. Burford *et al.*, Nucl. Phys. B **447**, 425 (1995).

[74] P. Ball, J. High Energy Phys. **9809**, 5 (1998).

[75] J.G. Körner and G.A. Schuler, Phys. Lett. B **231**, 306 (1989).

[76] A. Aoki *et al.*, Nucl. Phys. B (Proc. Suppl.) **63A-C**, 380 (1998).

[77] H. Matsufuru *et al.*, Nucl. Phys. B (Proc. Suppl.) **63A-C**, 368 (1998).